Università di Genova

Gonadotoxicity of targeted therapies in young breast cancer patients and impact of carrying a germline *BRCA* mutation.

Ph.D. program in Biotechnology in Translational Medicine

Curriculum: Translational and Precision Medicine

XXXVIII cycle

Candidate: Silvia Ottonello

Tutor: Matteo Lambertini

Coordinator: Sveva Bollini

Table of Contents

Abstract

Background:

Breast cancer is the most common malignancy arising in women of reproductive age and its treatment often results in long-term sequelae and impaired quality of life (QoL). Among the possible negative consequences of anticancer therapies, treatment-induced gonadotoxicity leading to premature ovarian insufficiency (POI) represents one of the major sources of distress in this patient population. POI has a negative impact on global health and QoL of young breast cancer survivors being associated with several side effects including infertility. Carrying a germline deleterious BRCA pathogenic/likely pathogenic variant (PV) can add additional burden on this regard.

Aim:

The overall objective of this doctoral project was to evaluate the gonadotoxic potential of the targeted therapies Olaparib and Abemaciclib using a translational experimental approach based on human ovarian cortical tissue. Due to the limited availability of non-BRCA ovarian samples, the experimental phase was completed for Olaparib only, focusing on BRCA1/2- mutated ovarian tissues. Consequently, the lack of a non-BRCA control group prevented the evaluation of the second aim of the project namely, to determine whether the treatment exerts an impact on the ovarian reserve.

Methods:

Ovarian cortical fragments obtained from BRCA1/2 mutation carriers undergoing risk-reducing salpingo-oophorectomy were cultured for three days under four experimental conditions: control, Olaparib alone, standard chemotherapy (carboplatin and paclitaxel), and Olaparib combined with chemotherapy. Histological (H&E, Masson's trichrome), immunohistochemical, and immunofluorescence analyses were performed to assess follicular morphology, collagen deposition, apoptosis, DNA damage, and activation markers, including γH2AX, TUNEL, cleaved Caspase-3, and Yap-1. In parallel, cytokine release in culture media was evaluated at 24, 48, and 72 hours using a multiplex immunoassay to explore treatment-related inflammatory and angiogenic responses.

Results:

Exposure to Olaparib alone did not induce significant alterations in follicular health status, morphology, or stromal integrity compared with controls. Apoptotic and DNA damage markers remained at baseline levels, suggesting minimal direct ovarian toxicity. As expected, chemotherapy-treated tissues displayed clear signs of follicular atresia and increased apoptosis. The combination of Olaparib with chemotherapy resulted in a modest increase in apoptotic marker expression (γH2AX) compared with chemotherapy, indicating a potential additive effect on ovarian damage. Cytokine analyses revealed that control and Olaparib-treated tissues exhibited similar profiles with high levels of released cytokines, whereas chemotherapy and combined treatments consistently showed lower levels of the selected analytes.

Conclusions:

These findings suggest that Olaparib alone has no evident gonadotoxic effects in human ovarian tissue in vitro, whereas its combination with chemotherapy may enhance ovarian damage. Although preliminary, these results provide valuable insight into the reproductive safety of targeted therapies. Cytokine analyses revealed consistent differences between control/Olaparib and chemotherapy/combined treatment groups, reflecting respectively possible tissue stress and cytotoxic effects rather than physiological inflammation. While these data complement morphological and functional findings, further studies are necessary to validate these observations, clarify the biological significance of cytokine changes, and improve detection sensitivity. Additional research is also needed to elucidate the underlying molecular mechanisms and to extend the analysis to Abemaciclib to comprehensively assess the fertility impact of modern anticancer treatments in young women with breast cancer. Lastly, further investigations should clarify whether germline BRCA status influences reproductive toxicity.

1. Introduction

1.1 Breast cancer in young women: epidemiology and clinical challenges

Breast cancer is the most frequently diagnosed malignancy among women worldwide and represents a leading cause of cancer-related mortality. Recent global cancer statistics indicate that it accounts for the highest number of new cancers diagnoses in women and a substantial proportion of cancer deaths. Although incidence varies geographically, the absolute number of cases continues to rise due to population aging, lifestyle factors, and improved detection. In Italy, breast cancer is likewise the most common cancer in women, with approximately 55,000-56,000 new diagnoses each year and around 13,000 deaths. Among these, an estimated 2,500-3,000 cases occur in women under the age of 40, confirming that, while less frequent, breast cancer in young women represents a clinically significant subgroup with specific needs (1).

Breast cancer diagnosed in women under the age of 40 is relatively uncommon, representing less than 10% of all cases, yet it is associated with distinctive clinical and psychosocial challenges. From an oncological perspective, young patients often present with biologically more aggressive tumors, including higher grade, hormone receptor–negative, and triple-negative subtypes, which contribute to poorer prognosis compared with older women. Beyond tumor biology, the diagnosis at a young age raises critical survivorship concerns, particularly regarding fertility and endocrine health (2).

Systemic anticancer treatments, especially chemotherapy, are known to exert gonadotoxic effects by damaging the ovarian reserve, leading to a substantial risk of premature ovarian insufficiency and infertility. This risk is particularly relevant given that many patients at this age have not yet completed their reproductive plans. The degree of gonadotoxicity depends on several factors, including the type and dose of cytotoxic agents, age at treatment, and baseline ovarian function. Building on this evidence, authoritative reviews highlight that alkylating agents and anthracyclines are consistently associated with the highest risk of ovarian damage and earlier menopause, with risk modulated by cumulative exposure and patient age (2,3).

Complementary mechanistic studies in vivo have shown that cyclophosphamide and cisplatin induce rapid DNA double-strand breaks in primordial-follicle oocytes, triggering TAp63-mediated apoptosis and acute depletion of the ovarian reserve (4–6). Similar dose-dependent ovarian toxicity has been reported for doxorubicin, which impairs follicle development and accelerates follicular atresia (7,8).

Human translational data reinforce these findings. In vitro exposure of ovarian cortex to the active cyclophosphamide metabolite 4-hydroperoxy-cyclophosphamide results in direct damage to primordial follicles and increased apoptosis, while co-treatment with anti-Müllerian hormone has shown partial protective effects (9,10). Ex vivo and xenograft models using human ovarian tissue similarly demonstrate significant follicular loss following treatment with alkylating agents supporting a shared mechanism of chemotherapy-induced ovarian reserve depletion (11,12).

Importantly, newer targeted agents are being increasingly used in the treatment of young women with breast cancer, but their long-term impact on fertility and gonadal function remains insufficiently understood and is an area of ongoing research (13).

In addition, newer targeted agents are being increasingly used in the treatment of young women with breast cancer, but their long-term impact on fertility and gonadal function remains insufficiently understood and is the subject of ongoing research (13). Alongside these biological and therapeutic aspects, young women face unique psychosocial challenges, including concerns related to body image, sexuality, career, and family planning. These elements underline the importance of integrating oncofertility counselling and fertility preservation strategies into the standard management of this population, ensuring that therapeutic efficacy is balanced with quality of life and long-term survivorship considerations (2).

Thanks to advances in systemic therapy, early detection, and multidisciplinary management, survival rates for breast cancer have significantly improved. As a result, the population of breast cancer survivors has grown steadily, shifting clinical priorities toward long-term health, quality of life, and tailored follow-up care. Comprehensive survivorship models emphasize the management of treatment-related toxicities, endocrine and bone health, cardiovascular risk, psychosocial wellbeing, fertility, and sexual health (14).

Recent consensus statements and expert recommendations in oncology underline the need for structured survivorship plans and integrated care pathways that ensure continuity between oncology, primary care, and supportive services (15). Furthermore, updated epidemiological analyses confirm the growing burden of survivorship worldwide and highlight the importance of designing healthcare systems capable of addressing the diverse needs of breast cancer patients across different life stages (1).

1.2 Genetic predisposition: *BRCA* germline pathogenic/likely pathogenic variant (PV) and clinical significance

The *BRCA1* and *BRCA2* genes encode tumor suppressor proteins that are crucial for the repair of DNA double-strand breaks through the homologous recombination (HR) pathway, thereby preserving genomic integrity (16). Pathogenic germline mutations in these genes lead to homologous recombination deficiency (HRD), which results in genomic instability and a markedly increased lifetime risk of developing breast and ovarian cancers. BRCA1- and BRCA2-associated breast cancers often present with distinct biological features: *BRCA1* carriers typically develop triple-negative tumors, whereas *BRCA2* associated cancers are more frequently hormone receptor–positive, with implications for prognosis and therapeutic responsiveness (17).

From a clinical perspective, these germline mutations are particularly relevant in young women, who not only face an earlier onset of disease but also unique survivorship concerns, especially regarding fertility. Several studies suggest that *BRCA1* mutation carriers may have a diminished ovarian reserve, as evidenced by lower anti-Müllerian hormone (AMH) levels and a potentially earlier age at menopause, raising concerns about gonadotoxic risk even before the initiation of systemic treatments (17,18).

Recent data further support this hypothesis. A large multicentered analysis found that women with germline *BRCA1/2* pathogenic variants had significantly lower AMH levels compared with non-carriers (23 % lower overall; and for BRCA1 carriers, a 33 % reduction) after adjustment for age and other covariates (19). Another recent observational study in healthy young women with hereditary breast/ovarian cancer (HBOC) syndrome showed a consistent trend toward reduced reproductive potential,

particularly among *BRCA1* carriers, when assessed by AMH and antral follicle count (AFC) (20). Conversely, a meta-analysis comparing women with and without *BRCA* mutations concluded that evidence of reduced ovarian reserve (in terms of AMH) is mixed and not uniformly confirmed (21,22).

Furthermore, preclinical models provide mechanistic insight: conditional ablation of Brca1 in mouse oocytes leads to accelerated depletion of the follicular pool and impaired oocyte maturation with advancing maternal age, supporting the concept that BRCA1 function is important for maintaining ovarian reserve over time (23).

Overall, while the body of evidence points toward a plausible link between *BRCA1* mutations and diminished ovarian reserve, discrepancies among clinical studies persist. The heterogeneity may arise from differences in study populations (healthy vs cancer-affected), age distributions, ovarian stimulation protocols, and the sensitivity of reserve biomarkers. Continued investigation is warranted to clarify the magnitude of effect, particularly in younger, non-treated *BRCA* carriers, and its implications for fertility preservation strategies.

The gonadotoxicity of chemotherapy, already a major issue in young breast cancer patients, may therefore have compounded effects in this genetically predisposed subgroup, further highlighting the need for early oncofertility counselling and proactive fertility preservation strategies (18).

In addition, *BRCA* mutation carriers face complex reproductive decisions related to the potential transmission of pathogenic variants to offspring and the timing of risk-reducing surgeries, such as risk reducing salpingo-oophorectomy, which are often recommended at a younger age and may conflict with reproductive intentions. For these reasons, the integration of genetic counselling, oncofertility expertise, and multidisciplinary care is essential in order to provide personalized and comprehensive management to young breast cancer patients carrying a *BRCA* mutation (17).

1.3 Anticancer therapies and gonadotoxicity risk

Systemic anticancer therapies can significantly impair ovarian function, either transiently or permanently, depending on the agent, dosage, and age of the patient at exposure. The term gonadotoxicity refers to the detrimental effect of oncologic treatments on the gonads, primarily through damage to the ovarian follicle pool, the stromal and vascular microenvironment, and the hypothalamic-pituitary-gonadal axis. This damage may manifest clinically as reduced ovarian reserve, menstrual dysfunction, infertility, or premature ovarian insufficiency (POI) (24,25).

The concept of gonadotoxic risk encompasses the likelihood that a given therapy will induce such effects, which varies according to drug class, cumulative dose, patient age at exposure, and the presence of genetic predispositions, such as *BRCA* mutations (25).

Chemotherapy remains the leading cause of iatrogenic gonadotoxicity in young women with breast cancer, primarily by inducing apoptosis of primordial follicles and accelerating follicular depletion (17). Beyond conventional cytotoxic treatments, the increasing use of targeted therapies introduces new uncertainties regarding their potential long-term reproductive consequences, since their effects on ovarian physiology are still poorly characterized (26). Understanding the gonadotoxic profile of each drug class is therefore essential for tailoring fertility preservation strategies and providing appropriate counselling.

1.3.1 Chemotherapy

1.3.1.1 Alkylating agents

Alkylating agents, such as cyclophosphamide, are widely recognized as the most gonadotoxic class of chemotherapeutic drugs. Their mechanism involves DNA cross-linking and direct damage to both dividing and quiescent oocytes, leading to follicular depletion and premature ovarian insufficiency. The risk is dose-dependent and cumulative, with higher rates of amenorrhea and infertility observed in patients treated with regimens containing high cumulative doses of cyclophosphamide (17,26). Consequently, alkylating agents represent a major concern for fertility preservation planning in young breast cancer patients (27).

1.3.1.2 Platinum and taxane-based regimens

Platinum compounds (e.g., cisplatin, carboplatin) exert their cytotoxic effects by forming DNA adducts and inducing double-strand breaks, which can also damage ovarian follicles. Taxanes (e.g., paclitaxel, docetaxel) act through microtubule stabilization, impairing cell division, and their gonadotoxic potential appears lower than that of alkylating agents but not negligible. When combined in modern breast cancer regimens, platinum and taxanes may increase the risk of treatment-induced amenorrhea, though the long-term effects on ovarian reserve are less clearly established (3,17). Current evidence suggests that the gonadotoxicity of platinum- and taxane-based therapies is intermediate, highlighting the importance of fertility preservation discussions even in patients receiving these regimens (27).

1.3.2 Novel Targeted Therapies

Targeted therapies are increasingly utilized in the management of young breast cancer patients, offering more precise mechanisms of action compared to conventional chemotherapy. Unlike cytotoxic agents, which broadly target proliferating cells, targeted therapies act on specific molecular pathways that drive cancer growth and survival. This specificity raises the possibility of a more optimized reproductive toxicity profile. However, the long-term gonadotoxic effects of these agents remain largely unexplored due to limited follow-up data and the absence of systematic assessment of fertility endpoints in most clinical trials (28,29).

In current treatment algorithms, targeted therapies may be administered either sequentially to chemotherapy or in combination with it, depending on tumor subtype and disease stage. PARP inhibitors, for example, are often introduced post-chemotherapy or used as maintenance in BRCA-mutated patients, whereas CDK4/6 inhibitors are commonly combined with endocrine therapy or integrated after cytotoxic regimens in hormone receptor–positive disease. The sequence of administration is particularly relevant when considering ovarian exposure, as the potential reproductive impact may vary when targeted agents are delivered before, during, or after chemotherapy. Recent analyses have highlighted that the broader incorporation of targeted therapies in earlier lines of treatment, especially in high-risk young women, has not been accompanied by parallel evaluation of fertility-related outcomes (30,31).

Although preclinical data suggest that some targeted agents may exert a lower degree of ovarian toxicity compared to traditional chemotherapy, the combined or sequential administration with cytotoxic drugs raises questions about cumulative or delayed effects. Moreover, as treatment durations extend and maintenance strategies become more common, the absence of long-term reproductive follow-up represents a substantial knowledge gap (32). Emerging research has also underlined the need to include fertility endpoints in clinical trials investigating immunotherapy and targeted agents in breast cancer, particularly in younger populations (33).

Given the relatively recent introduction of targeted agents and their prolonged use in some treatment settings, careful evaluation of reproductive safety is essential. Understanding the mechanisms by which these drugs may impact ovarian physiology is crucial for developing fertility preservation strategies and guiding oncofertility counseling (28,29).

1.3.2.1 CDK4/6 Inhibitors

Cyclin-dependent kinase 4 and 6 (CDK4/6) inhibitors, such as Palbociclib, Ribociclib, and Abemaciclib, have become standard of care in combination with endocrine therapy for hormone receptor–positive, HER2-negative advanced breast cancer. These agents arrest the cell cycle at the G1–S checkpoint, primarily affecting proliferating tumor cells. To date, no clinical evidence has demonstrated a direct gonadotoxic effect of CDK4/6 inhibitors, but most pivotal trials did not systematically evaluate fertility outcomes or ovarian reserve parameters (29).

Biologically, CDK4/6 pathways are also critical in ovarian function, including granulosa cell proliferation, follicular development, and oocyte maturation. Preclinical studies suggest that exogenous inhibition of CDK4/6 could interfere with these processes, potentially affecting ovarian reserve and fertility. Given their increasing use in young women and the potential for long-term administration, dedicated research on ovarian safety, including prospective monitoring of ovarian reserve markers, is warranted (28).

In addition, CDK4/6 inhibitors are being increasingly explored not only in the metastatic setting but also in earlier stages of the disease, including neoadjuvant and adjuvant contexts. This shift implies longer exposure time in premenopausal patients, raising questions about cumulative effects on ovarian physiology. Although available clinical data suggest an optimized safety profile from the reproductive standpoint, current evidence is indirect and mostly extrapolated from menstrual function, amenorrhea rates, or surrogate endocrine markers. Recent observational reports and translational studies have also highlighted that the ovarian microenvironment expresses CDK4/6-regulated targets, supporting the rationale for further investigation into potential subclinical effects on follicular dynamics (28).

Moreover, as some combinations with endocrine therapy or targeted agents are being extended to younger populations, the absence of structured fertility endpoints leaves an important knowledge gap. Taken together, the growing use of CDK4/6 inhibitors in women of reproductive age underscores the need for prospective studies assessing ovarian reserve, long-term menstrual function, and fertility outcomes with adequate follow-up (34).

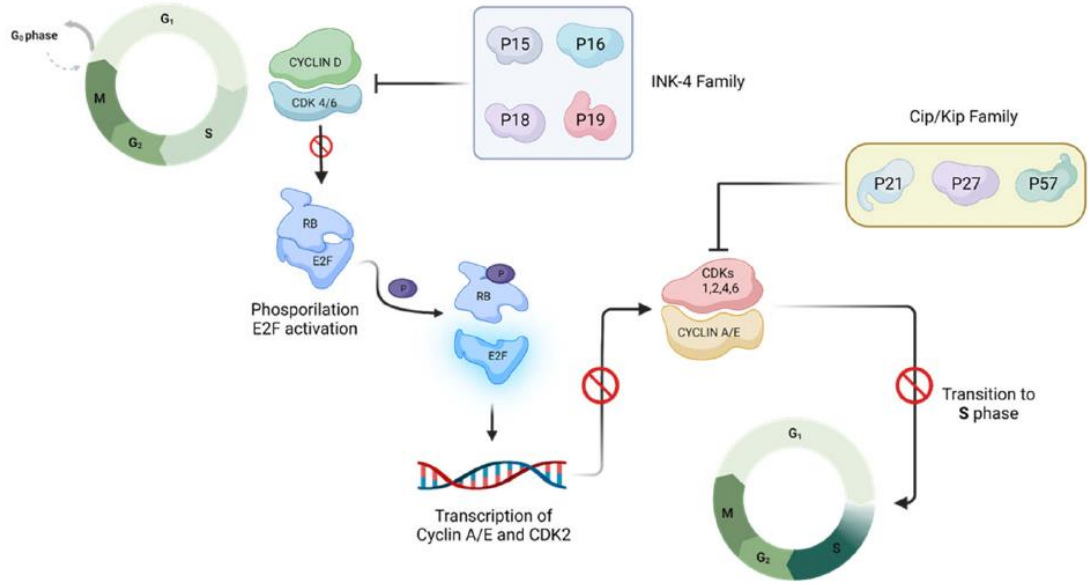

Fig 1. Cyclin–CDK pathway regulation in the cell cycle. The INK-4 family and the CIP/KIP-type family inhibit the cyclin D-CDK4/6 complex and cyclin A/E-CDK1, CDK2, CDK4 and CDK6, respectively. On the one hand, these complexes' inactivation leads to a state of cell quiescence in the G0 phase, and on the other, it prevents transition to the S phase. *Reproduced from:* Scavone, G.; Ottonello, S.; Blondeaux, E.; Arecco, L.; Scaruffi, P.; Stigliani, S.; Cardinali, B.; Borea, R.; Paudice, M.; Vellone, V.G.; Condorelli, M.; Demeestere, I.; Lambertini, M. The Role of Cyclin-Dependent Kinases (CDK) 4/6 in the Ovarian Tissue and the Possible Effects of Their Exogenous Inhibition. *Cancers* 2023, *15*(20), 4923. https://doi.org/10.3390/cancers15204923

1.3.2.2 PARP Inhibitors

Poly (ADP-ribose) polymerase (PARP) inhibitors, including Olaparib, Talazoparib, and Niraparib, target tumors with defects in homologous recombination DNA repair, such as BRCA1/2-mutated cancers (35). By blocking base excision repair, PARP inhibitors induce accumulation of DNA damage and selective death of tumor cells. While their oncologic efficacy is well established, data regarding their gonadotoxicity are limited (36).

Preclinical evidence indicates that PARP inhibitors may reduce primordial follicle counts and impair granulosa cell function, as demonstrated by olaparib-treated mice showing a 36% depletion of primordial follicles (37) and granulosa cell dysfunction in vitro (38). Moreover, since these drugs interfere with DNA repair pathways that are active in oocytes, there is a theoretical risk of follicular depletion, particularly in young women with BRCA mutations. Most clinical trials, however, have not systematically assessed fertility endpoints, making it difficult to quantify the true reproductive risk (36).

Considering the expanding use of PARP inhibitors, especially in BRCA-mutated young patients, monitoring ovarian function during and after treatment is recommended. Assessment of ovarian reserve through biomarkers such as anti-Müllerian hormone (AMH) and antral follicle count (AFC), along with individualized fertility counseling, should be integrated into clinical protocols to ensure optimal long-term reproductive care (36).

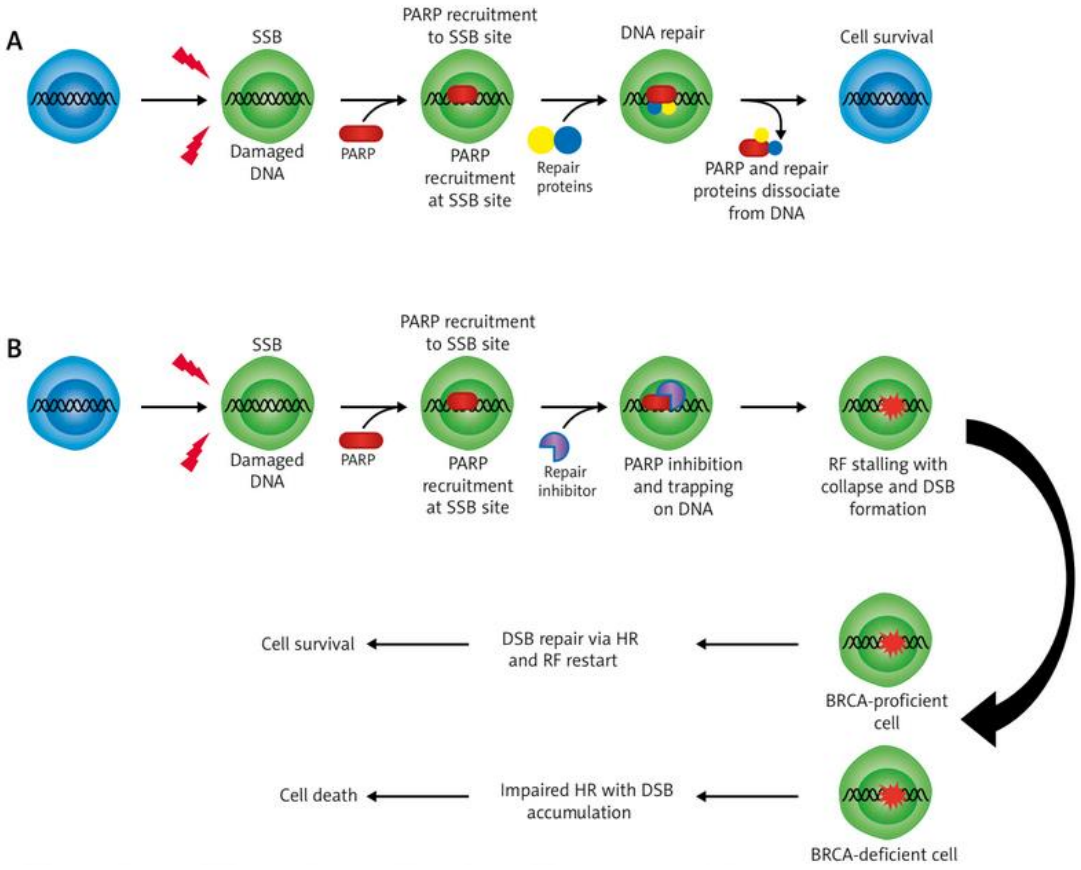

Fig. 2 Mechanism of action of PARP inhibitors.

A) Proper DNA repair mechanism with functional PARP protein and DNA repair proteins. B) Attempted DNA repair of SSB in the presence of PARP inhibitor resulting in DSB formation. BRCA-proficient cells can repair the DSB and restart, maintaining survival. BRCA-deficient cells are unable to repair the accumulating DSB–s which inevitably results in cell death. Reproduced from Mazurek et al., 2016 [PMID: 27981036], with permission. Source: Nowak-Markwitz E., Spaczyński M. *PARP inhibitors in ovarian cancer treatment*. *Przegląd Menopauzalny* (Menopause Review). 2016;15(3):215–219. doi:10.5114/pm.2016.65667

1.4 Gonadal function and reproductive health in young women with breast cancer

1.4.1 Female gonads: the ovary

The ovary is the central organ of the female reproductive system, responsible for both gamete production and hormone secretion. It is a paired structure located in the pelvic cavity and connected to the uterus and pelvic wall through ligamentous structures that also carry its blood supply and innervation (39).

Structurally, the ovary is organized into two regions: the cortex, which contains follicles at different stages of development, and the medulla, rich in blood vessels, nerves, and connective tissue (40,41). The ovarian follicles are the functional units of the ovary, each consisting of an oocyte surrounded by granulosa and theca cells. These cells support oocyte growth and mediate steroid hormone production, primarily estrogens (42).

The process of folliculogenesis starts with primordial follicles, established during fetal life, containing oocytes arrested in meiosis. A fraction of these follicles is gradually activated and progresses through primary, secondary, and antral stages, becoming sensitive to follicle-stimulating hormone (FSH). Eventually, a dominant follicle is selected, which undergoes ovulation under the influence of luteinizing hormone (LH). After ovulation, the residual follicle transforms into the corpus luteum, a temporary endocrine structure producing progesterone, crucial for early pregnancy support (43,44).

A key concept is the ovarian reserve, defined as the finite pool of primordial follicles present from birth. This pool declines progressively with age, as no new oocytes are generated after birth in humans. By age 30, only about 12% of the original pool remains, and by age 40, around 3%, explaining the marked decline in fertility with advancing age (45).

Ovarian function is tightly regulated by the hypothalamic–pituitary–gonadal axis, through gonadotropins such as follicle-stimulating hormone (FSH) and luteinizing hormone (LH), and by intra-ovarian signaling pathways, including Transforming growth factor beta (TGF-β) members and transcription factors like FOXL2 and FOXO3, which coordinate follicle growth and maturation (40,44).

In summary, the ovary sustains reproductive capacity through the coordinated processes of follicle recruitment, growth, ovulation, and hormone production. The gradual depletion of ovarian reserve underlies the biological basis of female reproductive aging.

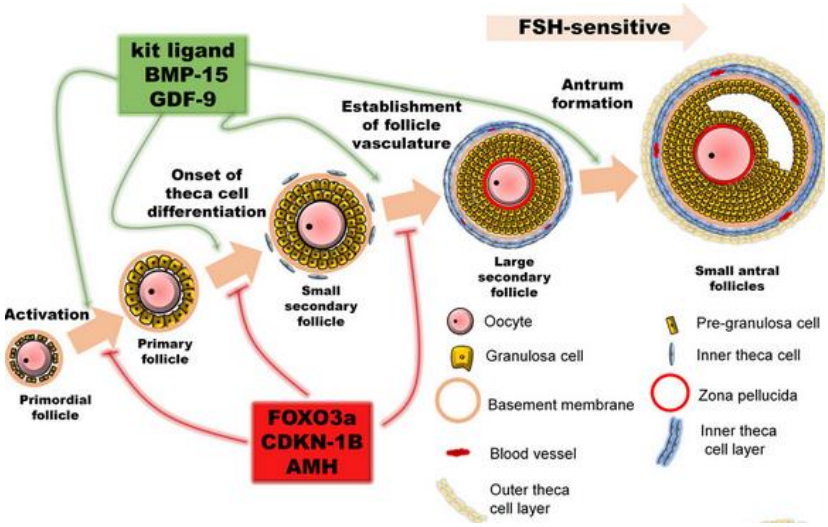

Fig. 3 Schematic representation of the main mechanisms that regulate ovarian follicular development. Reproduced from Guzmán A, Hernández-Coronado CG, Gutiérrez CG, Rosales-Torres AM. The vascular endothelial growth factor (VEGF) system as a key regulator of ovarian follicle angiogenesis and growth. Mol Reprod Dev. 2023 Apr;90(4):201-217. doi: 10.1002/mrd.23683. Epub 2023 Mar 26. PMID: 36966489.

1.4.2 Impact of anticancer treatments on ovarian reserve and hormonal function

Systemic anticancer therapies, including chemotherapy and targeted treatments, can significantly affect ovarian function, leading to both transient and permanent reproductive impairments. Ovarian reserve refers to the quantity and quality of primordial follicles present in the ovaries at a given time, representing a woman's reproductive potential. It can be assessed indirectly through biomarkers such as AMH levels, antral follicle count (AFC), and, in some cases, FSH measurements. A reduced ovarian reserve is associated with diminished fertility and an increased risk of premature ovarian insufficiency (45,46).

Chemotherapy, particularly regimens involving alkylating agents, induces DNA damage and apoptosis in primordial follicles, resulting in accelerated depletion of ovarian reserve. Platinum-and taxane-based regimens also contribute to ovarian damage, although their gonadotoxic potential may vary. Clinically, this can manifest

as amenorrhea, decreased AMH levels, reduced AFC, and, in some cases, early menopause. The extent of ovarian impairment depends on patient age, baseline ovarian reserve, cumulative drug dose, and treatment duration (2,27).

Emerging targeted therapies, such as CDK4/6 inhibitors and PARP inhibitors, are increasingly used in young breast cancer patients. Preclinical studies suggest that CDK4/6 inhibitors may interfere with ovarian cell proliferation and follicular maturation, while PARP inhibitors, such as olaparib, may impair DNA repair in oocytes, leading to potential follicular depletion and reduced ovarian function (28,47). Although clinical data are limited, these findings highlight the need for individualized monitoring of ovarian function and reproductive counseling.

1.4.3 Age-related decline in ovarian reserve: physiological mechanisms and clinical implication

Ovarian reserve progressively declines across a woman's reproductive lifespan due to a combination of intrinsic biological processes and environmental influences. At birth, the follicular pool is already dramatically reduced compared to the fetal stage and continues to decrease through ongoing follicular atresia and cyclical recruitment. The rate of follicle depletion accelerates notably after the age of 35, leading to a decline in ovarian hormone production and reduced reproductive capacity (48).

In addition to the numerical loss of follicles, ovarian ageing is characterized by a deterioration in oocyte quality. Recent studies have highlighted mitochondrial dysfunction and oxidative stress as key drivers of meiotic errors and increased aneuploidy in women of advanced reproductive age (49). Concurrently, chronic low-grade inflammation referred to as "inflammaging" disrupts the ovarian microenvironment by impairing granulosa cell function and follicular development (50).

The clinical consequences of this decline are reflected in reduced natural fertility rates and poorer outcomes in assisted reproductive technologies. However, a recent cross-sectional study demonstrated considerable interindividual variability in ovarian reserve among women of the same chronological age, underscoring the importance

of biomarkers such as Anti-Müllerian Hormone (AMH) and antral follicle count as more reliable predictors of reproductive potential than age alone (51).

In summary, age remains the primary determinant of ovarian reserve, yet its interpretation must be contextualized alongside functional biomarkers and individual genetic and environmental factors. A deeper understanding of the physiological mechanisms underpinning ovarian ageing is essential for optimizing fertility preservation strategies and improving reproductive counselling—particularly in women facing gonadotoxic cancer therapies.

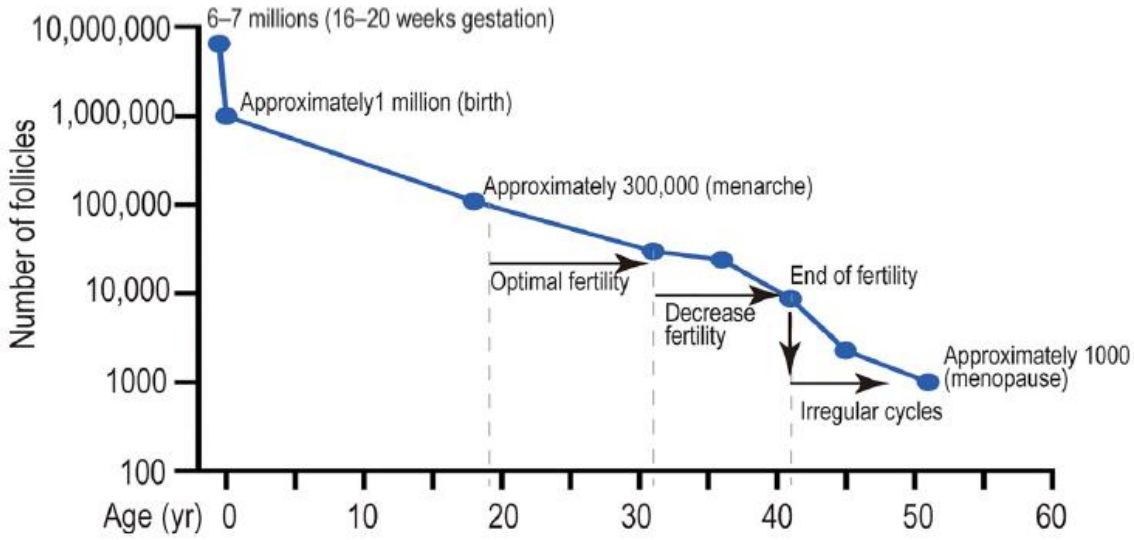

Fig. 4 Age-related decline in ovarian follicle number.
Reproduced from Pohl E, Pohl M, Walther A. *From reproductive age to menopause: the role of ovarian reserve and hormonal changes.* Mol Reprod. 2022;19(1): e0031. DOI: 10.1515/mr-2022-0031. Open Access under CC-BY license.

1.5 Fertility preservation and special considerations in *BRCA* mutation carriers

Fertility preservation is a crucial component of supportive care in young breast cancer patients, and it assumes relevance in carriers of pathogenic *BRCA1* or *BRCA2* germline mutations. In addition to conferring a markedly elevated lifetime risk of breast and ovarian cancers, *BRCA* mutations may be associated with biological features that compromise reproductive potential even in the absence of oncologic treatment. Several studies have suggested that *BRCA1* carriers tend to exhibit a reduced ovarian reserve, as reflected by lower AMH concentrations, decreased antral follicle count, and a potentially earlier age at menopause compared with non-carriers (17,52).

Although the evidence remains heterogeneous, these findings underscore the importance of timely fertility counseling and preservation strategies in this high-risk population.

Standard approaches for fertility preservation in breast cancer include oocyte and embryo cryopreservation, which are established as the most effective options, as well as ovarian tissue cryopreservation, increasingly offered in experimental or selected settings. Temporary ovarian suppression with gonadotropin-releasing hormone (GnRH) agonists during chemotherapy is another strategy with proven efficacy in reducing the risk of treatment-induced premature ovarian insufficiency(27,53). In BRCA mutation carriers, however, unique challenges arise: (a) a possibly lower baseline ovarian reserve may impact the success rates of controlled ovarian stimulation; (b) ovarian tissue cryopreservation, while technically feasible, raises theoretical concerns due to the intrinsic risk of future ovarian malignancies; and (c) the possibility of transmitting the germline mutation necessitates careful reproductive planning.

Patients should also be informed about reproductive options, including the possibility of preimplantation genetic testing (PGT) to reduce the risk of transmitting BRCA mutations to offspring (13). In parallel, risk-reducing strategies such as risk reducing salpingo-oophorectomy, usually recommended between 35 and 40 years of age for *BRCA1* and slightly later for *BRCA2* carriers, impose an additional time constraint on reproductive planning, making early intervention essential.

Fertility preservation in *BRCA* mutation carriers requires an individualized and multidisciplinary approach, integrating oncologists, reproductive endocrinologists, and genetic counsellors. This coordinated framework ensures that patients receive comprehensive information on their oncologic prognosis, reproductive risks, and available technologies, thereby facilitating informed choices that balance cancer outcomes with family planning aspirations(13,27).

1.6 Ethical and multidisciplinary aspects

The management of fertility preservation in young breast cancer patients requires a multidisciplinary approach and careful ethical consideration. Optimal care involves collaboration among oncologists, reproductive endocrinologists, geneticists, and psychosocial support professionals to ensure timely counseling and personalized decision-making (1,2). Multidisciplinary coordination is essential to integrate cancer treatment planning with reproductive goals without compromising oncologic outcomes (13,27).

Ethical considerations include respecting patient autonomy, providing comprehensive and balanced information about risks, benefits, and uncertainties of fertility preservation options, and supporting informed decision-making (13). For BRCA mutation carriers, additional ethical complexities arise from the potential transmission of pathogenic variants to offspring and the implications of preimplantation genetic testing (17). Psychosocial aspects, including anxiety related to infertility risk and treatment timing, should also be addressed to support patients' emotional well-being.

Furthermore, equitable access to fertility preservation techniques and adherence to international guidelines are critical to ensure that all eligible patients receive appropriate counseling and interventions (2,3). Integrating these ethical and multidisciplinary principles fosters patient-centered care and optimizes both reproductive and oncologic outcomes (1,3).

2. Aims of the Thesis

The overall aim of this thesis is to improve the current understanding of treatment-related gonadotoxicity in young women with breast cancer, an increasingly relevant issue in modern oncology where survival rates are high and reproductive health has become a major survivorship concern. While the detrimental effects of chemotherapy on ovarian function are well established, the reproductive safety profile of targeted therapies remains poorly defined, particularly for agents such as CDK4/6 inhibitors and PARP inhibitors that are now widely incorporated into therapeutic strategies.

Within this broader framework, the primary experimental objective of this doctoral project was to evaluate the gonadotoxic potential of the PARP inhibitor Olaparib using a translational experimental model based on short-term culture of human ovarian cortical tissue. Due to the limited availability of non-carrier samples, the study was conducted on ovarian tissue obtained from BRCA1/2 mutation carriers undergoing risk-reducing salpingo-oophorectomy, a population of clinical relevance given the possible intrinsic impairment of ovarian reserve associated with BRCA mutations.

A secondary and exploratory objective was to generate preliminary data on the ovarian effects of CDK4/6 inhibition, focusing on Abemaciclib. However, this component could only be partially addressed because of sample availability constraints and should therefore be considered hypothesis-generating rather than conclusive.

More broadly, the thesis also aims to investigate how germline BRCA1/2 mutations known to increase cancer susceptibility and potentially associated with reduced ovarian reserve and earlier reproductive senescence may interact with systemic therapies in shaping gonadal outcomes. By integrating experimental findings with clinical and biological evidence, this work seeks to contribute to individualized fertility preservation strategies and to improve multidisciplinary counseling for young breast cancer patients.

3. Materials and Methods

3.1 Experimental plan

This study focused on the assessment of potential gonadotoxicity of target therapy Olaparib, a PARP inhibitor currently used in clinical practice for BRCA1 and *BRCA2* carriers with early breast cancer at high risk of recurrence on ovarian cortical tissues alone or in combination with Carboplatin and Paclitaxel, which is standard chemotherapy for patients with triple negative breast cancer. The other target therapy objective of this study is Abemaciclib, a CDK4/6 inhibitor currently used in the early setting alone or in combination with its standard chemotherapy 4-hydroperoxy cyclophosphamide (4-HC), the active metabolite of cyclophosphamide, the most gonadotoxic agent used in breast cancer with a clearly defined mechanism of gonadotoxicity.

3.2 Ethical aspects and collection of ovarian cortical tissues

Approval for the use of human biological material was granted by the Ethical Committee of Regione Liguria on May 27th, 2020. Ovarian tissue was obtained from patients after written informed consent and collected according to standard clinical indications by laparoscopic surgery. In those who met the requirements for the present analysis and consented to donate part of the tissue for research purposes, the ovarian cortex was immediately rinsed in IVF-buffered medium (Cook Medical) and transported on ice to the IVF laboratory. The medullary compartment was removed using a sharp scalpel, and the cortex was cut into small, thin cubes that were placed in tubes containing slow-freezing medium (OVARSTORE, EOS Srl). After incubation at 4 °C for 45 minutes, the ovarian cortex fragments were transferred into 1.5 ml cryovials, four to five fragments per vial, frozen using a slow-cooling protocol in a programmable vertical freezer (Planer Kryo 360) and stored in liquid nitrogen. To date, ovarian tissue has been collected from one 31-year-old BRCA-negative woman who underwent ovarian surgery for a condition not associated with reduced ovarian reserve, as well as from eight healthy young *BRCA* mutation carriers who underwent bilateral risk-reducing salpingo-oophorectomy at an age of 45 years or younger, as reported in Table 1.

Women were considered eligible if they underwent risk reducing adnexectomy or ovarian surgery for benign conditions not associated with a reduction in ovarian reserve and if they were between 18 and 45 years of age. Exclusion criteria included postmenopausal status, active malignant disease, and prior treatment with gonadotoxic drugs.

European guidelines recommend risk reducing salpingo-oophorectomy (removal of ovaries and fallopian tubes) at the age of 35-40 years for BRCA1 mutation carriers and of 40-45 years for BRCA2 mutation carriers. Consequently, the ovarian tissues collected in this setting are more frequently obtained from women with a reduced baseline ovarian reserve due to their older reproductive age (>35 years), which may have an impact on the quality of the cortical samples available for research purposes.

Patient ID	Anatomy Pathology Unit ID	Age at surgery (years)	Parity	Ovarian stored fragments	Thawed and treated ovarian fragments	Type of mutation
1	I- 9337 2021/OSAP	39	1	R:2 L:6	R:2 L:6	*BRCA1*
2	I- 19597 -2021/OSAP	39	3	R:4 L:3	R:4	*BRCA2*
3	I- 22800-2021/OSAP	44	2	R:4 L:4	R:4	*BRCA1*
4	I-3104-2022/OSAP	43	2	R:3 L:4	R:4	*BRCA2*
5	I -5727-2022/OSAP	45	2	R:5 L:6	R:5	*BRCA2*
6	I-6437-2022/OSAP	42	2	R:4 L:4	R:4 L:4	*BRCA2*
7	I-10875-2022/OSAP	38	1	R:8 L: n/a	R:4	*BRCA1*
8	I-5810-2023/OSAP	41	1	R:5 L:8	R:5 L:4	*BRCA1*

Table 1. Clinical and biological characteristics of the 8 healthy BRCA 1/2 women. R= right ovary L= left ovary

3.3 Preliminary experiments

Before proceeding with the tests on the ovarian cortical tissue, preliminary experiments have been performed to optimize the doses of the drugs (Olaparib and Abemaciclib) and treatment times on two different cell models: human cumulus cells (CC) and non-mutated human/ *BRCA1* mutated breast cancer cell lines: MCF7 and MDA-MB-436 (Biobank, IRCCS Ospedale Policlinico San Martino, Genoa, Italy).

3.3.1 Human cumulus cells

CC are specialized granulosa cells that closely surround the oocyte, forming the cumulus–oocyte complex (COC). They play a crucial role in supporting oocyte growth, maturation, and competence acquisition through bidirectional communication mediated by gap junctions and paracrine signaling. The metabolic and molecular status of CC reflects, to a large extent, the microenvironment and quality of the corresponding oocyte, making them a valuable cellular model for studying ovarian physiology, follicular health, and the impact of pharmacological agents on female reproductive function. The CC were obtained from cumulus cell-oocyte complexes (COC) retrieved after assisted reproduction techniques by transvaginal oocyte aspiration 36 h after injection of human chorionic gonadotropin (54). All COC derived from women < 40 years old, with a normal ovarian reserve, without any ovarian pathology. A standard controlled ovarian stimulation protocol including gonadotropin administration in combination with GnRH antagonist was applied. Under SZX7 stereomicroscope (Olympus Corporation), oocytes were denuded by enzymatic treatment with 80 IU/mL hyaluronidase solution. After washing, CC were counted and placed in 96-well microplates containing Sydney IVF Fertilization medium (Cook Medical) at 37°C in a humidified atmosphere of 6% CO2, 5% O2 using Galaxy 48R incubator (New Brunswick Scientific). After 24 h of culture the CC were exposed to different concentrations of Abemaciclib (diluted in DMSO) and DMSO alone. Based on the literature (55,56) different Abemaciclib concentrations (10, 3.1, 0.178 μM) were tested at defined timepoints (24, 48 or 72h).

CCs were also treated with Olaparib, based on available literature data (38,57), at concentrations of 23, 10, and 2 μM (diluted in DMSO), i.e. a PARP inhibitor currently used in clinical practice for BRCA1 and BRCA2 carriers with early breast cancer at high risk of recurrence.

Cell viability was measured by incubating cells with 3-(4,5- Dimethylthiazol2-yl)-2,5-diphenyltetrazoliumbromide (MTT) for 4 h and the optical density (OD) of the Formazan product was measured at 555 nm.

3.3.2 Human breast cancer cells

Analogous experiments were conducted on MCF7 cell lines, which represent a good model of epithelial like breast cancer expressing estrogen and progesterone receptors but not HER2 (notably, the current clinical indication of Abemaciclib in early breast cancer is for patients affected by high-risk hormone receptor-positive/HER2-negative disease). The MCF7 cell line was cultured in Dulbecco's modified Eagle's medium (DMEM), High Glucose (Sigma Aldrich) supplemented with 10% heat-inactivated fetal bovine serum (FBS), 2 mM L-glutamine, 100 U/ml penicillin, 100 µg/ml streptomycin. Prior to drug exposure, growth curves were established up to 72 hours to optimize the number of cells to be seeded per well and ensure consistent confluency at the time of treatment. Toxicity tests were conducted in 96 well plate treating 6×10^4 cells per well for 24, 48 and 72 h with the three different Abemaciclib concentrations. Experiments were repeated three times. Based on viability test results, the chosen concentration for Abemaciclib was 10 µM.

To optimize doses and treatment times of Olaparib, MDA-MB-436, a BRCA1-mutated triple negative breast cancer cell line, was used. The MDA-MB-436 cells were grown in RPMI-1640 medium supplemented with 10% heat-inactivated fetal bovine serum (FBS), 2 mM L-glutamine, 100 U/ml penicillin, 100 µg/ml streptomycin at 37°C in a humidified atmosphere with 5% CO2, 95% air. Similarly to MCF7, growth curves up to 72 hours were first established to determine the optimal seeding density before drug treatments. Experiments were conducted using $4x10^4$ cells/well. Based on the literature, cells were exposed to different concentrations of Olaparib (23, 10, 2 µM diluted in DMSO) and DMSO alone.

After 24, 48 or 72 h, cell viability was measured by incubating cells with MTT for 4 h. Experiments were replicated 3 times. Based on viability test results, the chosen concentration for Olaparib was 23 µM.

3.4 Culture of ovarian cortical tissues

Due to lack of non-*BRCA* mutated tissues as previously described as shown in Table 1, experiments have been conducted only on *BRCA1/2* mutated tissues using Olaparib as case study for targeted therapy and its chemotherapy treatments, alone or in combination as explained in Fig.1 The *BRCA* mutated ovarian cortex fragments obtained from eligible patients were placed in cryovials (4-5 fragments/each), frozen by a slow-cooling protocol and stored in liquid nitrogen. A preliminary follicular count was carried out by Anatomy Pathology Unit of IRCCS San Martino Hospital on hematoxylin and eosin (H&E)-stained sections from the entire right and left ovary of each patient, with the aim of providing a baseline assessment of follicle number.

Thawing was conducted using a rapid protocol. Cryovials containing the ovarian tissue fragments were first brought to room temperature for two minutes and then transferred to 25 °C for an additional two minutes. The tissues were then washed for five minutes in a sequence of solutions with decreasing cryoprotectant concentrations (0.5, 1, 0.5, and 0 mol/l). After thawing, the fragments were placed in culture in four-well plates containing 500 µl of Leibovitz medium (Gibco, Life Technologies) supplemented with 2 mM sodium pyruvate (Sigma Aldrich), 2 mM glutamine (Sigma), 3 mg/ml human serum albumin (Vitrolife), 30 µg/ml penicillin G (Sigma), and 50 µg/ml streptomycin (Sigma).

After rapid thawing, the cryopreserved ovarian cortical tissues were not further sectioned, as is usually performed to standardize fragment dimensions (58); this procedure was avoided in order to prevent additional follicular loss, given the already low follicle density observed, as demonstrated by the follicle count carried out by the Anatomy Pathology Unit of San Martino Hospital.
The fragments were individually cultured for three days (D0, D1,D2); the culture was stopped on D3 and it was based on recent literature (59).

Ovarian fragments were randomly assigned to one of the four conditions: (a) control (culture medium) (b) Olaparib (AZD2281**;**Selleck Chemicals, Houston, TX, USA), 23 µm diluted in McCoy's 5A modified medium, (c)10 µg/ml carboplatin (C2538; Merck, Darmstadt, Germany) diluted in McCoy's 5A modified medium

(Thermofisher Scientific, Waltham, MA, USA), and 10 µg/ml paclitaxel (46868, Accord Healthcare, Italy) diluted in NaCl 0,9 %, (d) 10 µg/ml carboplatin and 10 µg/ml paclitaxel and Olaparib 23 µm . The culture medium consisted of McCoy's 5A modified medium, 0.1% v/v HSA, 3 mM L-glutamine, 30 µg/ml penicillin G, 50 µg/ml streptomycin G, 50 µg/ml ascorbic acid (Merck, Darmstadt, Germany), 2.5 µg/ml transferrin (10652202001, Merck, Darmstadt, Germany), and 4 ng/ml selenium (Merck, Darmstadt, Germany). The medium was prepared under sterile conditions, stored at 4°C, and considered stable for up to 7 days. Before use, it was equilibrated in the incubator for 2 hours to allow temperature and gas-phase calibration prior to tissue exposure. On day D1 of culture 10 mg/ml human insulin (I9278, Merck, Darmstadt, Germany) and hFSH (Bemfola 300 UI/0,50 ml, IRCCS San Martino Hospital) were added to the culture medium. Drugs (Olaparib, Carboplatin and Paclitaxel) were added into the medium since D0, each day of culture both the medium and the drugs were fully changed (1 ml/well). During the whole culture, fragments were incubated at 37°C, 5% CO_2, 6% O_2 to recreate the hypoxia environment of ovarian tissue in vivo. On D3 the ovarian cortical tissues fragments were collected and fixed in 4% w/v PFA (KLESSIDRA 30, Bio-Optica Milano Spa, Italy) for 22 h at 4°C and delivered to the Anatomy Pathology Unit of San Martino Hospital for the paraffin embedding process.

3.5 Histological analysis

After paraffin embedding process, tissues were cut at 5 µm thickness and arranged so that all treatment conditions were on the same slide (n=4 fragments /per slide).

To assess the number of ovarian follicles per slide and per condition, hematoxylin/eosin staining was performed on every 10th section. Follicle density and follicle classification as well as atresia assessment followed the procedures established at the Research Laboratory on Human Reproduction (Brussels, Belgium). Each follicle was categorized by developmental stage as follows: (a) primordial, an oocyte surrounded by a flattened layer of granulosa cells (GCs); (b) transitory, an oocyte enclosed by both flattened and cuboidal GCs; (c) primary, an oocyte encircled by a complete layer of cuboidal GCs; and (d) secondary, an oocyte surrounded by at least two layers of cuboidal GCs (60). Follicular health was evaluated by identifying atretic follicles, defined by (a) nuclear or granulosa cell alterations (karyolysis,

pyknosis, or karyorrhexis), (b) eosinophilic oocyte cytoplasm, or (c) disruption of overall follicular morphology (61).

In order to assess potential collagen deposition and thereby the extent of tissue fibrosis after treatments, basing on current literature (62,63), histological analysis was carried out using Masson's trichrome staining (04-010802, Bio-Optica Milano Spa, Italy). It stains nuclei and games in black, cytoplasm/keratin/muscles fibers/acidophil granules in red, collagen in blue and erythrocytes in yellow. The assessment of collagen deposition was limited to a qualitative, observer-based evaluation of Masson's trichrome–stained sections.

3.6 Immunohistochemistry and immunofluorescence analysis

To assess follicle activation, survival, apoptosis as well as vascular damage, proliferation and DNA repair mechanisms, immunostaining of several proteins was performed, as well as a DNA fragmentation assay. Prior to performing the staining procedures on BRCA patient samples, an immunostaining protocol was optimized for both immunohistochemistry (IHC) and immunofluorescence (IF), employing healthy and pathological ovarian tissue samples supplied by the Anatomy Pathology Unit of San Martino Hospital. After deparaffination using X-free (06-1305Q, Bio-Optica Milano Spa, Italy) for five minutes (x 3), B-Alcohol 100 for five minutes (06-10077Q, Bio-Optica Milano Spa, Italy) and B-Alcohol 70 (06-10075Q, Bio-Optica Milano Spa, Italy) for 5 minutes. After a brief rinse in running water, the slides were incubated in hydrogen peroxide to quench endogenous peroxidase activity in the blood vessels, which could otherwise generate background staining. Antigen retrieval was performed in a microwave, firstly at 800 W for 3 minutes and then at 300 W for 13 minutes, in a pH 6 Citrate buffer/ pH 9 Tris EDTA buffer depending on the antibody manufacturer instruction. After cooling, the slides were incubated with serum to block nonspecific binding sites. Normal goat serum (ab7481, Abcam Limited, Cambridge, UK), diluted to 15% in Phosphate buffered saline (PBS) w/o Calcium & Magnesium (ECB4004L, Euroclone S.p.A, Italy) was used for this purpose, and the slides were incubated for 30 minutes. Without rinsing, the slides were subsequently incubated with the primary antibody: for 1 h in the case of immunohistochemistry and for 2 h in the case of immunofluorescence, both at room

temperature in a humidified chamber. After PBS washing, secondary antibody incubation was carried out. For IHC, slides were treated with MACH 4 Universal HRP-Polymer (M4U534G, Bio-Optica Milano Spa, Italy) for 30 minutes, followed by Betazoid DAB Chromogen Kit (BDB2004H, Bio-Optica Milano Spa, Italy) for 2–3 minutes.

A hematoxylin (05-06002/L, Bio-Optica Milano Spa, Italy) counterstain was then applied for 5 minutes.

For IF, slides were incubated with the secondary antibody for 45 minutes at room temperature in a humidified chamber. Following three PBS washes (5 minutes each), Hoechst 33342 (62249, Thermofisher Scientific, Waltham, Massachusetts, USA) was used as a nuclear counterstain.

3.6.1 Antibody Validation

For optimal staining efficiency, each antibody was validated for IHC and IF. Validation was carried out on healthy and pathological ovarian tissue obtained from the Anatomy Pathology Unit of San Martino Hospital (Genoa), where different antibody concentrations were tested according to the manufacturer's datasheet.

ANTIBODY	CLONE	CAT. NUMBER	SUPPLIER	DILUITION	TARGET
Recombinant Anti-YAP1 antibody	[EP1674Y]	ab52771	Abcam	IHC 1:100 IF 1:100	FOLLICULAR ACTIVATION
Phospho-Akt (Ser473) (D9E) XP®		cs4060	Cell Signaling	IHC 1:100	
Mis Antibody B-11		SC166752	Santa Cruz Biotechnology	IHC 1:30	
Anti-Inhibin alpha antibody	[4A2F2]	ab47720	Abcam	IHC 1:200	
ZP3 Polyclonal Antibody		21279-1-AP	Thermofisher	IHC 1:100 IF 1:100	
GDF9 Polyclonal Antibody		bs-4720R	Thermofisher	IF 1:100	

Anti-FSH-R antibody		ab113421	Abcam	IHC 1:400	FOLLICULAR STRUCTURE
Connexin 43 Antibody - GAPJALFA1 3516		3516	Cell Signaling	IHC 1:200	
Anti-Vimentin antibody	[RV202]	ab8978	Abcam	IHC 1:400	
Anti-Cytokeratin 8 antibody	[M20]-Cytoskeleton	ab9023	Abcam	IHC 1:10	
Anti-SCF antibody		ab64677	Abcam	IHC 1:400	
Caspase 3 (Cleaved Asp175)		PA5114687	Invitrogen	IHC 1:200 IF 1:100	APOPTOSIS
Anti-Histone H2A.X antibody	[EPR22820-23]	ab229914	Abcam	IHC 1:200 IF 1:200	
Phospho-Histone H2AX (Ser139)		05-636	Cell signaling	IHC 1:240 IF: 1:200	
Anti-phospho histone H2AX		05636	Merk life science	IHC 1:100 IF 1:100	
Ki-67 (30-9) 5278384001-		5278384001	Roche Diagnostics-S.P.A Italia	IHC 2 ug/ml	PROLIFERATION
Recombinant Anti-YAP1 antibody	[EP1674Y]	ab52771	Abcam	IHC 1:100 IF:100	
Recombinant Anti-RPS6		ab101691	Abcam	IHC 1:100 IF 1:100	

Anti-CD34 antibody	[EP373Y]	Ab81289	Abcam	IHC 1:200 IF 1:100	
Anti-beta Actin antibody		ab8227	Abcam	IHC 1:250 IF 1:100	VASCULARIZATION
Anti-CD31 antibody	[EPR3094]	ab76533	Abcam	IHC 1:100 IF 1:250	
Anti-CD45 antibody		ab10558	Abcam	IHC 1:200	IMMUNOPHENOTYPE
Rabbit monoclonal to CD3	[SP162]	ab135372	Abcam	IHC 1:150	
Rabbit monoclonal to CD20	[SP32]	ab64088	Abcam	IHC 1:200	

Table 2. Summary of all antibodies validated and applied for IHC/IF to assess follicular activation, structure, apoptosis, vascular damage, and proliferation.

3.6.2 Evaluation of follicular apoptosis and activation

Following antibody validation, specific markers were selected to investigate both treatment-induced DNA damage and potential follicular activation. Two complementary immunofluorescence assays were employed to detect different stages of DNA damage–related apoptosis. Phosphorylated histone H2AX (γ-H2AX) was used as an early indicator of DNA double-strand breaks, as γ-H2AX rapidly accumulates at chromatin sites surrounding the lesion (64). In contrast, the TUNEL assay detects DNA fragmentation occurring at a later stage of apoptosis, thus providing information on cells undergoing irreversible damage (65). In both cases, co-staining with the oocyte-specific marker ZP3 was performed to ensure the localization of the signal within follicles.

To further characterize apoptotic commitment, cleaved Caspase-3 was analyzed by immunohistochemistry as a marker of execution-phase apoptosis.

In parallel, Yes-associated protein 1 (YAP1) was investigated as an exploratory marker of stress-induced follicular activation (66). YAP1 is a central effector of the Hippo signaling pathway, a conserved mechanotransduction cascade that regulates cell proliferation, survival, and organ size in response to physical and biochemical cues. Under physiological conditions, activation of the Hippo core kinase cassette (MST1/2–LATS1/2) results in the phosphorylation of YAP1, which is thereby retained in the cytoplasm and targeted for degradation, maintaining follicles in a quiescent state(66).

Conversely, mechanical stimuli such as extracellular matrix stiffening or cytoskeletal rearrangements can disrupt Hippo pathway activity. Increased actin polymerization from globular (G-) to filamentous (F-) actin generates cytoskeletal tension that inhibits LATS1/2-mediated phosphorylation of YAP1. Consequently, dephosphorylated YAP1 translocate into the nucleus, where it associates with TEAD transcription factors and drives the expression of genes involved in cell growth and metabolic activation. In the ovarian context, this mechanosensitive switch has been implicated in primordial follicle awakening following tissue fragmentation or culture-induced stress (67). Therefore, nuclear localization of YAP1 was assessed as a readout of potential activation of dormant follicles in response to experimental manipulation.

3.7 Immunological analysis

For three of the eight treated patients, the culture medium of each condition was collected at 24, 48, and 72 hours to evaluate potential fluctuations in pro- and anti-inflammatory cytokine levels in non-physiological conditions related to the ovary, as suggested by current literature (68–71) using Milliplex Human Cytokine/Chemokine/Growth Factor Panel A Magnetic bead Panel- Immunology Multiplex assay (HCYTA-60K, Merck, Darmstadt, Germany). In one of these three patients, further collections were performed at 1, 2, 3, and 6 hours (D0) for each condition. The analytes choice was based on current literature (69,70).

The panel of analyzed cytokines was composed of VEGF-A, TNF- α, IL-4, MIP-1-α, IFN- α-2, IL-8, MCP-1, IP-10, IL-6, IL-2,IL 1-B, IL-17A, IL-10, IFN- γ based on current literature (71–73). To validate the results obtained from cytokine analysis in the culture medium, immunohistochemical staining for CD45, a leukocyte marker, was also performed to confirm the presence of lymphocytic/inflammatory cells, which were presumed to be responsible for the production of the detected cytokines (71,73).

3.7.1 Experimental Procedure

The samples were thawed at 4 °C in a refrigerator and subsequently centrifuged. Before beginning the experimental procedure, all reagents supplied with the kit were brought to room temperature (20–25°C), and the required laboratory equipment, including two 96-well plates, multichannel pipettes, sterile tips, reservoirs, and waste containers, was prepared. The assay began with the preparation of the Wash Buffer. The 10X concentrate was equilibrated to room temperature, mixed thoroughly to ensure complete dissolution of salts, and diluted to 1X in three 50 mL Falcon tubes, each containing 5 mL of concentrate and 45 mL of deionized water. The unused portion was stored at 2–8°C for up to one month. The plate was pre-wetted by dispensing 200 µL of Wash Buffer into each well, sealing it with adhesive film, and placing it on a shaker for ten minutes.

During this time, quality controls (QC) were prepared. QC1 and QC2 were dissolved in 250 µL of deionized water, gently inverted, briefly vortexed, and allowed to rest for 5–10 minutes in the kit box. Any unused aliquots were stored at −20°C. The assay standards were similarly prepared by reconstituting the provided vial with 250 µL of deionized water, mixing thoroughly, and allowing it to stabilize before conducting a series of six serial dilutions in 200 µL of Assay Buffer, following the dilution scheme indicated by the manufacturer. After reconstitution, the standard was referred to as Standard 7, according to the internal protocol. The unused portion was stored at −20 °C.

Subsequently, the Mixing Bottle containing the antibody-coated magnetic beads was prepared. Each antibody vial was vortexed for two minutes, three at a time, and 60 µL of each antibody were transferred into the Mixing Bottle. The volume was then

adjusted to 3 mL with Bead Diluent and thoroughly vortexed to ensure homogeneity. This mix could be stored at 2–8°C for up to one month. Once the pre-wetting step was completed, the plate was emptied by inversion and gently blotted on absorbent paper. The assay solutions were then dispensed into the designated wells. Standards were loaded by adding 25 µL of the appropriate standard dilution, 25 µL of D1 medium, and 25 µL of the bead mixture into each well. The same scheme was applied to the quality controls, using QC1 or QC2 instead of the standard. Background wells received 25 µL of Assay Buffer, 25 µL of D1 medium, and 25 µL of Mixing Bottle. For the sample wells, 25 µL of Assay Buffer, 25 µL of vortexed sample, and 25 µL of Mixing Bottle were added. Throughout this step, the Mixing Bottle was vortexed frequently and kept in motion to prevent bead sedimentation during dispensing.

After loading all wells, the plate was sealed, wrapped in aluminum foil to protect the beads from light, and incubated with continuous shaking for 16–18 hours at 2–8°C, or alternatively for two hours at room temperature. On the following day, the adhesive seal was removed, and the plate was placed on a magnetic separator for two minutes to immobilize the beads. The liquid was discarded, and three wash cycles were performed by adding 200 µL of Wash Buffer, shaking for two minutes, returning the plate to the magnet for two minutes, and discarding the liquid. Any bubbles were removed with a pipette tip to ensure accurate subsequent readings.

Following the washing steps, 25 µL of Detection Antibodies were added to each well. The plate was sealed, protected from light, and incubated for one hour at room temperature on a shaker. Without removing the contents, 25 µL of Streptavidin-Phycoerythrin were then added to each well under light-protected conditions. The plate was resealed, wrapped in foil, and incubated for an additional thirty minutes with shaking. After incubation, the plate was magnetized again and washed three more times using the same procedure as before, ensuring light protection throughout.

To prepare the plate for acquisition on the Luminex® instrument, 150 µL of Sheath Fluid Plus were added to each well. The plate was kept protected from light and shaken for ten minutes to fully resuspend the beads. Finally, the plate was transferred to the acquisition system for data collection and subsequent analysis of cytokine, chemokine, and growth factor concentrations.

3.8 Research Internship at the Université libre de Bruxelles

As part of my fellowship at the Research Laboratory on Human Reproduction, Université libre de Bruxelles (ULB), Brussels, Belgium from November the 4th 2024 to May 1st, 2025, I conducted in vitro experiments on healthy human ovarian cortical tissue obtained from breast cancer patients not previously exposed to chemotherapy, with the aim of evaluating the gonadotoxic effects of targeted therapy (PARP inhibitor-Olaparib) in combination with chemotherapy (4HC-cyclophosphamide), by comparing samples with and without *BRCA* mutations. This work represents part of a broad experimental project conducted by this laboratory, which focuses on investigating the potential gonadotoxicity of the targeted therapy Olaparib.

3.8.1 Preliminary experiments

Before proceeding with the experiments on ovarian cortical tissues, it was necessary to establish the optimal dose of Olaparib to be evaluated. Based on current literature (38) and on experiments previously performed on *BRCA1*-mutated MDA-MB-436 cells in Genoa, three concentrations of Olaparib (20, 35, and 50 μM, diluted in DMSO) were evaluated. The concentration of 4HC had previously been established by the laboratory group at 10 μM. Experiments were performed on three healthy patients' ovarian tissues that were not exposed to chemotherapy prior to ovarian tissue cryopreservation (OTC), characteristics are shown in Table 3.

Patient ID	Age prior OTC	Diagnosis
2018-02	5	Ependyomoma
2010-38	25	Lupus
2015-13	23	Lymophoma

Table 3. Baseline characteristics of patients undergoing ovarian tissue cryopreservation prior to chemotherapy exposure.

The tissues were thawed on ice in decreasing concentrations of DMSO solutions (1.5 M, 1 M, 0.5 M, 0 M) (Merck, Darmstadt, Germany) in Leibovitz L-15 medium (Thermofisher Scientific, Waltham, MA, USA) supplemented with 0.1 M sucrose, as previously described (74,75). Tissues were then cut into 4×2×1 mm^3 fragments in dissection medium consisting of Leibovitz L-15 medium, 2 mM sodium pyruvate (Merck, Darmstadt, Germany), 0.3% human serum albumin (HSA) (CAF DCF, Belgium), 2 mM L-glutamine (Merck, Darmstadt, Germany), 30 µg/ml penicillin G (Merck, Darmstadt, Germany), and 50 µg/ml streptomycin G (Merck, Darmstadt, Germany).

Regarding the assessment of Olaparib concentration, ovarian fragments (n = 4/condition/population) were randomly assigned to one of the four conditions: (a)control with DMSO 0.1%, (b) Olaparib (AZD2281**;** Selleck Chemicals, Houston, TX, USA) 20 µM, (c) Olaparib 35 µM and (d) Olaparib 50 µM diluted in culture medium. The culture media consisted of McCoy's 5A modified medium, 0.1% v/v HSA, 3 mM L-glutamine, 30 µg/ml penicillin G, 50 µg/ml streptomycin G, 50 µg/ml ascorbic acid (Merck, Darmstadt, Germany), 2.5 µg/ml transferrin (Roche Diagnostics, Diegem, Belgium), and 4 ng/ml selenium (Merck, Darmstadt, Germany). During the whole culture, fragments were incubated at 37°C. Olaparib in different concentrations was added after 24 h of culture and the culture media was supplemented with 1 ng/ml hFSH (Gonal-F, Belgium) and 10 ng/ml insulin (Merck, Darmstadt, Germany) for the remaining 48 h. After 3 days of *in vitro* culture, the fragments were collected and fixed in 4% w/v PFA for 24 h at 4°C before paraffin embedding. After paraffin embedding, all the fragments were serially sectioned (every five sections) at 5 µm thickness. To evaluate follicular health and classification to determine the appropriate drug dosage, hematoxylin–eosin staining was performed every five sections.

3.8.2 Evaluation of treatment toxicity of Olaparib

After establishing the optimal dosage of Olaparib, I proceeded with the experiments in combination with chemotherapy, 4HC 10 µM. The ovarian tissues used was from four *BRCA1*-mutated and four non-mutated healthy women. The mean age of the patients was 29.8 ± 0.5 years in the BRCA1 group and 31.3 ± 2.6 years in the non-BRCA group, respectively as shown in Table 4.

BRCA 1 mutated patients ID	Age	Non-*BRCA* mutated patients ID	Age
2007-06	29	2007-02	29
2006-14	30	2008-03	34
2007-12	30	2009-33	29
2009-25	30	2012-05	33

Table 4. Characteristics of *BRCA1* and non-*BRCA* mutated patients used in the experiments.

The tissues were processed as previously described for the experiments conducted to optimize concentration. Following thawing, they were randomly assigned (n = 4) to four culture conditions: control with 0.1% DMSO, 20 µM Olaparib (AZD2281; Selleck Chemicals, Houston, TX, USA) diluted in culture medium, 10 µM 4HC, and 20 µM Olaparib together with 10 µM 4HC (SML4103, Merck, Darmstadt, Germany). The culture period lasted three days (D0, D1, and D2).

To reproduce in vivo treatment conditions, only 4HC was administered on D0. On D1, during the complete medium change, Olaparib was administered, and the chemotherapeutic agent was no longer supplied; the same procedure was followed on D2. The culture was terminated on D3. The culture medium was prepared exactly as described in section 3.8.1, and insulin and hFSH were therefore added on D1, after 24 hours. In the control group, DMSO was added in the same way and at the same final concentrations used for the drug dilutions, corresponding on D0 to the concentration used for 4HC (since it was administered only on that day) and on D1 and D2 to the concentration used for Olaparib.

3.8.3 Histological Analysis

As previously reported, following paraffin embedding all tissue fragments were serially sectioned at a thickness of 5 µm, collecting one section every five. To evaluate follicle density, activation, and survival, the first slide of each series was stained with hematoxylin–eosin. In brief, after deparaffinization in toluene and a graded ethanol series, the slides were stained with hematoxylin (Vector Laboratories, Oxford, UK) and subsequently counterstained with eosin prior to mounting.

Follicle classification and atresia assessment were conducted as previously described in Chapter 3.6, following the criteria adopted and taught at the hosting laboratory where the experiments were performed.

To avoid double counting, only follicles with a visible oocyte nucleus were considered. The surface of each section was then measured to calculate follicle density (total number of follicles per mm^2). These analyses were performed after returning from the hosting laboratory, using the FIJI image analysis software on slide scans acquired with the NanoZoomer scanner.

The proportions of quiescent and atretic follicles were calculated as the ratio of primordial follicles to the total follicle count (percentage of quiescent follicles) and the ratio of unhealthy follicles to the total follicle count (percentage of atretic follicles), respectively.

3.8.4 Assessment of follicle density

Follicle density was quantified by normalizing the total number of follicles to the analyzed tissue area. For each experimental condition and for each patient, all hematoxylin–eosin (HE) stained sections were acquired and individually measured to determine their surface area (mm^2). The areas of all sections belonging to the same condition were then summed to obtain the total analyzed tissue area.

The total number of follicles counted across these sections was subsequently divided by the corresponding cumulative area, yielding a density value expressed as number of follicles per mm^2.
This approach allowed an accurate estimation of follicle density based on the real surface of the analyzed tissue, rather than relying on approximate assumptions about fragment size thus ensuring improved precision and comparability across samples.
For logistical reasons, digital scans of the HE-stained slides for each patient and experimental condition were provided instead of the physical sections. Each section present on the scanned slides was individually measured using the FIJI image analysis software to determine its surface area (mm^2). The areas of all sections belonging to the same condition were then summed to obtain the total analyzed tissue area. Follicle density was finally calculated by dividing the total number of follicles identified in the HE-stained scans by the corresponding cumulative area and expressed as number of follicles per mm^2.
This method allowed an accurate quantification based on the real tissue surface rather than on theoretical fragment dimensions, ensuring greater precision and consistency across samples.

3.8.5 Immunofluorescence analysis

Immunofluorescence experiments were carried out at the San Martino Hospital laboratory in Genoa, upon receipt of the slides from the laboratory in Belgium. All staining procedures were performed according to the protocol previously described in Chapter 3.2.

To assess DNA damage and repair, two complementary approaches were employed. DNA fragmentation was evaluated using Terminal deoxynucleotidyl transferase dUTP Nick-End Labelling (TUNEL), following the manufacturer's protocol (In Situ Cell Death Detection Kit, Roche Diagnostics, Roche Diagnostics- S.P.A Italia). In parallel, activation of DNA repair pathways was investigated through immunostaining for phosphorylated HISTONE 2X family protein (γH2AX; 05-636, Merck, Darmstadt, Germany). To enable follicle visualization, co-staining with ZONA PELLUCIDA 3 protein (ZP3; 21279-1-AP, Proteintech, Manchester, UK) was

performed. Quantification was conducted by calculating the percentage of follicles positively stained for TUNEL and γH2AX over the total number of follicles counted.

3.8.6 Validation of Apoptosis Markers: p63 and Cleaved Parp

To further validate the detection of apoptosis in ovarian tissue and to complement the results obtained with γH2AX and Cleaved Caspase-3, two additional markers, p63 and Cleaved PARP, were tested. p63, a member of the p53 family, is highly expressed in oocytes and serves as a key regulator of DNA damage–induced apoptosis in primordial follicles. Its activation has been described following exposure to genotoxic agents and is therefore relevant for assessing ovarian response to treatments affecting DNA integrity (74). Cleaved PARP, a downstream substrate of Caspase-3, represents a late apoptotic marker associated with the execution phase of programmed cell death (77,78). Given that Olaparib acts as a PARP inhibitor targeting the same DNA repair pathway, the evaluation of Cleaved PARP provides additional insight into the apoptotic mechanisms and potential effects of PARP inhibition on ovarian cells.

For this validation, ovarian cortical tissue slices previously exposed for 24 hours to 20 µM 4-hydroperoxycyclophosphamide (4HC), a known inducer of apoptosis, were used. Several antibody concentrations were tested according to the manufacturer's recommendations; however, the optimal working dilution has not yet been fully established.

4. Results

4.1 Preliminary results

To determine the drug concentrations to be used in the subsequent experiments, cell viability was first assessed following exposure to Olaparib and Abemaciclib. In the case of Olaparib, MDA-MB-436 cells, which harbour a *BRCA* mutation, were treated with different concentrations of the drug and viability was evaluated at 24, 48 and 72 hours. Compared with the DMSO control, a progressive reduction in cell viability was observed from the earliest point, particularly at 23 µM and 10 µM, with the effect becoming more pronounced over time (as shown in Fig.5A). The 2 µM concentration produced only a modest and less consistent decrease. Based on the overall trend and reproducibility across time points, 23 µM was selected as the working concentration for the subsequent assays.

For Abemaciclib, the assessment was performed on MCF-7 cells, which are BRCA wild-type. Multiple concentrations (10 µM, 3 µM, 1 µM and 0.178 µM) were tested and viability was measured at the same time intervals. Although the reduction in cell viability was less marked than that observed with Olaparib, the concentration of 10 µM consistently produced the most evident and stable decrease over time compared with the control as shown in Fig. 5B. On this basis, 10 µM was chosen as the reference concentration for the following experimental phases.

To further explore the potential ovarian impact of the selected drugs, viability assays were also performed on human cumulus cells (CC). These cells represent a simplified ex vivo ovarian model and allow preliminary evaluation of the direct effects of pharmacological exposure on somatic follicular components. The same concentrations used in tumor cell lines were tested, and cell viability was assessed at 24, 48 and 72 hours. In cumulus cells, no appreciable reduction in viability was detected at any concentration or time point following Olaparib exposure as shown in Fig. 5C, whereas for Abemaciclib a light decrease in viability was observed at the

highest concentration (10 µM), while lower doses showed minimal variation over time as shown in Fig. 5D.

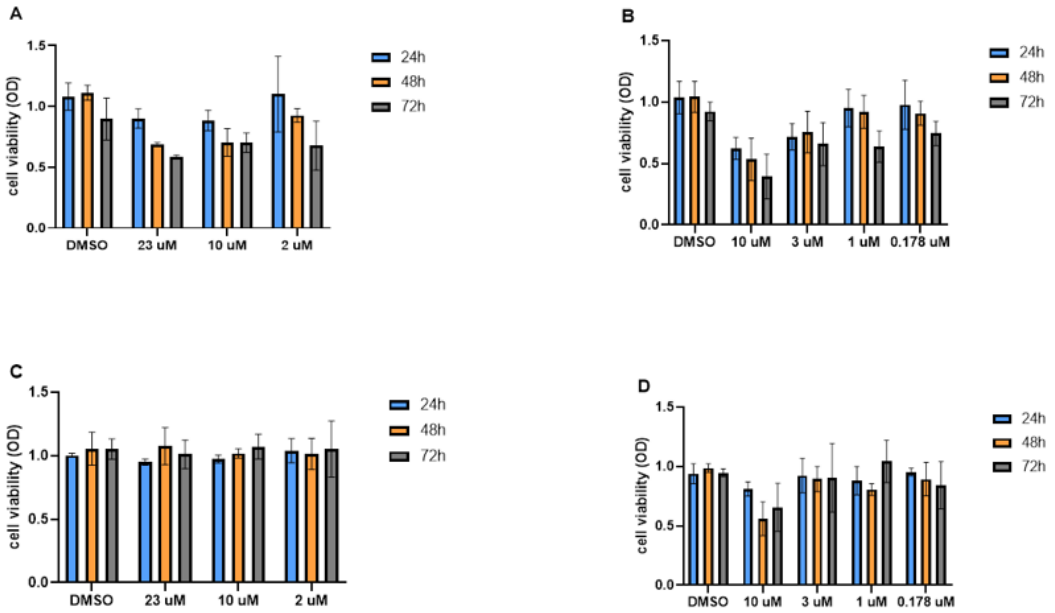

Fig. 5. Dose-response experiments with Olaparib (DMSO control 23 µM, 10 µM, 2 µM) and Abemaciclib (DMSO control, 10 µM, 3 µM, 1 µM, 0.178 µM) in breast cancer and cumulus cells. (A) BRCA-mutated breast cancer cells (MDA-MB-436) treated with Olaparib. (B) Non-mutated breast cancer cells (MCF-7) treated with Abemaciclib. (C) Cumulus cells treated with Olaparib. (D) Cumulus cells treated with Abemaciclib. Cell viability was evaluated at 24 h (blue), 48 h (orange), and 72 h (grey). Data represent mean optical density (OD) ± SD from n = 3/4 replicates per condition.

4.2 Analytical approach in relation to sample limitations

Due to the limited availability of follicles in the collected ovarian cortical tissues, as previously discussed, analyses could only be performed on four of the eight patients whose samples were thawed and treated. Even within these four cases, the follicle yield per condition was low, remaining below the commonly accepted threshold of approximately 25 follicles per treatment group, as reported in previous histological studies (58). For this reason, the analyses were conducted on a follicle-based rather than patient-based approach, pooling all follicles across the four experimental conditions (CTRL, OLA, CB+PTX, and OLA+CB+PTX). In addition, tissues allocated to the same condition showed marked inter-sample heterogeneity, both in terms of fragment size and follicle density, which further limited the possibility of standardizing the evaluation.

4.3 Statistical Analysis

Categorical data on follicle counts across treatment groups were analyzed using the Chi-square test of independence. When more than 25% of the expected cell frequencies were below 5, Fisher's exact test was applied as a more reliable alternative.

To compare the proportion of marked versus unmarked follicles per sample (Rate), non-parametric comparisons were performed using the Kruskal–Walli's test, followed by Wilcoxon rank-sum scores for ranked data.

All analyses were conducted using SAS software, version 9.4 (SAS Institute Inc., Cary, NC, USA), and statistical significance was defined as $p < 0.05$.

4.4 Histological analysis

4.4.1 Morphological Assessment of Follicular Stages

To evaluate whether the treatments influenced follicular development, the proportions of primordial, transitional, primary, and secondary follicles were assessed in ovarian cortical fragments exposed to control (CTRL), Olaparib (OLA), carboplatin plus paclitaxel (CB+PTX), and the combined treatment (OLA+CB+PTX).

The control group showed the highest median proportion of primordial follicles, while the OLA group displayed the lowest values. The CB+PTX and OLA+CB+PTX conditions were characterized by wider variability, with some samples reaching values similar to or above the control (Fig. 6A). However, the Kruskal-Walli's test did not reveal statistically significant differences among treatment groups (χ^2 = 1.5616, df = 3, p = 0.6681). Transitional follicles represented the most abundant category in all groups. Median values were slightly higher in the OLA group, whereas the CB+PTX condition showed the greatest inter-sample variability (Fig 6B). Nevertheless, no statistically significant differences were detected (χ^2 = 3.0221, df = 3, p = 0.3882). Primary follicles were observed at comparable proportions across treatments. The CB+PTX condition showed a modest increase in median values relative to the other groups, although variability remained substantial (Fig 6C), and the Kruskal-Walli's analysis confirmed the absence of significant differences (χ^2 = 1.6544, df = 3, p = 0.6471). Secondary follicles were the least represented stage across all conditions. Slightly higher variability was observed in the OLA group, whereas CTRL, CB+PTX and OLA+CB+PTX showed narrow distributions and lower medians (Fig. 6D). Statistical testing showed no significant differences among treatments (χ^2 = 1.1137, df = 3, p = 0.7738).

A quantitative evaluation of follicular density revealed a clear reduction in the number of morphologically preserved follicles following exposure to the different treatments compared with control tissues (CTRL). As shown in the box plot, Olaparib alone (OLA) induced a mild decrease in follicle count relative to controls, whereas chemotherapy (CB+PTX) caused a more pronounced reduction. Notably, the

combined treatment (OLA+CB+PTX) showed the lowest median follicle count among all experimental conditions (Fig.6E).

Overall, none of the treatments induced statistically significant changes in the proportional distribution of follicle stages. The heterogeneity of the tissue samples and the low number of follicles per condition likely contributed to the observed variability. The boxplots visually represent these distributions, with individual values (patients) shown as circles. Percentages were calculated on pooled follicles across the four available patients due to the low follicle yield per sample.

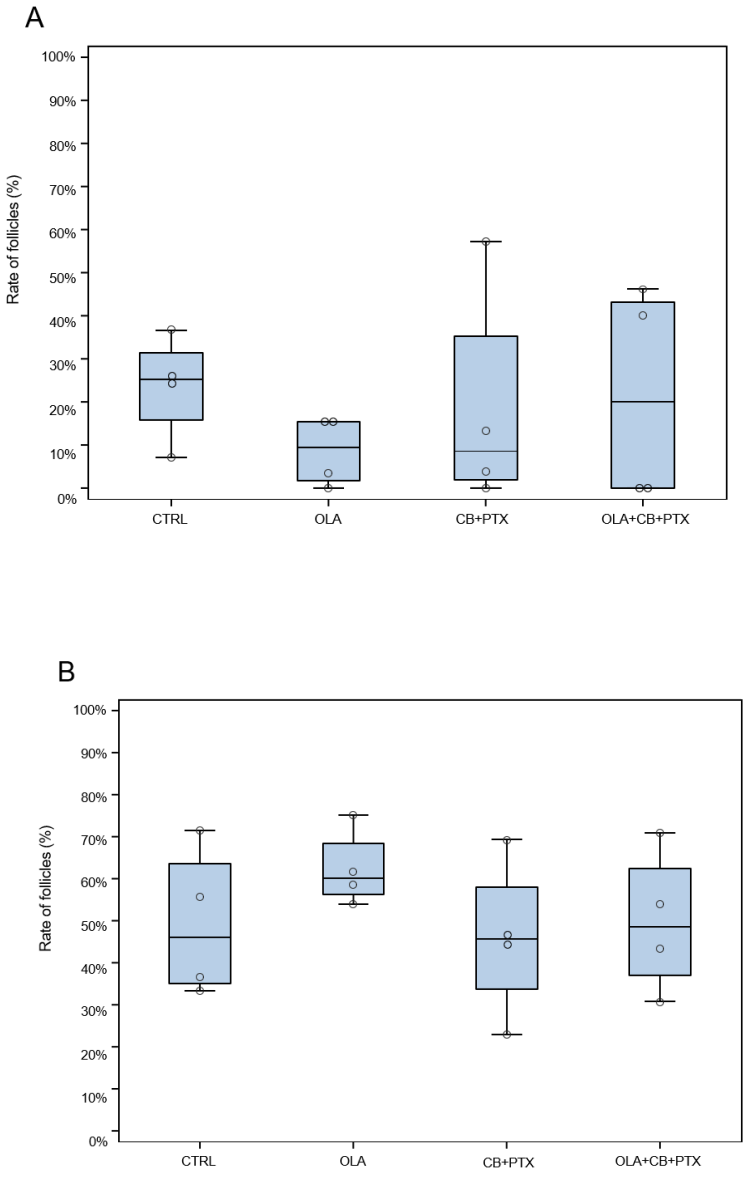

C

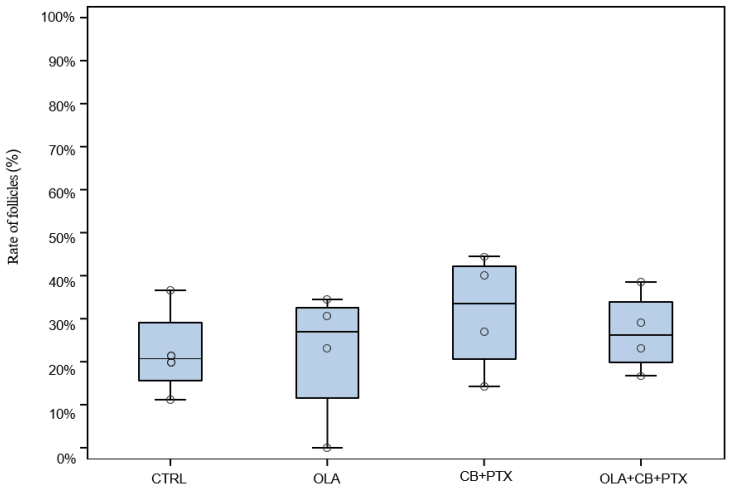
Rate of follicles (%)
100%
90%
80%
70%
60%
50%
40%
30%
20%
10%
0%
CTRL
OLA
CB+PTX
OLA+CB+PTX

D

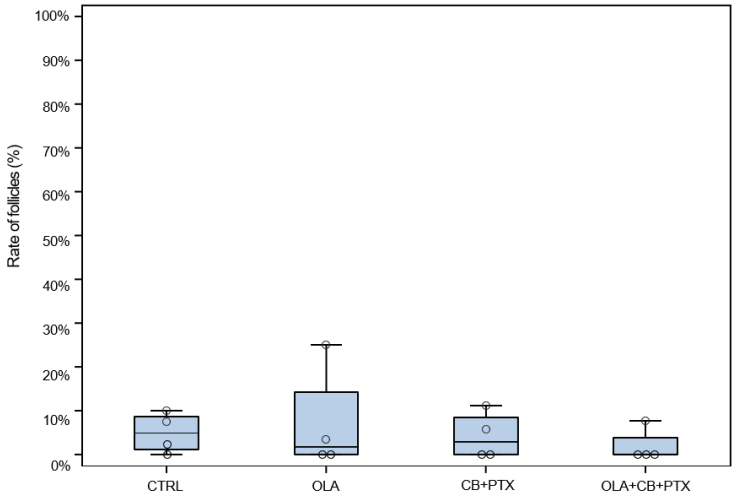
Rate of follicles (%)
100%
90%
80%
70%
60%
50%
40%
30%
20%
10%
0%
CTRL
OLA
CB+PTX
OLA+CB+PTX

E

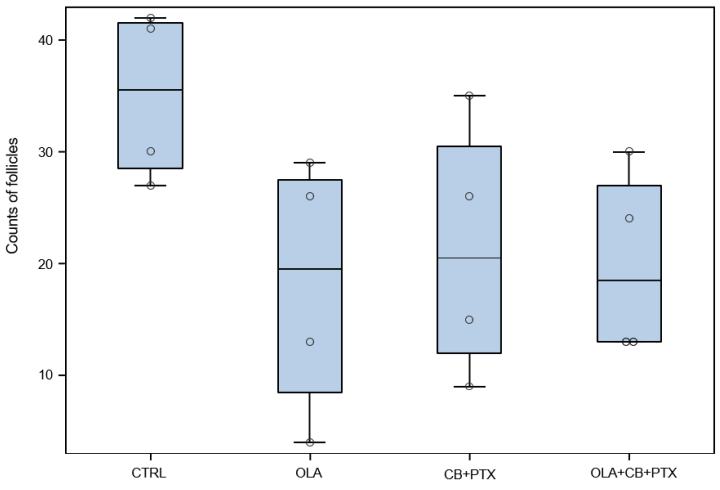
Counts of follicles
40
30
20
10
CTRL
OLA
CB+PTX
OLA+CB+PTX

Fig. 6 Follicle stage distribution and total follicles count.

(A) Primordial follicles. (B) Transitional follicles. (C) Primary follicles. (D) Secondary follicles. (E) Total number of follicles counted per condition. Boxplots display the distribution of follicle proportions (A–D) or absolute follicle counts (E) in ovarian cortical fragments exposed to CTRL, Olaparib (OLA), carboplatin plus paclitaxel (CB+PTX), or the combined treatment (OLA+CB+PTX). Circles indicate patient-level values within each group; Statistical analysis were conducted using a pooled follicle-based approach. No statistically significant differences were detected among treatment groups for any follicle stage (Kruskal–Walli's test, $p > 0.05$).

4.4.2 Assessment of follicle atresia

Follicles were classified as healthy or atretic to evaluate treatment-related differences in follicular integrity (Fig. 7). When all follicles were pooled, the stacked bar plot (Fig. 7A) showed that atretic follicles represented the majority in all treatment groups, with CTRL and OLA exhibiting slightly higher proportions of healthy follicles compared with CB+PTX and OLA+CB+PTX. At the individual level, variability across patients was observed in both healthy (Fig. 7B) and atretic follicles (Fig. 7C). Statistical analysis revealed a significant association between treatment and follicle health status when considering pooled counts (Chi-squared test, $p = 0.0054$). However, no significant differences were detected at the patient level using Kruskal–Walli's test for either healthy ($p = 0.0821$) or atretic follicles ($p = 0.0821$).

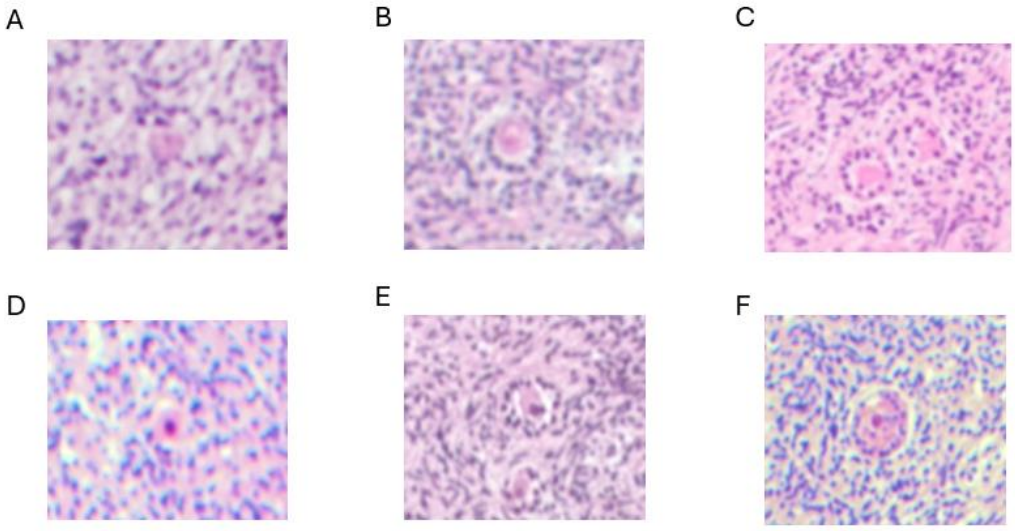

Fig. 7 Representative histological features of healthy and atretic ovarian follicles.
Hematoxylin and eosin staining illustrates the morphological criteria used to distinguish intact from degenerating follicles. Figures A–C show healthy examples of primordial (A), transitional (B) and primary follicles (C), all characterized by well-preserved oocyte morphology and orderly granulosa cell arrangement, with nuclei displaying uniform chromatin. In contrast, Figures D–F depict atretic counterparts of the same follicular stages: the primordial follicle in Figure D exhibits oocyte pyknosis with hyperchromatic nuclear condensation, while Figure E shows a transitional follicle with disorganized granulosa cells and nuclear degeneration. The primary follicle in Figure F presents evident oocyte cytoplasmic shrinkage and nuclear fragmentation, consistent with advanced atresia. Images were acquired at 10× magnification using a Nikon Eclipse E-800 microscope equipped with NIS-Elements imaging software.

A

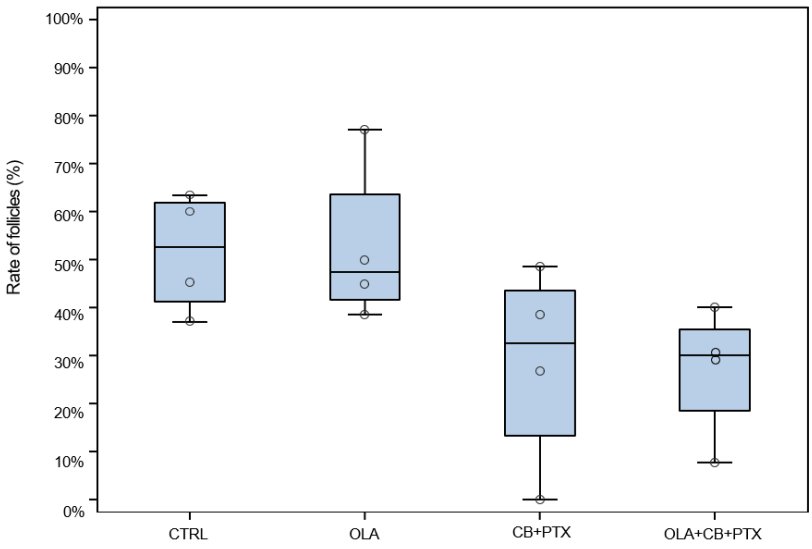
Rate of follicles (%)
100%
90%
80%
70%
60%
50%
40%
30%
20%
10%
0%
CTRL
OLA
CB+PTX
OLA+CB+PTX

B

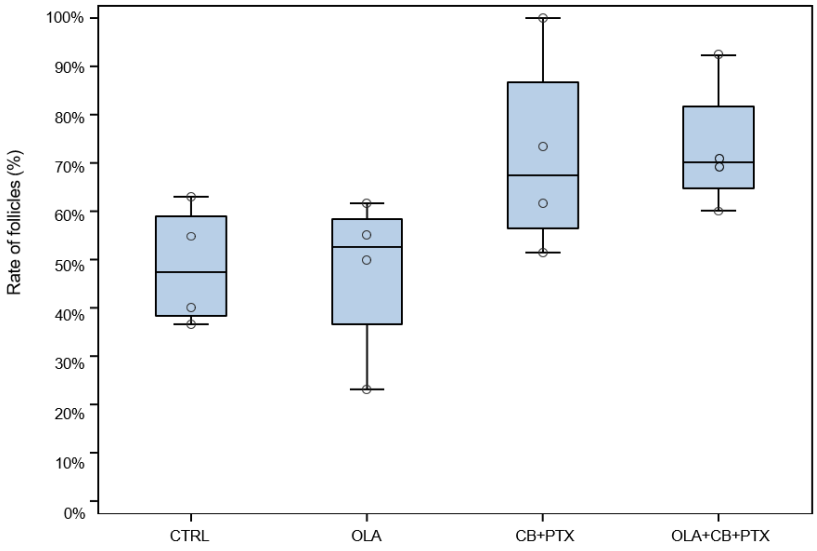
Rate of follicles (%)
100%
90%
80%
70%
60%
50%
40%
30%
20%
10%
0%
CTRL
OLA
CB+PTX
OLA+CB+PTX

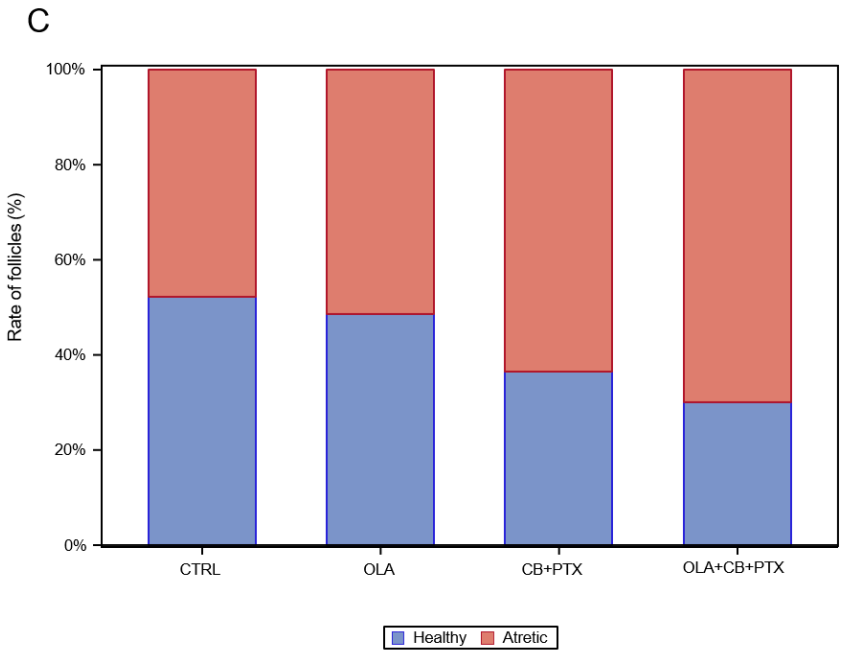

Fig. 8 Assessment of follicle health status across treatment conditions. (A) Boxplot of healthy follicle proportions by treatment. (B) Boxplot of atretic follicle proportions by treatment. (C) Stacked bar plot showing the overall proportion of healthy and atretic follicles pooled across all patients for each treatment group (CTRL, Olaparib; OLA, carboplatin plus paclitaxel CB+PTX, and the combined treatment OLA+CB+PTX). Circles in panels B and C represent individual patient-level values, while panel A displays aggregated data across all follicles. When considering pooled counts, a significant association between treatment and follicle health status was observed (Chi-squared test, $p = 0.0054$). However, no significant differences were detected at the patient level using Kruskal–Walli's analysis for either healthy ($p = 0.0821$) or atretic follicle proportions ($p = 0.0821$).

4.4.3 Assessment of collagen deposition

Masson's trichrome staining was performed to qualitatively assess potential alterations in stromal architecture and extracellular matrix composition following treatment exposure. Representative sections are shown in Figure 8 (A = CTRL, B = OLA, C = CB+PTX, D = OLA+CB+PTX), acquired at 10× magnification using a Nikon Eclipse E-800 microscope and NIS-Elements Basic Research software. Overall, no marked differences were observed in collagen distribution or general stromal organization across the groups.

However, the combined treatment condition (D) exhibited slightly more intense blue staining within the cortical stroma compared with the control and single-agent treatments. As no quantitative image analysis was performed, these observations remain descriptive and should be interpreted cautiously.

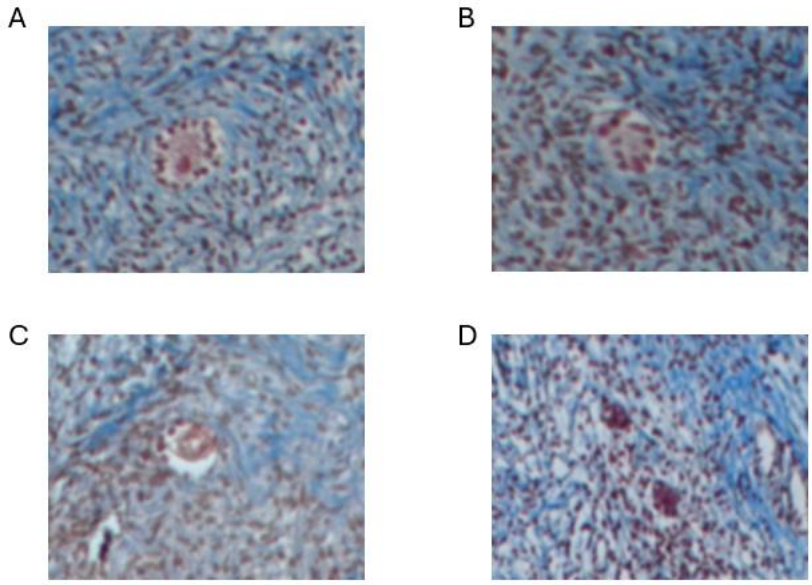

Fig. 9 Masson's trichrome staining of ovarian cortical tissue following 3 days in vitro culture exposure to different treatment conditions. (A) Control (CTRL), (B) Olaparib (OLA), (C) Carboplatin + Paclitaxel (CB+PTX), (D) Olaparib + Carboplatin/Paclitaxel (OLA+CB+PTX). Sections were acquired at 10× magnification using a Nikon Eclipse E-800 microscope and NIS-Elements Basic Research software. Collagen fibers appear in blue, while cellular components are counterstained in red. No marked alterations in stromal morphology or extracellular matrix distribution were detected across conditions; however, the combined OLA+CB+PTX treatment (D) showed slightly increased collagen staining within the cortical stroma compared with control and single-agent treatments.

4.5 Immunostaining results

4.5.1 TUNEL Assay

TUNEL staining was employed to assess apoptotic incidence within granulosa cells (GC) and oocyte (O) across the four experimental conditions (CTRL, OLA, CB+PTX, OLA+CB+PTX). ZP3 co-labelling was utilized only to facilitate follicular structure identification and was not considered analytically.

In Fig. 10A, the proportion of TUNEL-positive GC demonstrated substantial inter-individual variability, with no evident treatment-dependent pattern. No statistically significant differences were detected by Kruskal–Walli's testing ($\chi^2 = 4.253$, df = 3, $p = 0.235$). Likewise, Fig. 10B, representing TUNEL-positive oocyte nuclei, showed no detectable treatment effect (Kruskal–Wallis $\chi^2 = 1.8129$, df = 3, $p = 0.612$).

Fig. 10C reports the percentage of non-marked follicles, corresponding to structures without detectable apoptotic signal. No statistically significant differences were observed (Kruskal–Wallis $\chi^2 = 3.8316$, df = 3, $p = 0.280$).

A cumulative comparison of all follicular outcomes (GC-positive, O-positive, and non-marked follicles) is shown in Fig. 10D. Chi-square testing indicated a tendency towards differential distribution across treatments ($\chi^2 = 13.8935$, df = 6, $p = 0.0308$); however, this effect did not withstand Fisher's exact test (two-sided $p = 0.0605$), suggesting that the apparent shift may be influenced by the reduced number of follicular units contributing to each group, rather than reflecting a robust treatment-dependent mechanism.

A

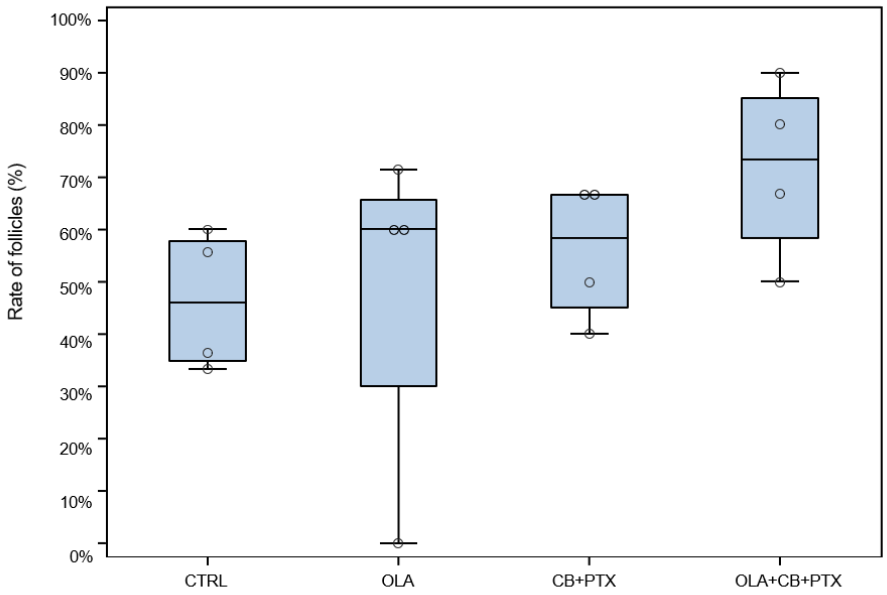
Rate of follicles (%)
100%
90%
80%
70%
60%
50%
40%
30%
20%
10%
0%
CTRL
OLA
CB+PTX
OLA+CB+PTX

B

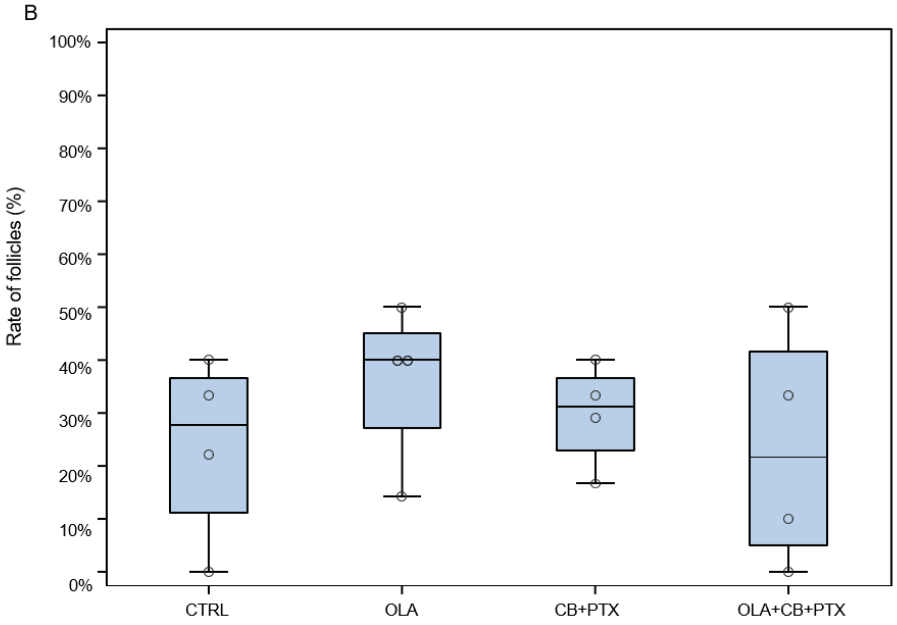
Rate of follicles (%)
100%
90%
80%
70%
60%
50%
40%
30%
20%
10%
0%
CTRL
OLA
CB+PTX
OLA+CB+PTX

C

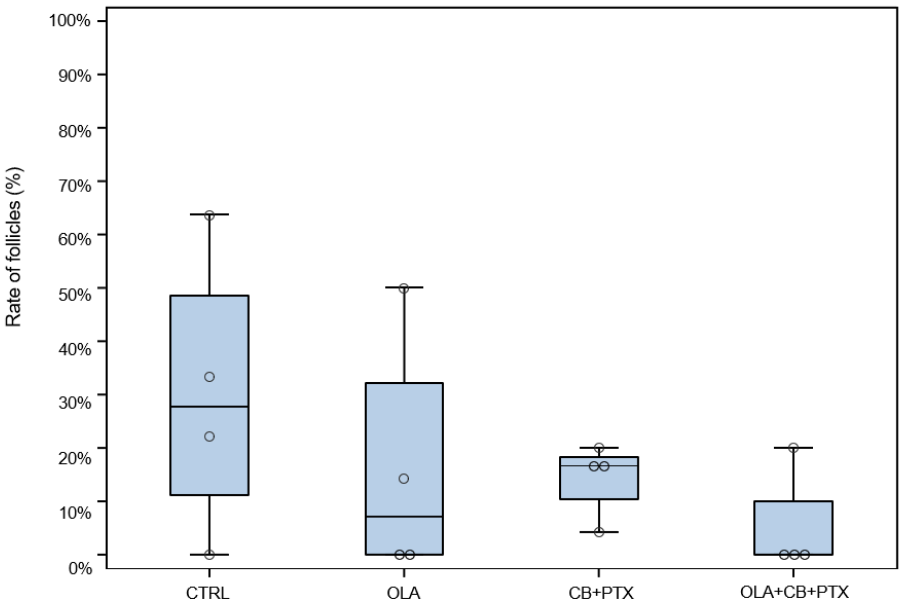
100%
90%
80%
70%
60%
50%
40%
30%
20%
10%
0%
Rate of follicles (%)
CTRL
OLA
CB+PTX
OLA+CB+PTX

D

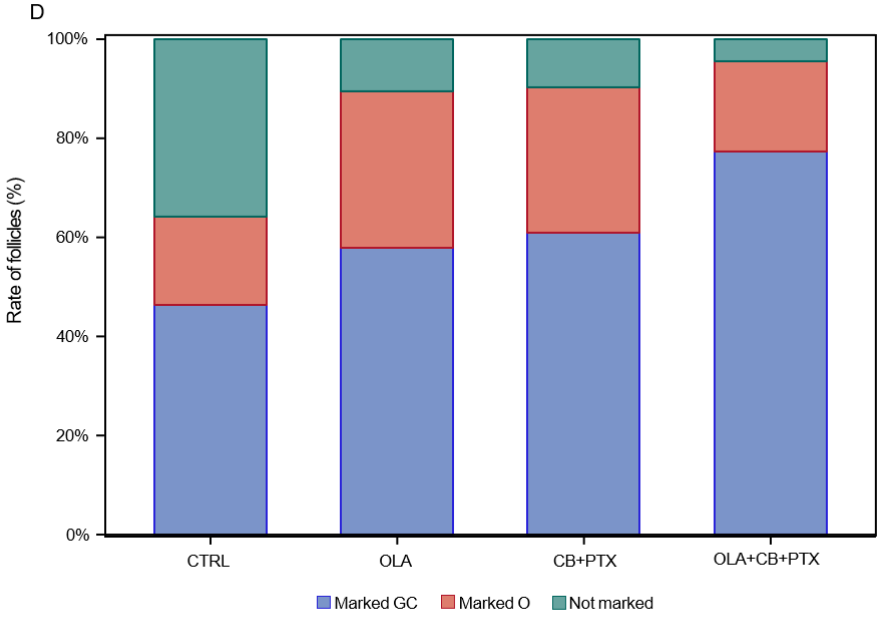
100%
80%
60%
40%
20%
0%
Rate of follicles (%)
CTRL
OLA
CB+PTX
OLA+CB+PTX
Marked GC
Marked O
Not marked

Fig. 10. Apoptotic assessment with TUNEL in human follicles following 3 days in vitro culture exposure to different treatment conditions. The percentage of TUNEL-positive granulosa cells (GC) is shown in Fig. 10A, while Fig. 10B reports the proportion of TUNEL-positive oocyte nuclei. Fig. 10C illustrates the percentage of non-labelled follicles, corresponding to structures with no detectable apoptotic signal. Fig 10D displays the cumulative distribution of the three outcomes across treatments. Each data point represents an individual biological donor. Statistical comparisons were performed using Kruskal–Wallis tests for Fig 10A–C and Chi-square/Fisher's exact test for Figure 10D. Although the cumulative comparison in Fig. 10D marginally approached statistical significance (χ^2 p = 0.0308), this result was not confirmed by Fisher's exact test (p = 0.0605).

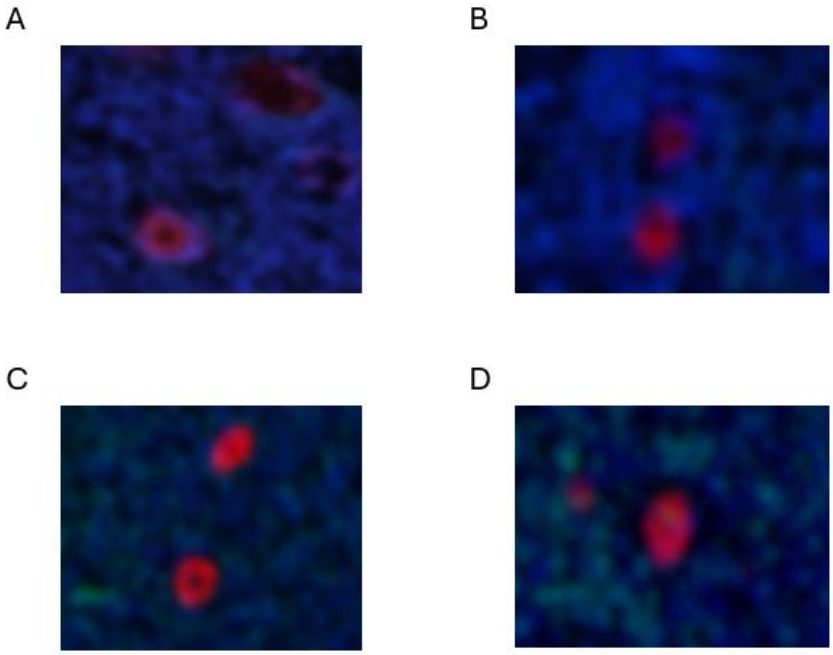

Fig. 11 TUNEL assay in human ovarian cortical tissue after in vitro exposure to different treatment conditions. Representative immunofluorescence images showing TUNEL staining (green) in ovarian tissue sections under the four experimental conditions: (A) Control (CTRL), (B) Olaparib (OLA), (C) Carboplatin + Paclitaxel (CB+PTX), and (D) Olaparib + Carboplatin + Paclitaxel (OLA+CB+PTX). Follicles are identified by ZP3 staining (red)**,** and nuclei are counterstained with Hoechst (blue)**.** Images were acquired at 10× magnification using a Nikon Eclipse E-800 fluorescence microscope**.** Scale bar = 100 µm.

4.5.2 γH2AX

γH2AX immunostaining was evaluated to assess DNA damage within granulosa cells and oocyte across the four experimental conditions (CTRL, OLA, CB+PTX, OLA+CB+PTX). As shown in Fig. 12A, the proportion of γH2AX-positive granulosa cells displayed moderate variability across treatments, with slightly higher values observable under the combined condition (OLA+CB+PTX). However, no statistically significant differences were detected by Kruskal–Walli's testing (χ^2 = 3.8835, df = 3, p = 0.2743).

In Fig. 12B, γH2AX positivity in oocyte remained generally low and uniform across all groups, without evidence of marked treatment-driven variation (Kruskal–Wallis χ^2 = 1.8239, df = 3, p = 0.6097). Fig 12C illustrates the proportion of non-labelled follicles, which appeared comparatively reduced under the combined treatment. The combined treatment group showed the lowest proportion of non-labelled follicles in Fig. 12C; however, this difference was not statistically significant (Kruskal–Wallis χ^2 = 3.8316, df = 3, p = 0.2802). A cumulative representation of all follicular outcomes is presented in Fig. 12D. Chi-square testing indicated a significant difference in the overall distribution of γH2AX labelling patterns across treatments (χ^2 = 19.3117, df = 6, p = 0.0037), which was further supported by Fisher's exact test (p = 0.0024). While current sample size limits definitive conclusions, the consistent trend across treatment groups supports the hypothesis of a treatment-related effect, which is likely to emerge more clearly with an expanded follicle dataset.

A

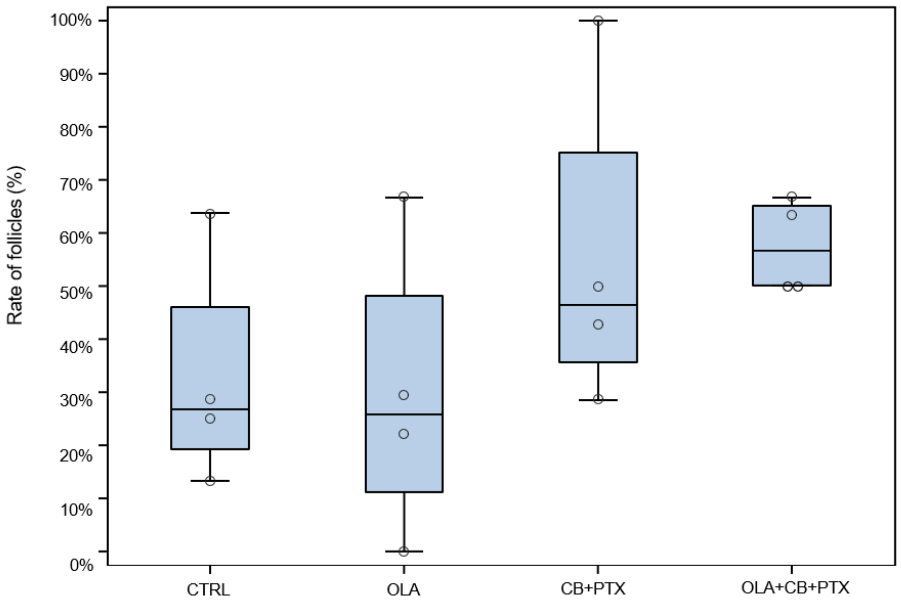
Rate of follicles (%)
100%
90%
80%
70%
60%
50%
40%
30%
20%
10%
0%
CTRL
OLA
CB+PTX
OLA+CB+PTX

B

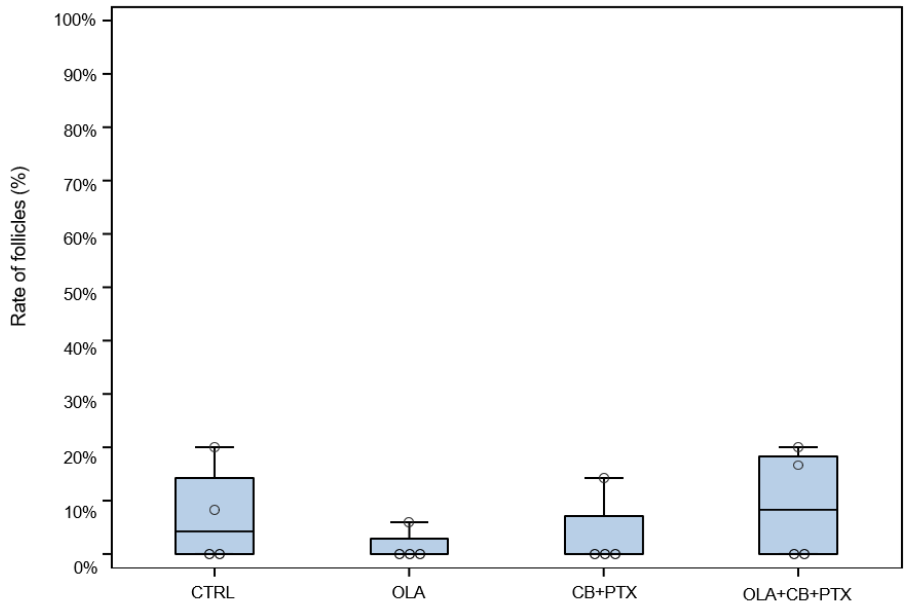
Rate of follicles (%)
100%
90%
80%
70%
60%
50%
40%
30%
20%
10%
0%
CTRL
OLA
CB+PTX
OLA+CB+PTX

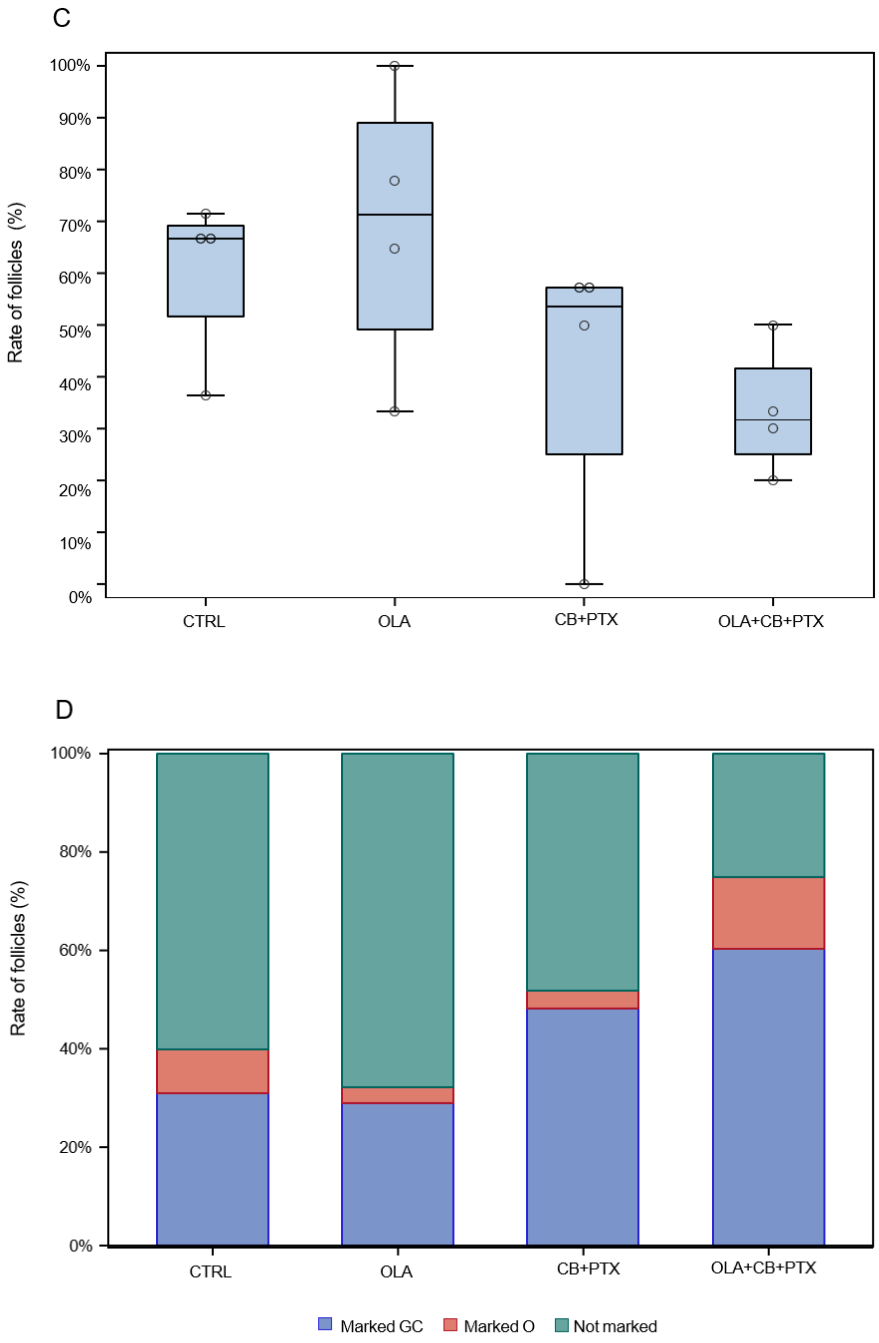

Fig. 12 γH2AX-based assessment of DNA damage in human follicles following 3 days in vitro culture exposure to different treatment conditions. Fig. 12A reports the percentage of γH2AX-positive granulosa cells, whereas Fig. 12B illustrates γH2AX positivity in oocyte nuclei. Fig. 12C depicts the proportion of non-labelled follicles. Fig. 12D presents the cumulative distribution of the three staining categories across treatments. Each data point represents an individual biological donor. Statistical comparisons were conducted using Kruskal–Wallis tests for Fig. 12A–C and Chi-square/Fisher's exact test for Fig. 12D.

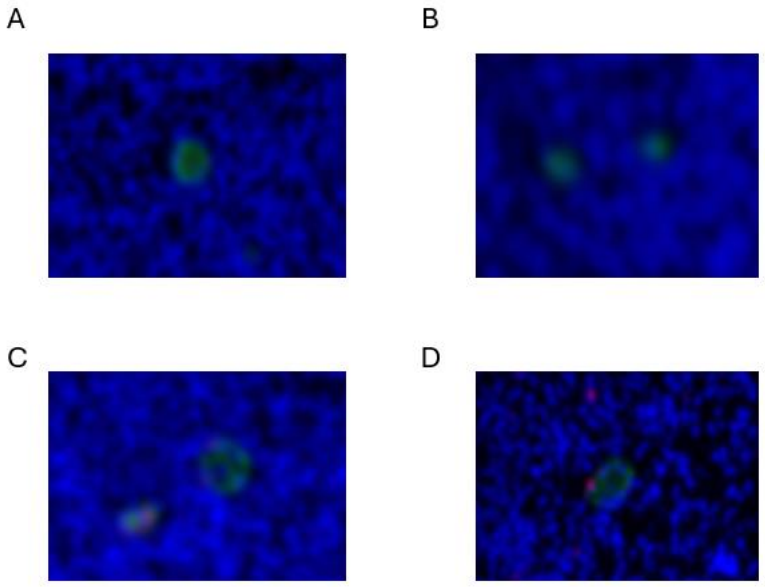

Fig. 13 γH2AX immunofluorescence in human ovarian cortical tissue after in vitro exposure to different treatment conditions. Representative immunofluorescence images showing γH2AX staining (red) in ovarian tissue sections under the four experimental conditions: (A) Control (CTRL), (B) Olaparib (OLA), (C) Carboplatin + Paclitaxel (CB+PTX), and (D) Olaparib + Carboplatin + Paclitaxel (OLA+CB+PTX). ZP3 staining (green) identifies follicles, while nuclei are counterstained with Hoechst (blue). Images were acquired at 10× magnification using a Nikon Eclipse E-800 fluorescence microscope. Scale bar = 100 μm.

4.5.3 Cleaved Caspase 3

Cleaved caspase-3 (CC3), an established executioner marker of apoptosis, was assessed in granulosa cells and oocyte across the four experimental treatments (CTRL, OLA, CB+PTX, OLA+CB+PTX). In Fig. 14A, the proportion of CC3-positive granulosa cells displayed a moderate increase in the treatment groups compared to CTRL. Median CC3 positivity in GC was lowest in CTRL (approximately 10–15%) and appeared slightly higher in OLA and CB+PTX (around 20–25%), with the highest values observed under the combined treatment OLA+CB+PTX (approaching 30%). However, Kruskal–Walli's testing indicated that these differences were not statistically significant ($\chi^2 = 2.6568$, df = 3, p = 0.4478). In Fig. 14B, CC3 nuclear positivity in oocytes remained consistently low

across all treatments, with values typically below 10% in all groups. No statistically significant variation was detected (Kruskal–Wallis $\chi^2 = 0.7750$, df = 3, p = 0.8550). Figure 14C highlights a clear reduction in the proportion of non-marked follicles under CB+PTX and OLA+CB+PTX, whereas CTRL and OLA retained higher levels of unstained follicles**.** Nevertheless, this distributional change did not reach statistical significance (Kruskal–Wallis $\chi^2 = 5.7209$, df = 3, p = 0.1255). A cumulative comparison of all outcomes is shown in Fig. 14D. Pearson's chi-square test detected a significant difference in the overall distribution of CC3 staining categories across treatments ($\chi^2 = 14.3628$, df = 6, p = 0.0258), corroborated by Fisher's exact test (two-sided p = 0.0262). Although based on a restricted follicular sample, the emerging trend suggests that a larger dataset may help consolidate this finding.

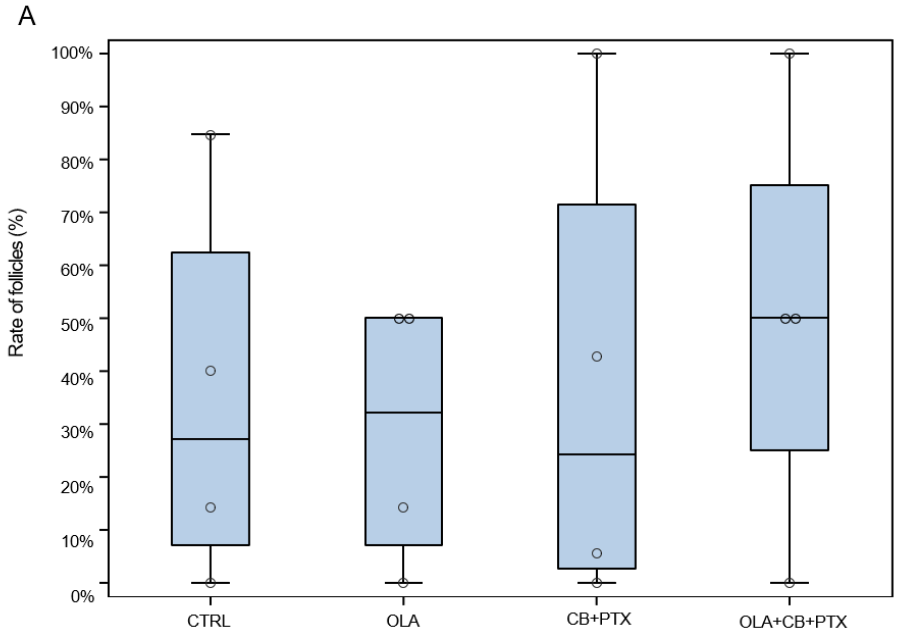

B

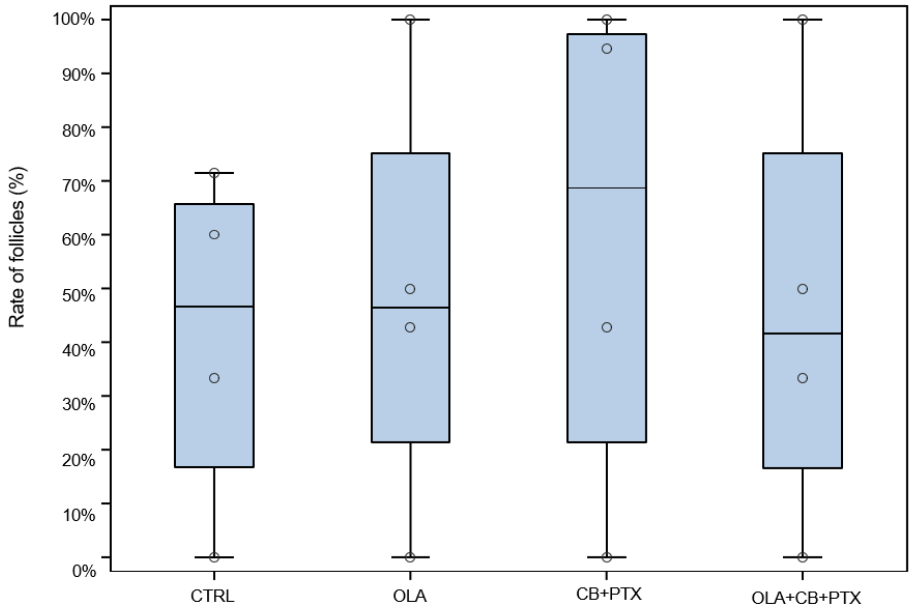
Rate of follicles (%)
100%
90%
80%
70%
60%
50%
40%
30%
20%
10%
0%
CTRL
OLA
CB+PTX
OLA+CB+PTX

C

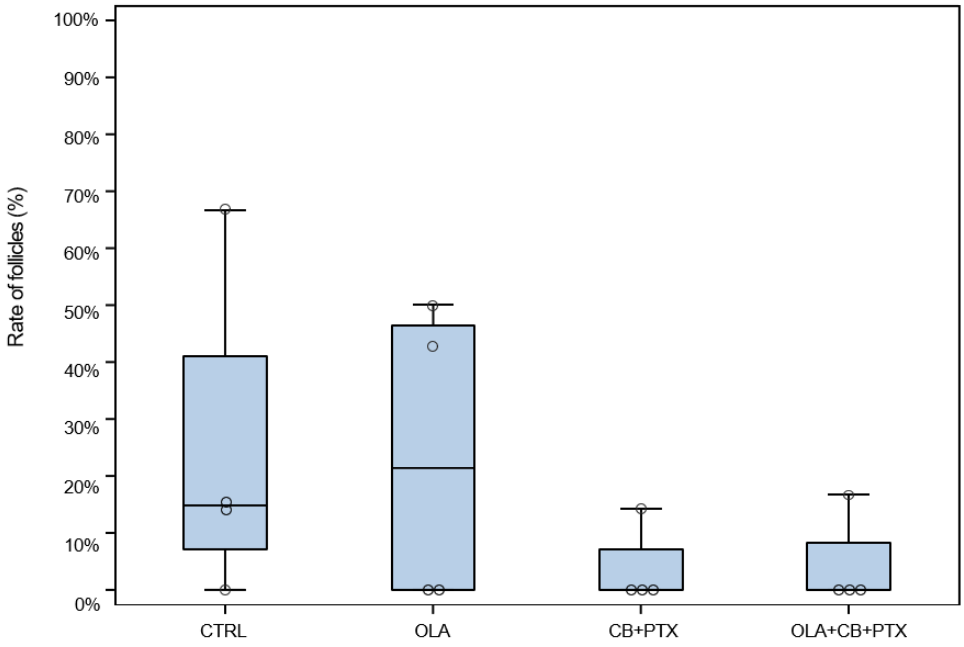
Rate of follicles (%)
100%
90%
80%
70%
60%
50%
40%
30%
20%
10%
0%
CTRL
OLA
CB+PTX
OLA+CB+PTX

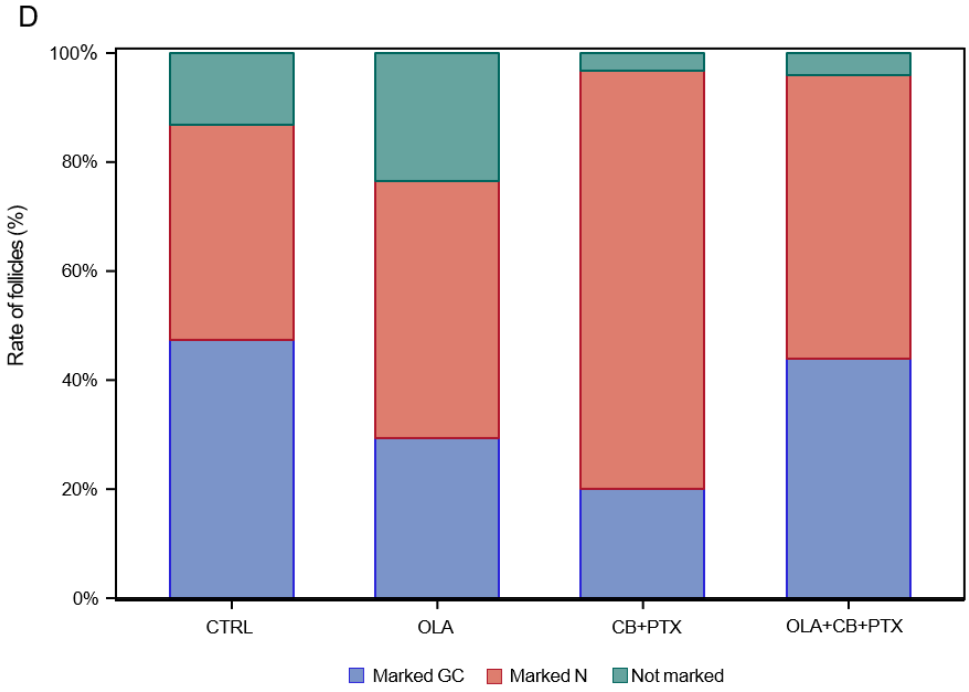

Fig. 14 Cleaved caspase-3 (CC3) staining in human follicles following 3 days in vitro culture exposure to different treatment conditions. Fig. 14A shows the percentage of CC3-positive granulosa cells, while Fig. 14B reports CC3 positivity in oocyte nuclei. Fig. 14C presents the proportion of non-marked follicles. Fig. 14D illustrates the cumulative distribution of the three staining categories across treatments. Each point represents an individual biological donor. Statistical analyses were performed using Kruskal–Wallis tests for Fig. 14A–9C and Chi-square/Fisher's exact test for Fig. 14D. Pearson's chi-square test detected a significant difference in the overall distribution of CC3 staining categories across treatments ($\chi^2 = 14.3628$, df = 6, p = 0.0258), corroborated by Fisher's exact test (two-sided p = 0.0262).

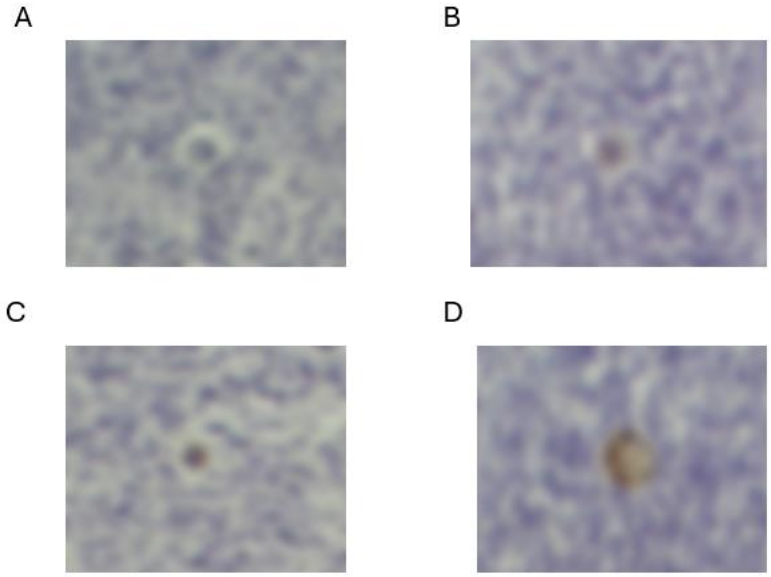

Fig. 15 Immunohistochemical detection of Cleaved Caspase-3 in human ovarian cortical tissue after in vitro exposure to different treatment conditions. Representative immunohistochemical staining for Cleaved Caspase-3, showing apoptotic follicles in ovarian tissue sections under the four experimental conditions: (A) Control (CTRL), (B) Olaparib (OLA), (C) Carboplatin + Paclitaxel (CB+PTX), and (D) Olaparib + Carboplatin + Paclitaxel (OLA+CB+PTX). Positive brown signal indicates Caspase-3 activation within granulosa and oocyte compartments. Images were acquired at 10× magnification using a Nikon Eclipse E-800 microscope. Scale bar = 100 μm.

4.5.4 Yes-associated protein 1 (Yap-1)

Yes-associated protein 1 (Yap-1), a transcriptional co-activator of the Hippo signaling pathway, was assessed as an indicator of follicular proliferative activity following treatment.

In Fig. 16A, YAP1 positivity in granulosa cells showed variable distribution across treatments. Median values were ~52% in CTRL and OLA, higher in CB+PTX (~70%), and comparable to CTRL/OLA in OLA+CB+PTX (~55–60%), with a wider inter-sample spread in CTRL and OLA+CB+PTX. Despite these apparent fluctuations, statistical comparison via Kruskal–Walli's test did not reveal significant differences among treatments ($\chi^2 = 3.0616$, df = 3, $p = 0.3822$).

Fig. 16B shows nuclear YAP1 positivity in oocytes. Median values were highest in OLA (~50%), intermediate in CTRL (~30%), and low in both CB+PTX and OLA+CB+PTX (around ~10%), with wider inter-sample spread in OLA. Group

differences were not statistically significant (Kruskal–Wallis $\chi^2 = 5.1090$, df = 3, p = 0.1640). Fig 16C reports the proportion of YAP1-negative follicles. Negativity was lowest in OLA (near 0–5%) and remained relatively low in CB+PTX (~5–10%), whereas it was higher in OLA+CB+PTX (~10–20%) and showed the widest spread with the highest upper values in CTRL. These differences were not statistically significant (Kruskal–Wallis $\chi^2 = 1.9860$, df = 3, p = 0.5753).

In Fig. 16D, the cumulative distribution of YAP1 staining patterns (GC-positive, N-positive, and negative follicles) revealed a treatment-dependent redistribution of follicular states. CB+PTX was characterized by a relative enrichment of GC-positive follicles, consistent with a potential shift toward granulosa-driven proliferative signaling, whereas OLA+CB+PTX displayed a larger proportion of YAP1-negative follicles, suggesting either suppression or delayed activation of the Hippo effector**.** CTRL exhibited a more balanced allocation across categories, while OLA uniquely showed an increased proportion of oocyte-positive follicles, indicating preferential YAP1 activation at the oocyte level.

Pearson's chi-square confirmed that this redistribution was statistically significant ($\chi^2 = 15.0401$, df = 6, p = 0.0199), further supported by Fisher's exact test (p = 0.0302). Although the number of follicles analyzed per group is limited, the emerging divergence in compartment-specific YAP1 activation suggests that different treatments may differentially modulate oocyte- versus granulosa-driven responses, warranting confirmation in a larger dataset.

A

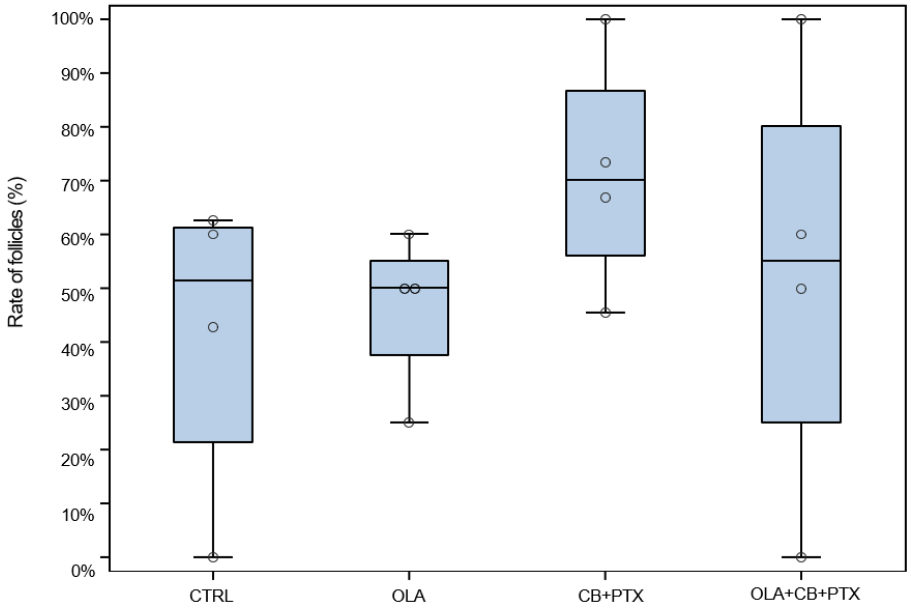
Rate of follicles (%)
100%
90%
80%
70%
60%
50%
40%
30%
20%
10%
0%
CTRL
OLA
CB+PTX
OLA+CB+PTX

B

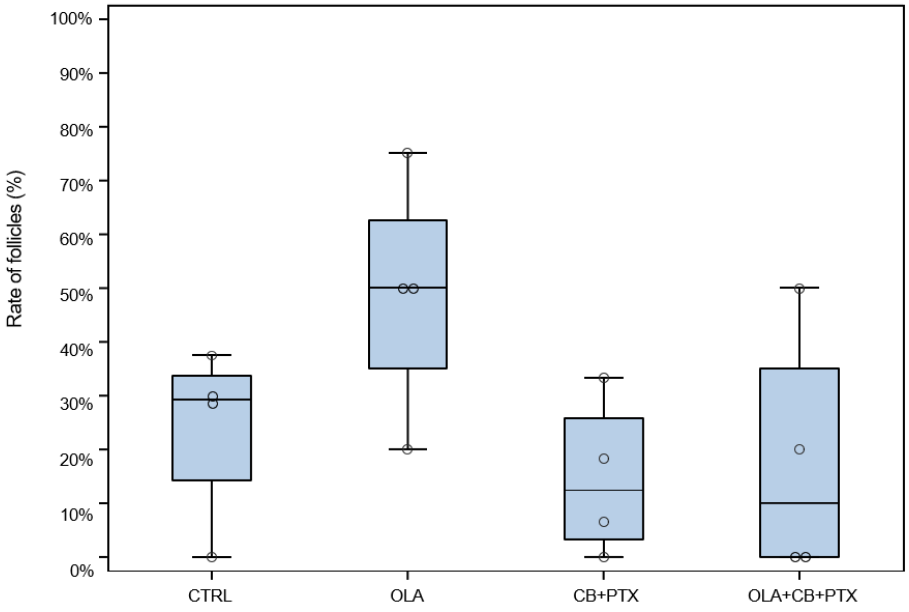
Rate of follicles (%)
100%
90%
80%
70%
60%
50%
40%
30%
20%
10%
0%
CTRL
OLA
CB+PTX
OLA+CB+PTX

C

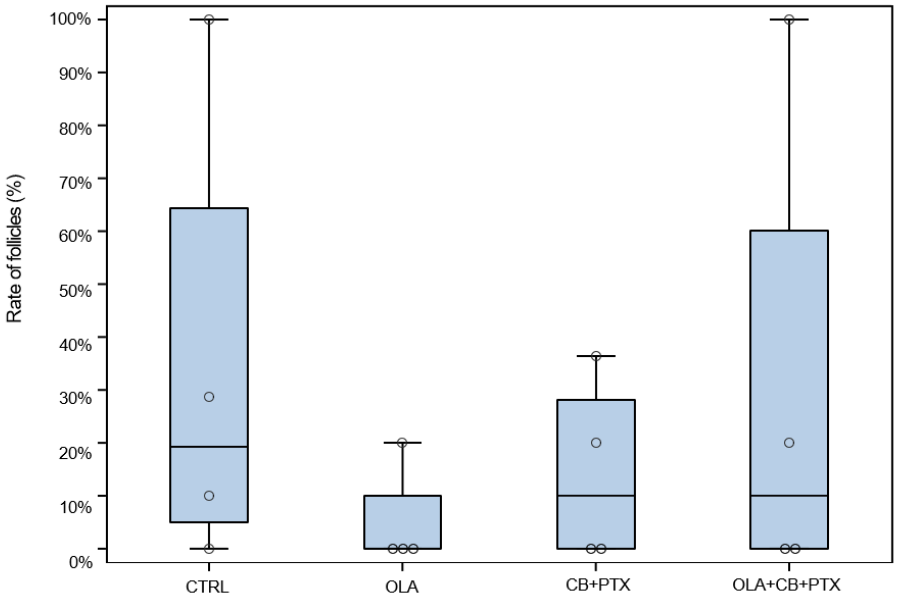
100%
90%
80%
70%
60%
50%
40%
30%
20%
10%
0%
Rate of follicles (%)
CTRL
OLA
CB+PTX
OLA+CB+PTX

D

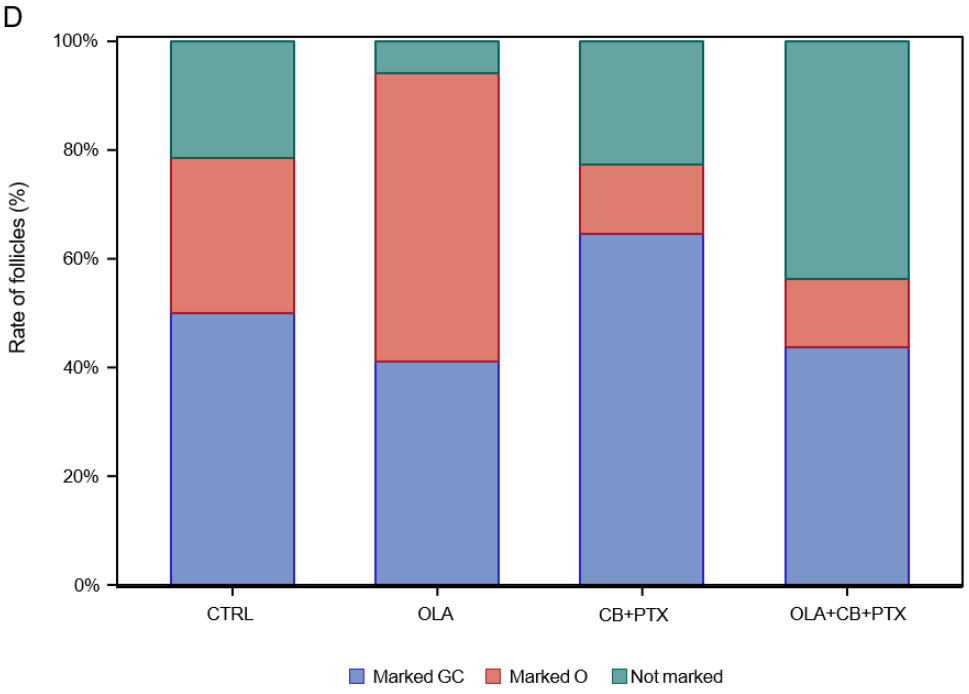
100%
80%
60%
40%
20%
0%
Rate of follicles (%)
CTRL
OLA
CB+PTX
OLA+CB+PTX
Marked GC
Marked O
Not marked

Fig. 16 YAP-1 staining in human ovarian follicles following 3 days in vitro culture exposure to different treatment conditions.

Fig. 16A reports the percentage of YAP1-positive granulosa cells, while Fig. 16B illustrates YAP1 positivity within oocyte nuclei. Fig. 16C displays the proportion of YAP1-negative follicles. Fig. 16D presents the cumulative distribution of the three staining categories (GC-positive, N-positive, and negative follicles) across treatments. Each point represents an individual biological donor. Statistical comparisons were conducted using Kruskal–Wallis tests for Fig. 16A–C and Chi-square/Fisher's exact testing for Fig. 16D. Distribution in Fig. 16D reached statistical significance (χ^2 p = 0.0199; Fisher's exact p = 0.0302).

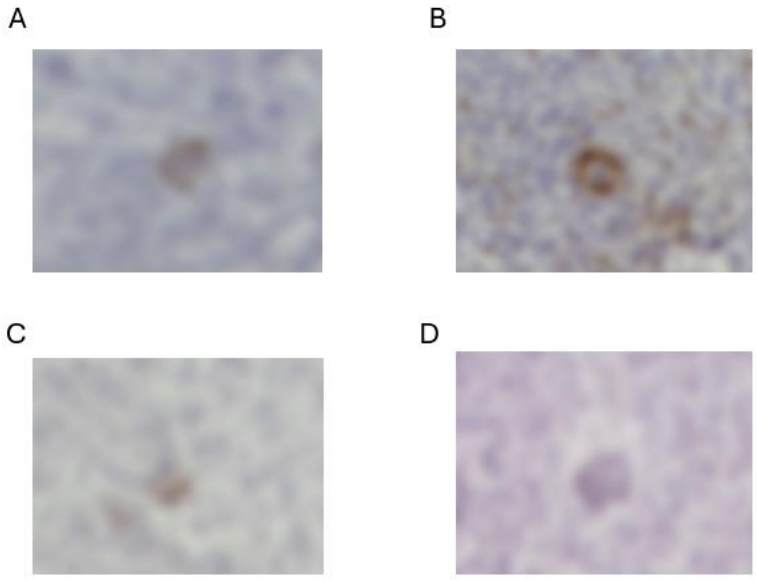

Fig. 17. Immunohistochemical detection of YAP1 in human ovarian cortical tissue after in vitro exposure to different treatment conditions. Representative immunohistochemical staining for YAP1 in ovarian tissue sections under the four experimental conditions: (A) Control (CTRL), (B) Olaparib (OLA), (C) Carboplatin + Paclitaxel (CB+PTX), and (D) Olaparib + Carboplatin + Paclitaxel (OLA+CB+PTX). Positive brown nuclear and cytoplasmic staining indicates YAP1 expression within granulosa and stromal cells. In OLA+CB+PTX samples, weak signal is observed, while treated tissues show variable YAP1 positivity. Images were acquired at 10× magnification using a Nikon Eclipse E-800 microscope. Scale bar = 100 μm.

4.6 Immunological analysis

The experiment was performed on culture media collected at 24, 48, and 72 hours, with two independent experimental replicates. In addition, a separate experiment was conducted to evaluate cytokine release at shorter time points (1, 2, 3, and 6 hours); however, for all early time points, cytokine concentrations were detected at levels below the minimum value of the standard curve range for each cytokine. Similarly, several cytokines included in the panel- namely TNF-α, MIP-1α, IFN-α2, IL-2, IL-1β, IL-17A, and IFN-γ were detected at low concentrations in the culture media and are therefore not reported for the 24-, 48-, and 72-hour time points.

Overall, for most of the cytokines analyzed, CTRL and OLA conditions displayed comparable concentration profiles over time, whereas CB+PTX and OLA+CB+PTX showed consistently lower values across all examined time points.

IL-4 and VEGF exhibited a similar temporal behavior, characterized by an increase in concentration from 24 to 72 hours, particularly under CTRL and OLA conditions. In contrast, CB+PTX and OLA+CB+PTX conditions showed a relatively moderate increase of cytokine levels over time, with limited variation between time points (Fig. 18A and 18G).

IL-10 and MCP-1 exhibited a comparable trend across all experimental conditions, characterized by a progressive decrease in concentration from 24 to 72 hours. Notably, for both cytokines, the OLA condition showed a pronounced elevation at 24 h compared with the other treatment groups, followed by a decline at later time points. This pattern was consistently observed across CTRL, OLA, CB+PTX, and OLA+CB+PTX conditions (Fig. 18D and 18F).

IL-6 showed a distinct profile, with CTRL and OLA conditions maintaining high and relatively stable concentrations from 24 to 72 hours. In contrast, CB+PTX and OLA+CB+PTX conditions exhibited a marked reduction in cytokine levels over time, with progressively lower concentrations at later time points (Fig. 18B).

IP-10 demonstrated a time-dependent decrease in concentration across all experimental conditions, with higher levels detected at 24 hours followed by reduced values at 48 and 72 hours. At each time point, CTRL and OLA conditions showed higher concentrations compared to CB+PTX and OLA+CB+PTX (Fig. 18E).

IL-8 was among the cytokines showing the highest absolute concentration levels compared to the other analytes, with the CTRL and OLA conditions displaying an

increase over time, whereas the CB+PTX and OLA+CB+PTX conditions remained lower and exhibited limited temporal variation (Fig. 18C).

All data are presented as mean values derived from two experimental replicates.

Regarding leukocyte detection by CD45 (IHC), a very limited number of positive cells was observed in the analyzed ovarian tissue sections.

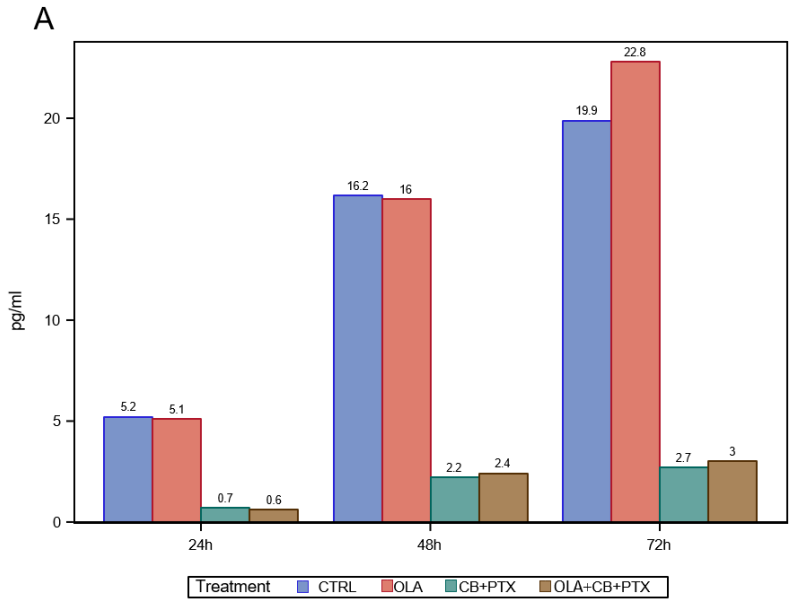

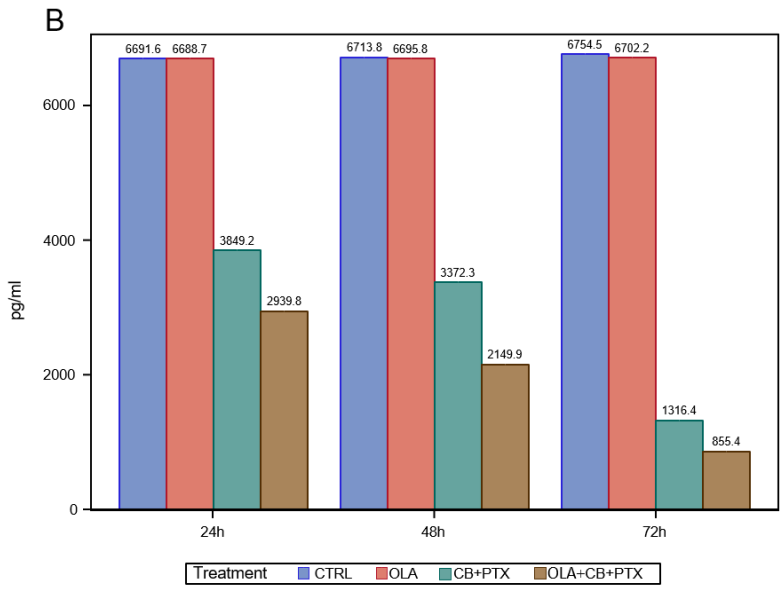

C

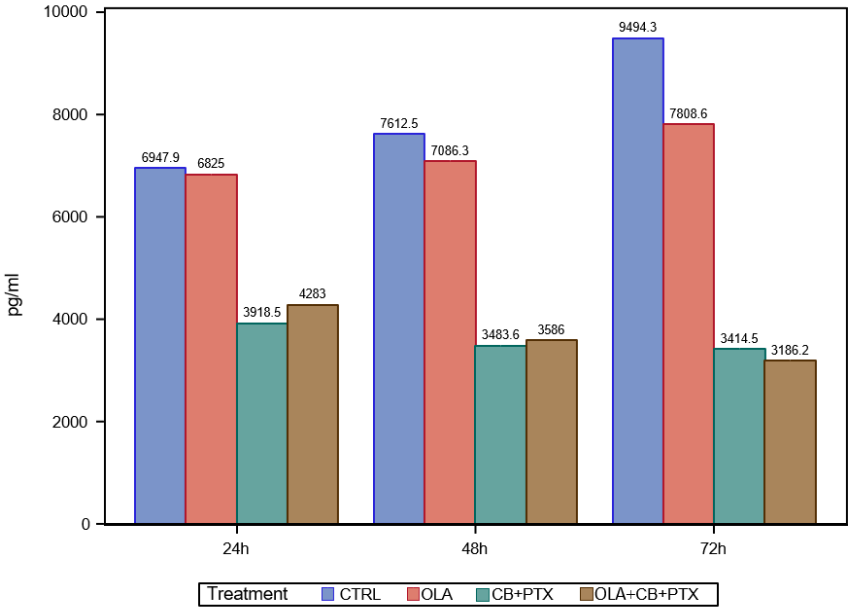
10000
8000
6000
4000
2000
0
pg/ml
6947.9
6825
3918.5
4283
7612.5
7086.3
3483.6
3586
9494.3
7808.6
3414.5
3186.2
24h
48h
72h
Treatment
CTRL
OLA
CB+PTX
OLA+CB+PTX

D

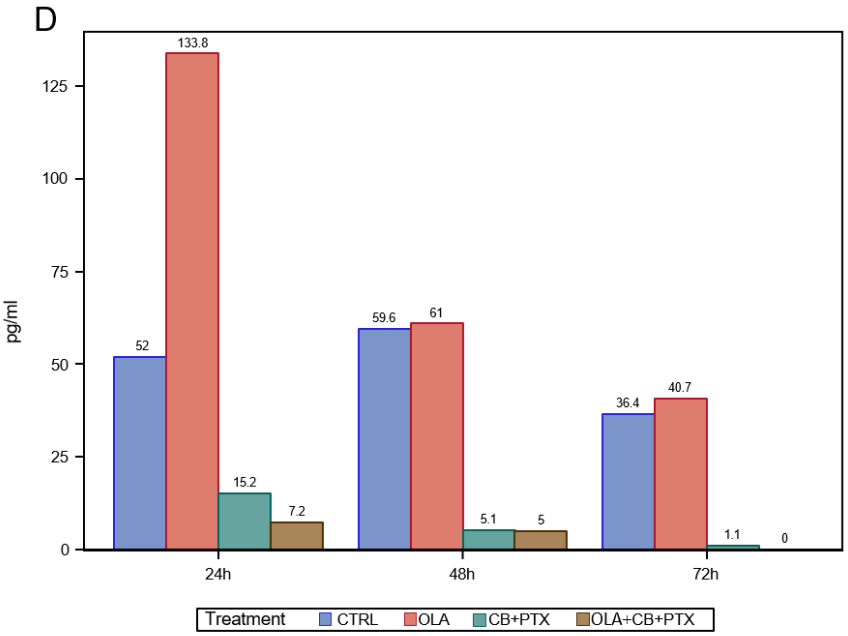
125
100
75
50
25
0
pg/ml
52
133.8
15.2
7.2
59.6
61
5.1
5
36.4
40.7
1.1
0
24h
48h
72h
Treatment
CTRL
OLA
CB+PTX
OLA+CB+PTX

E

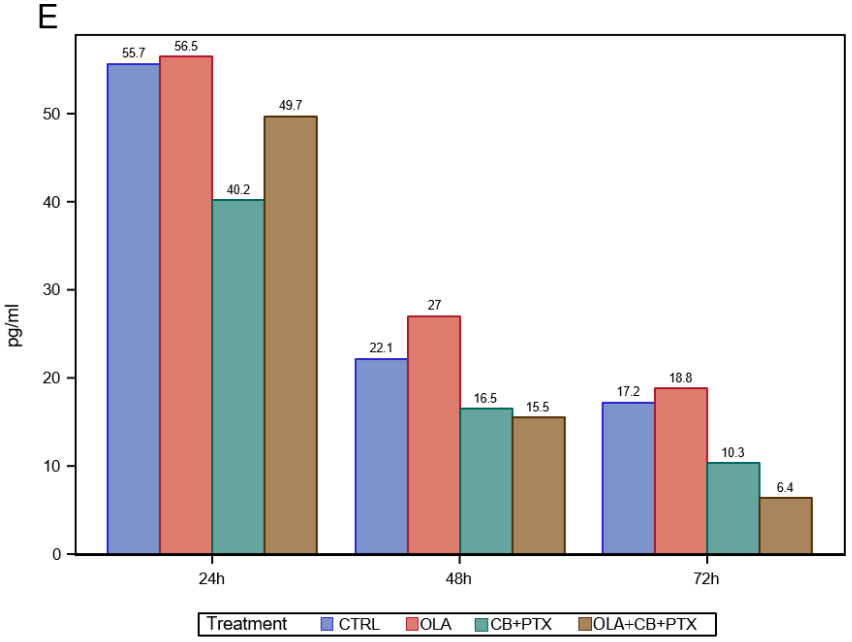
55.7
56.5
49.7
40.2
22.1
27
16.5
15.5
17.2
18.8
10.3
6.4
pg/ml
0
10
20
30
40
50
24h
48h
72h
Treatment
CTRL
OLA
CB+PTX
OLA+CB+PTX

F

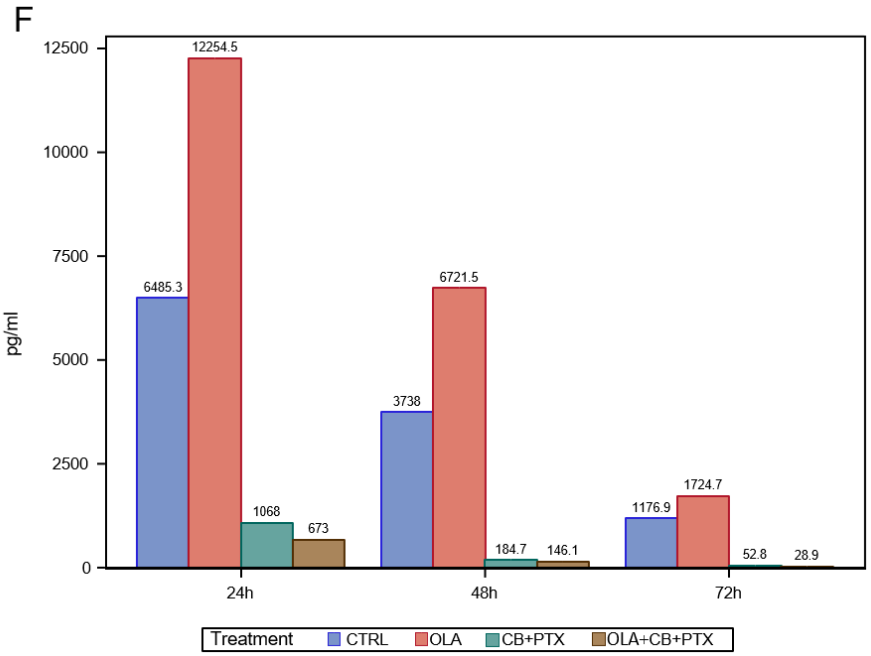
12254.5
6485.3
6721.5
3738
1068
673
184.7
146.1
1724.7
1176.9
52.8
28.9
pg/ml
0
2500
5000
7500
10000
12500
24h
48h
72h
Treatment
CTRL
OLA
CB+PTX
OLA+CB+PTX

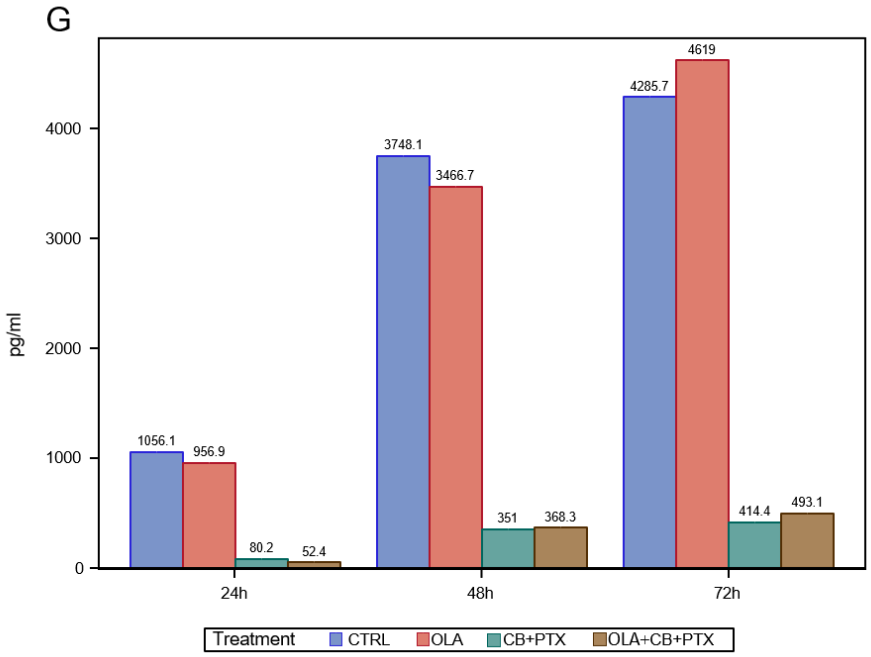

Fig. 18. Time-dependent modulation of cytokine release in culture media after 24, 48 and 72 hours of in vitro culture. Cytokine concentrations measured in culture media collected at 24, 48, and 72 h under different experimental conditions (CTRL, OLA, CB+PTX, OLA+CB+PTX) show distinct temporal patterns across analytes. (A) IL-4, (B) IL-6, (C) IL-8, (D) IL-10, (E) IP-10, (F) MCP-1, and (G) VEGF are displayed in the order of the cytokine panel. Data are shown for 24 h, 48 h, and 72 h and represent mean ± SD of two experimental replicates. Quantification ranges based on the standard curves were as follows: IL-4, IL-6, and IL-8, 0.64-10,000 pg/mL; IL-10, IP-10, and VEGF, 2.6-40,000 pg/mL; MCP-1, 3-50,000 pg/mL.

4.7 Brussels internship experiments

The experiments conducted on the tissues treated at the Research Laboratory on Human Reproduction in Brussels and continued in Genova. For this reason, the data are not yet supported by statistical analysis to determine their significance and are therefore partially incomplete. Consequently, the results presented here should be interpreted as providing a general overview rather than definitive conclusions.

4.7.1 Histological analysis

4.7.1.1 Morphology assessment of follicular stages

The distribution of follicle classes was evaluated in ovarian tissues treated *ex vivo* under four experimental conditions: control (CTRL), Olaparib 20 μM (OLA 20), cyclophosphamide (4HC), and the combination of 4HC + Olaparib (4HC + OLA). Samples were further stratified according to BRCA mutational status, distinguishing tissues derived from BRCA-mutated patients (pink dots) and non-mutated patients (green dots). Primordial follicles showed comparable proportions across all treatment groups, with no evident differences between conditions. Both BRCA-mutated and non-mutated samples exhibited similar inter-individual variability. Transitory follicles represented the predominant population in every experimental condition. No clear treatment-related variation emerged, and no trend appeared to be specifically associated with BRCA status. The distribution of values consistently ranged between approximately 50% and 90% across all samples. Primary follicles were detected at lower frequencies, showing similar levels across treatments. A slightly broader dispersion was observed in the 4HC and 4HC + OLA conditions; however, no consistent difference between BRCA-mutated and non-mutated tissues was observed. Secondary follicles were absent in all conditions, irrespective of chemotherapy exposure or BRCA status.

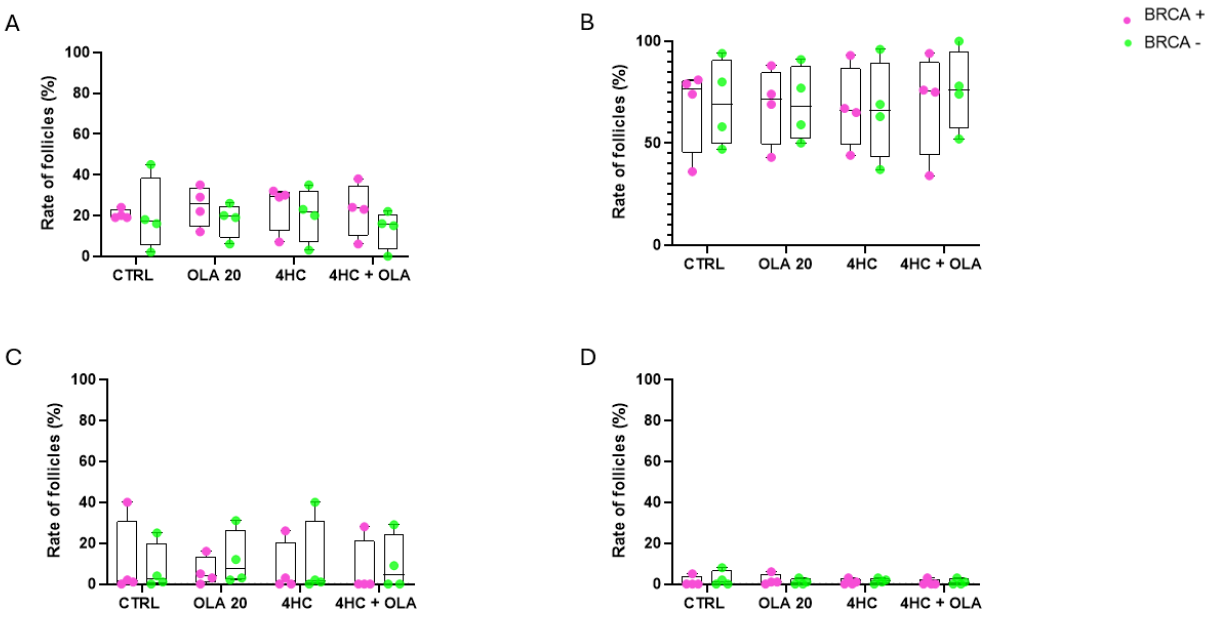

Fig. 19 Follicle stage distribution in ovarian cortical tissues following 3 days in vitro culture exposure to different treatment conditions. Samples were exposed to control medium with 0.1% DMSO (CTRL), Olaparib 20 µM (OLA 20), cyclophosphamide (4HC), or the combination of 4HC + Olaparib (4HC + OLA). BRCA-mutated patients are represented by pink dots, while non-mutated patients are shown in green. Fig. 19A shows the proportion of primordial follicles, Fig. 19B the transitory follicles, Fig. 19C the primary follicles, and Fig. 19D the secondary follicles. Data are presented as individual values and box plots.

4.7.1.2 Assessment of follicle atresia

The rate of atretic follicles was assessed across the four treatment conditions (CTRL, OLA 20, 4HC, and 4HC + OLA), stratified by BRCA mutational status (pink dots for BRCA-mutated samples, green dots for non-mutated samples). Primordial atretic follicles (Fig.1A) were detected at variable but generally comparable levels across all treatments. Both BRCA-mutated and non-mutated samples displayed similar inter-individual dispersion, with no consistent trend associated with either chemotherapy exposure or Olaparib treatment. Transitional atretic follicles (Fig. 17B) represented the largest proportion of atretic structures in all groups. Although a broader variability was observed in some conditions particularly in the OLA 20 group no clear treatment-related pattern emerged, and BRCA-mutated and non-mutated samples appeared intermingled across the distribution.

Primary atretic follicles (Fig.17C) were present at lower frequencies and remained similar between treatment groups. Slightly higher values were occasionally observed in the 4HC or 4HC + OLA conditions, but without a consistent BRCA-associated tendency. Secondary atretic follicles (Fig. 17D) were absent in all experimental conditions, regardless of treatment or BRCA status.

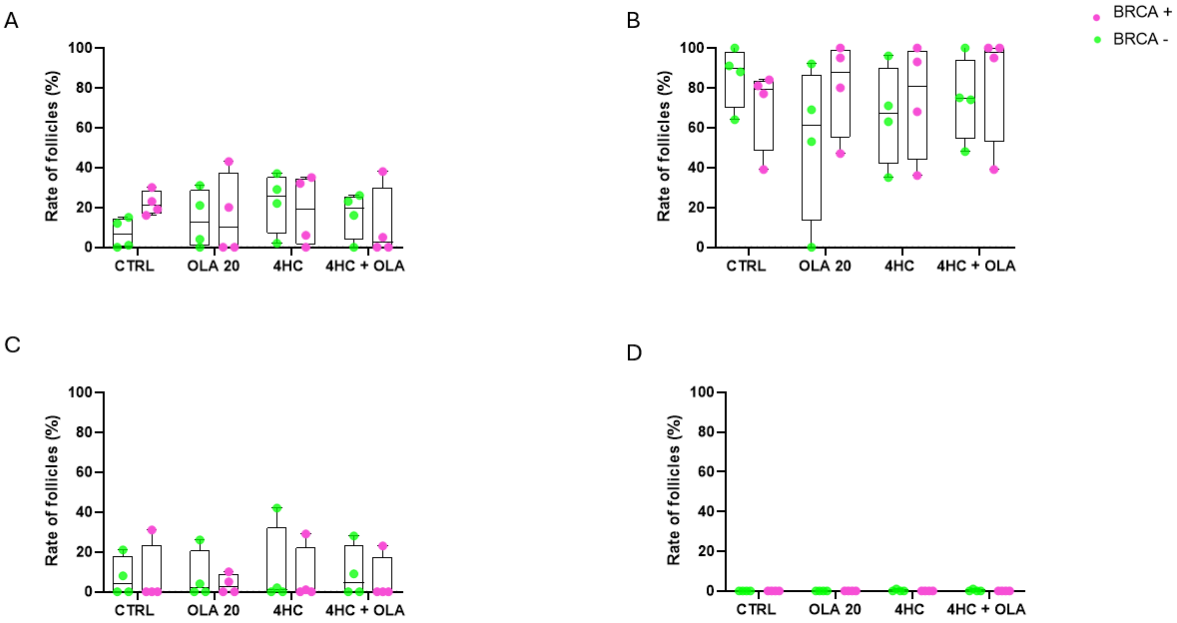

Fig. 20 Rate of atretic follicles in ovarian cortical tissues following 3 days in vitro culture exposure to different treatment conditions. Samples were exposed to control medium (CTRL), Olaparib 20 µM (OLA 20), cyclophosphamide (4HC), or the combination of 4HC + Olaparib (4HC + OLA). BRCA-mutated patients are represented by pink dots, while non-mutated patients are shown in green. Fig. 20A refers to primordial atretic follicles, Fig. 20B to transitional atretic follicles, Fig. 20C to primary atretic follicles, and Fig. 20D to secondary atretic follicles. Data are shown as individual values and box plots.

4.7.1.3 Assessment of follicle density

The impact of the different *in vitro* treatments on ovarian tissue was evaluated through the analysis of both follicle density and follicle classification. Density was assessed by normalizing the total number of follicles counted in each condition to the corresponding analyzed tissue area (mm^2), allowing a quantitative comparison between samples while accounting for tissue variability across patients.

In parallel, follicles were categorized according to their developmental stage (primordial, transitional, primary, and secondary) and further classified as healthy or atretic. Given that primordial and transitional follicles represent the most abundant populations in these tissues, specific analyses were dedicated to these two categories.

Results are presented separately for BRCA-mutated (BRCA+) and non-mutated (BRCA–) samples to explore potential differences in response to chemotherapy (4HC) and PARP inhibition (Olaparib), administered either alone or in combination.

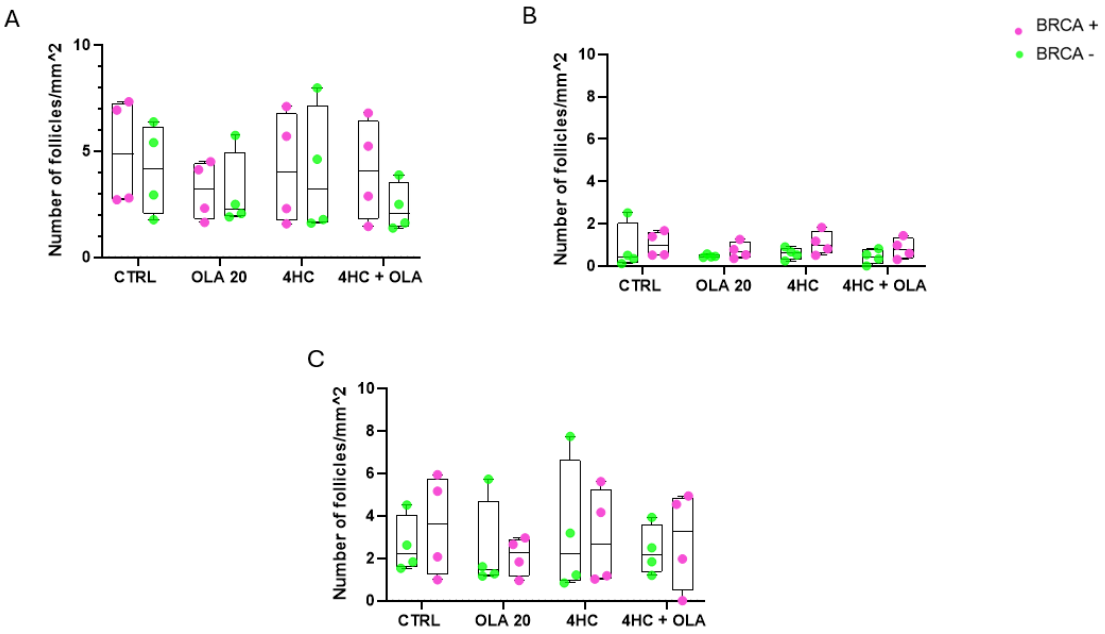

Fig. 19 Follicle density in ovarian cortical tissues following 3 days of in vitro culture exposure to different treatment conditions. Samples were exposed to control medium with DMSO 0.1% (CTRL), Olaparib 20 µM (OLA 20), cyclophosphamide (4HC), or the combination of 4HC + Olaparib (4HC + OLA). BRCA-mutated samples (BRCA+) are indicated by pink dots, while non-mutated samples (BRCA–) are shown in green. **(A)** Total follicle density expressed as number of follicles per mm². **(B)** Density of primordial follicles per mm². **(C)** Density of transitional follicles per mm². Data are presented as individual values and box plots.

4.7.1.4 Immunostaining results

DNA damage in ovarian follicles was evaluated by immunostaining for γH2AX, a marker of double-strand breaks, and by TUNEL assay, indicative of DNA fragmentation associated with apoptotic cell death. In both essays, ZP3 co-labelling was used to facilitate the identification of follicular structures. Positivity was quantified separately in granulosa cells (GC), in the oocyte nucleus, or simultaneously in both cell types. The percentage of positive cells was calculated over the total number of stained cells rather than on the total number of follicles identified. Data are presented for BRCA-mutated (BRCA+) and non-mutated (BRCA-) samples across all treatment conditions (CTRL, OLA 20, 4HC, 4HC + OLA).

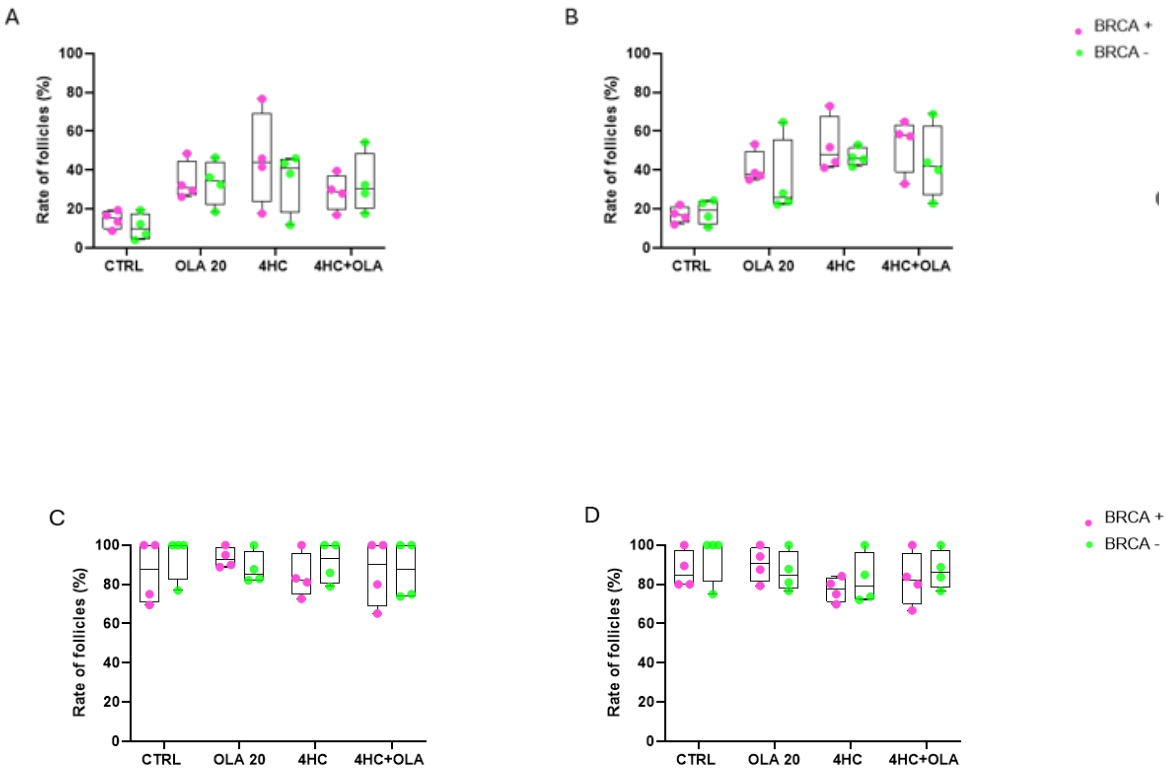

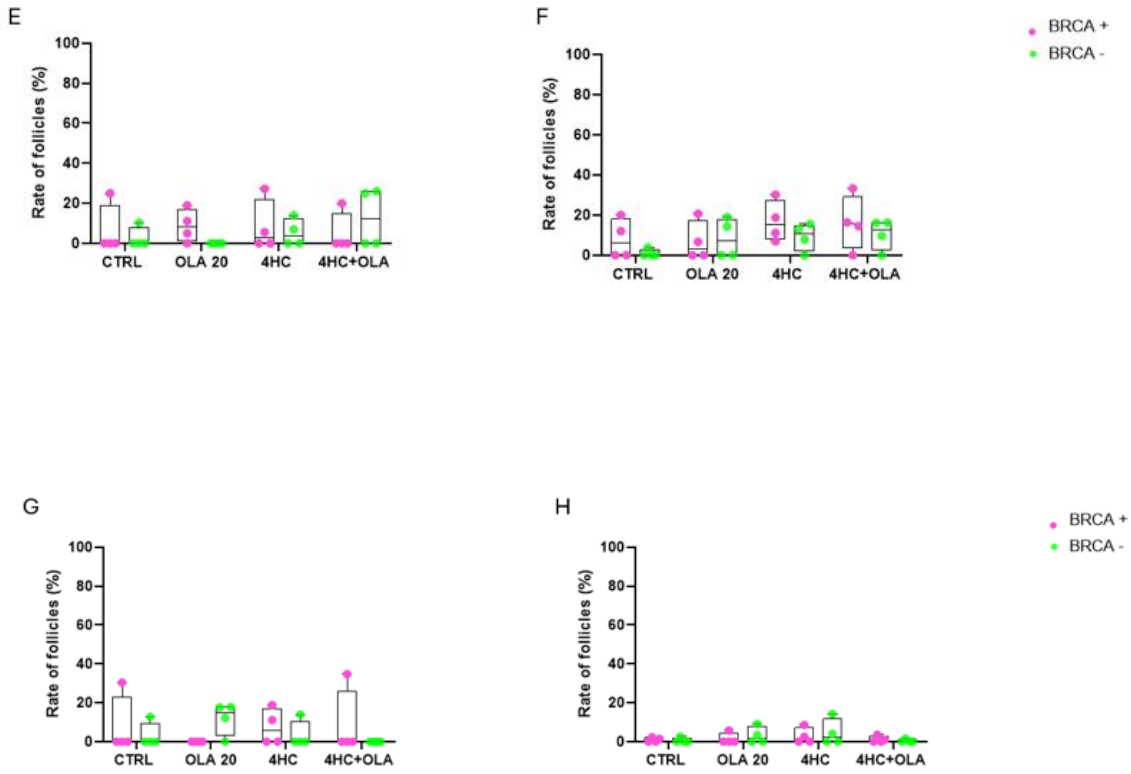

Fig. 20 Analysis of DNA damage in ovarian follicles following *ex vivo* exposure to CTRL, OLA 20, 4HC or 4HC + OLA. Follicular structures were identified through ZP3 staining and assessed for DNA double-strand breaks (γH2AX immunostaining) or apoptotic DNA fragmentation (TUNEL assay). BRCA-mutated samples (BRCA+) are represented by pink dots, while non-mutated samples (BRCA–) are shown in green. (A–B) Percentage of TUNEL-positive (A) and γH2AX-positive (B) follicles over the total number of labelled cells. (C–D) Rate of TUNEL-positive (C) and γH2AX-positive (D) granulosa cells (GC). (E–F) Rate of TUNEL-positive (E) and γH2AX-positive (F) oocytes. (G–H) Percentage of follicles showing double positivity in both granulosa cells and oocytes for TUNEL (G) and γH2AX (H).

5. Discussion

5.1 Follicle Morphology and Atresia

The distribution of follicular stages was similar across all treatment conditions with transitional follicles representing the most frequent category in every group as shown in Fig. 5B. This pattern suggests that none of the tested treatments induced a substantial shift toward follicular activation or growth arrest within the duration of culture. A modest reduction in the proportion of primordial follicles was noted in the Olaparib group compared with the control and the other treatment conditions as shown in Fig 5A. As primordial follicles represent the quiescent ovarian reserve from which growing follicles are recruited, such a decrease could be interpreted as an early indication of potential follicle depletion; however, this variation did not reach statistical significance (Kruskal–Wallis, $p = 0.6681$) and should therefore be interpreted with caution. Moreover, the control condition showed the highest totals, whereas all treatment groups—including Olaparib alone and in combination with chemotherapy—displayed lower yields.

Although morphology-based classification provides a practical estimation of follicular integrity, it is limited to the detection of late-stage degenerative changes. Increasing evidence indicates that early molecular perturbations—including activation of apoptotic pathways and mitochondrial stress—may precede overt histological damage and therefore remain undetected by conventional hematoxylin/eosin staining (5,79). For this reason, morphology alone may underestimate subtle treatment-related effects, particularly in settings with limited follicle numbers and heterogeneous tissue quality.

Morphological assessment by hematoxylin/eosin indicated similar proportions of healthy and atretic follicles in the Olaparib and control groups, suggesting that Olaparib monotherapy did not induce overt follicular degeneration under these conditions. It is also important to note that the presence of atretic follicles within the control group is expected, as tissue manipulation, cryopreservation/thawing, and in vitro culture inherently impose stress that can trigger baseline levels of follicular atresia even in the absence of treatment. In pooled analyses, however, the OLA+CB+PTX group exhibited a higher proportion of atretic follicles, and treatment was significantly associated with follicle health status (Chi-squared test, $p = 0.0054$).

While this pooled signal was not uniformly reflected across individual follicular subcategories, it suggests that modulation of DNA repair status may alter the way follicles respond to concomitant cytotoxic stressors without necessarily inducing direct damage on its own. In parallel, independent evidence shows that chemotherapy can trigger oocyte-intrinsic apoptotic pathways and mitochondrial stress before morphological degeneration becomes apparent(5,79) and that PARP inhibition can impact primordial follicles in vivo (37). Human data on Olaparib's ovarian effects remain limited and largely inferential (80). Taken together, while H&E-based scoring suggests stability with Olaparib alone, reliance on morphology may underestimate early or synergistic damage under combination treatment; these observations warrant cautious interpretation and confirmation in larger, follicle-sufficient cohorts.

5.2 Apoptosis and DNA damage

5.2.1 TUNEL assay

The TUNEL assay is widely recognized as a reliable method for detecting late-stage apoptosis through the identification of DNA strand breaks. In the context of ovarian follicular biology, TUNEL reactivity serves as an informative indicator of degenerative processes affecting either the somatic (granulosa) or germ cell compartments, thus providing insight into follicular atresia or stress-induced damage. An increase in TUNEL-positive structures may therefore be interpreted as evidence of pro-apoptotic pressure, whereas low reactivity may reflect either cellular resilience or activation of alternative non-apoptotic death pathways that remain undetected by this method. In the present study, no statistically significant differences in apoptotic incidence were detected among the experimental treatments when granulosa cells, oocyte nuclei, or non-labelled follicles were assessed independently. This suggests that none of the tested conditions exerts a pronounced pro- or anti-apoptotic effect at the level of individual follicular compartments. Nevertheless, the cumulative comparison shown in Figure 9D indicated a potential redistribution of apoptotic events across treatments.

Within this cumulative distribution, the combined treatment (OLA + CB+PTX) appeared to display a higher proportion of apoptotic outcomes compared to the control. Interestingly, both OLA and CB+PTX showed distributions that were more closely aligned with the combined treatment than with the CTRL group, suggesting

that even individual agents may contribute to a modest increase in apoptotic signatures relative to baseline conditions. These observations did not reach definitive statistical support, but they are compatible with a scenario in which cytotoxic and PARP-inhibitory exposure—whether isolated or combined—may subtly shift the follicular environment toward a more damage-prone state. While this trend did not reach definitive statistical support, it may suggest that concurrent exposure to multiple agents could impose a modestly increased apoptotic burden on the follicular environment. Similar pro-apoptotic responses to combined metabolic or pharmacological stressors have previously been reported in human ovarian tissue (65,81,82), supporting the hypothesis that follicular units may be particularly sensitive to cumulative insults rather than isolated stimuli. Such an effect should not be overinterpreted due to the reduced number of follicular units contributing to each group; nevertheless, it may warrant further investigation in studies with greater statistical power.

Overall, these findings should be regarded as descriptive rather than conclusive**.** It is plausible that apoptosis alone may not fully encompass the spectrum of treatment-induced responses in human follicles. Alternative mechanisms—such as autophagy, metabolic adaptation, or sublethal mitochondrial dysfunction—may coexist or precede detectable DNA fragmentation(83–85). Future studies should therefore aim to increase the number of follicular units per treatment group and consider integrating TUNEL analysis with additional markers of cellular stress or death pathways, to provide a more comprehensive understanding of treatment-induced follicular dynamics.

5.2.2 γH2AX

The γH2AX assay is widely recognized as a sensitive marker of DNA double-strand breaks, reflecting the early cellular response to genotoxic stress. Within the ovarian follicle, persistent γH2AX labelling has been associated with impaired genome stability and potential compromise of developmental competence. Accordingly, the evaluation of γH2AX reactivity provides important insight into treatment-induced alterations in DNA integrity (64).

γH2AX staining did not reveal marked differences between CTRL and OLA, supporting the notion that PARP inhibition alone did not elicit detectable DNA damage under these conditions. In contrast, a progressive increase in γH2AX positivity was observed in CB+PTX and became more evident in the combined treatment (OLA+CB+PTX), suggesting a graded rise in DNA damage across treatment intensity. This pattern was reflected in the cumulative distribution of staining outcomes, which was statistically significant, indicating that treatment exposure influenced the overall allocation of DNA-damaged follicles. Although these findings should be interpreted cautiously given the number of follicular units analyzed, the consistency of the CTRL/OLA similarity and the stepwise increase from CB+PTX to OLA+CB+PTX provide a coherent signal that warrants further investigation.

The combined treatment (OLA + CB+PTX) appeared to be associated with a relatively higher proportion of γH2AX-positive outcomes. While not definitive, this observation is noteworthy, particularly considering that the analyzed follicles originate from BRCA-mutated patients, in whom defective DNA repair capacity has been reported in ovarian tissue (86). Moreover, altered genome stability has been directly documented within BRCA-associated human follicles (87) supporting the possibility that even low-level or transient damage may be more persistent in this genetic context. Additional studies have shown sustained γH2AX activation in response to metabolic or pharmacological stressors (88,89), reinforcing the plausibility of an additive effect under combined treatment conditions.

Given the relatively small number of follicles analyzed, the present findings should be regarded as exploratory and interpreted with appropriate caution**.** Future investigations using a larger number of BRCA-derived follicles, potentially alongside functional assessments of DNA repair competence, will be essential to determine whether the increased γH2AX reactivity observed under the combined treatment reflects a genuine treatment-associated vulnerability or remains attributable to stochastic variation.

5.2.3 Cleaved Caspase 3

Cleaved caspase-3 (CC3) represents an established executioner of apoptosis and is widely employed as a terminal marker of follicular atresia. Previous studies have shown that caspase-3 activation is part of the physiological follicle selection process in both granulosa cells and oocytes (90) and its immunohistochemical assessment has been proposed as a sensitive indicator of chemotherapy-induced ovarian damage (91,92). In this framework, CC3 staining was used in the present study to assess potential treatment-related apoptotic responses within the follicular niche.

The cumulative analysis (Figure 13D) revealed a redistribution of CC3 labelling across treatment groups, with the C+P and combined OLA+C+P conditions displaying slightly higher proportions of apoptotic outcomes compared with CTRL and Olaparib alone. However, this trend was not uniformly reflected across follicular compartments. In contrast to expectations from previous literature—where chemotherapy-induced apoptosis is typically more pronounced in granulosa cells—the current dataset showed relatively intense nuclear/oocyte staining in the C+P group and a less consistent pattern in granulosa cells. Furthermore, CC3 positivity was also relatively high in the control condition, suggesting that a component of apoptosis may be intrinsically associated with ex vivo culture and tissue manipulation rather than exclusively treatment driven. This interpretation is supported by recent evidence indicating that cryopreservation, thawing and culture stress can independently activate apoptotic cascades in ovarian tissue, even in the absence of pharmacological exposure (93). In addition, intrinsic apoptotic mechanisms are a physiological component of follicular turnover and atresia, as follicle loss naturally accompanies selection and growth dynamics. This baseline apoptotic background arising from both technical handling and endogenous mechanisms should therefore be considered when interpreting treatment-induced differences. This baseline apoptotic activity should therefore be considered when interpreting treatment-induced differences**.**

Within this context, Olaparib alone did not emerge as a dominant pro-apoptotic inducer relative to chemotherapy exposure. The slightly lower apoptotic allocation observed in the OLA group compared with CB+PTX and OLA+CB+PTX suggests that PARP inhibition may not substantially potentiate CC3 activation in this setting.

Nevertheless, given the unexpectedly elevated CC3 levels detected in control follicles and the compartmental discrepancy between granulosa and nuclear staining under chemotherapy, a definitive interpretation remains premature.

Overall, these findings indicate that CC3 activation in vitro human follicles may reflect a composite of intrinsic culture-associated apoptosis and treatment-related effects**,** with conventional chemotherapy appearing to exert a more pronounced apoptotic influence than Olaparib monotherapy. Further investigations employing time-resolved assessment of caspase activation and compartment-specific quantification will be required to determine whether PARP inhibition contributes to delayed or secondary apoptotic responses beyond the early culture phase.

5.3 Follicular activation and proliferation

5.3.1 Yes-associated protein 1 (YAP-1)

Previous studies demonstrated that Yes-associated protein 1 (YAP-1) plays a pivotal role in ovarian follicle physiology, acting as a pro-survival and proliferative co-activator within granulosa cells**.** It has been shown that timely expression and activation of YAP-1 in granulosa cells is essential for ovarian follicle development (94). Rather than serving as a marker of treatment efficacy or inefficacy, such diffuse YAP-1 expression may reflect a physiological requirement for Hippo pathway activity during early follicular maintenance (95), with potential subtle modulation — rather than overt activation of the pathway under different treatment conditions.

Notably, elevated YAP-1 labelling was also detected within the control samples**,** suggesting that tissue manipulation itself may have contributed to transient Hippo pathway disruption. Previous studies demonstrated that mechanical interference with ovarian tissue architecture is sufficient to interrupt Hippo signaling and induce follicular activation, even in the absence of pharmacological stimulation (67). Therefore, the excision and sectioning of ovarian cortex used for culture preparation may have provided a mechanical stimulus capable of triggering YAP-1 nuclear translocation, partially masking treatment-specific variations.

Regarding treatment effects, Olaparib was included as the primary pharmacological target; however, no clear directional modulation of YAP-1 was observed across treated groups. Previous studies explored possible interactions between PARP inhibition and Hippo/YAP-1 pathway dynamics (96), but the present data do not provide sufficient evidence to support either activation or repression of YAP-1 under Olaparib exposure. This may indicate that Hippo/YAP-1 signaling is predominantly influenced by intrinsic follicular activation cues and tissue manipulation**,** rather than by PARP inhibition alone within the current experimental setting.

Taken together, these observations suggest that YAP-1 expression in ex vivo human follicles is shaped by multiple overlapping influences, including mechanical disruption and intrinsic activation states. Nonetheless, a compartment-specific pattern emerged: granulosa cells showed higher YAP-1 positivity in chemotherapy-treated tissues, consistent with a potential pro-survival or reparative response to cytotoxic stress, in line with the recognized role of YAP-1 in supporting granulosa cell function. Conversely, in the OLA condition, YAP-1 was more frequently localized within the oocyte than in any other treatment, indicating that PARP inhibition may preferentially modulate Hippo signaling in the oocyte compartment rather than in somatic cells.
These preliminary compartmental shifts suggest that pharmacological inputs do not act in a uniform manner but may differentially regulate YAP-1 across follicular cell types. Future studies employing non-invasive follicle isolation or dynamic culture systems, coupled with temporal (rather than endpoint) assessment of YAP-1 localization, will be essential to clarify whether such signals reflect transient adaptation, delayed activation, or early signs of pathway dysregulation.

5.4 Immunological analysis

The cytokine profiles observed in the present study seems to be broadly consistent with previously described functional interactions among pro-inflammatory, immunomodulatory, and angiogenic mediators within ovarian and tumor-associated microenvironments (97). In particular, the coordinated behavior of IL-6, IL-8, MCP-1, and VEGF across experimental conditions reflects their well-established synergistic roles in the regulation of inflammatory responses, angiogenesis, and tissue remodeling (73,98–100).

Among the cytokines analyzed, IL-6 appears to play a central role as a pro-inflammatory upstream mediator. Recent evidence highlights IL-6 as a key regulator of ovarian inflammatory responses, contributing to immune cell activation, cytokine amplification, and modulation of the local microenvironment (101). Through JAK/STAT3-dependent signaling pathways, IL-6 has been shown to induce the expression of IL-8, MCP-1, and VEGF, thereby promoting inflammatory amplification and angiogenic responses (72,73,98,102). The coordinated temporal patterns observed for these cytokines in the present study are therefore consistent with the established regulatory role of IL-6 within inflammatory and angiogenic cytokine networks.

A major finding of this study is the overall reduction in cytokine concentrations observed under CB+PTX and OLA+CB+PTX treatment conditions compared with CTRL and OLA alone. This generalized decrease, involving both anti/ pro-inflammatory and angiogenic mediators, may reflect a reduced cytokine production by ovarian tissue exposed to chemotherapy. Chemotherapeutic agents such as carboplatin and paclitaxel are known to induce DNA damage, leading to cellular dysfunction and cell death (58,103,104). It could be therefore plausible that chemotherapy exposure may compromise not only follicular and stromal cells but also immune cells residing within the ovarian microenvironment. Based on this premise, their damage or depletion could be associated with a reduction in cytokine release, including IL-6, IL-8, MCP-1, and VEGF. These interpretations would benefit from further investigation and should be supported by additional analyses; however, evidence reported in the literature indicates that chemotherapy can alter immune cell populations and inflammatory signaling within ovarian tissue (101).

However, the relatively higher cytokine levels detected under CTRL and OLA conditions may be related to tissue stress responses rather than reflecting a physiological inflammatory state. Ovarian tissue culture represents a non-physiological condition, and procedures such as cryopreservation, thawing, and subsequent manipulation are known to induce cellular stress, structural damage, and activation of inflammatory pathways (105–107). It is therefore conceivable that the elevated concentrations of pro-inflammatory cytokines observed under CTRL and OLA conditions are, at least in part, associated with stress-induced activation of resident stromal and immune cells following tissue handling and vitro culture. Nevertheless, the immunological significance of these responses remains controversial and incompletely characterized.

The parallel behavior of IL-4 and VEGF observed in this study reflects their similar temporal patterns, characterized by increasing concentrations over time, particularly under CTRL and OLA conditions.

In contrast, IL-8 and VEGF did not display comparable temporal dynamics. Indeed, an inverse relationship between these mediators may be hypothesized, whereby higher levels of one factor at early time points are associated with lower levels of the other. In this context, IL-8 appeared relatively stable over time and across experimental conditions, whereas VEGF showed a more pronounced and generalized increase with prolonged culture duration. Despite these distinct kinetic profiles, previous studies have reported cooperative roles for IL-8 and VEGF in the regulation of angiogenesis and stromal remodeling, including within ovarian and reproductive tissues (97,101,107).

MCP-1 integrates into this inflammatory angiogenic network by regulating immune cell recruitment and indirectly influencing angiogenic signaling (108). Notably, in the present study MCP-1 and IL-10 exhibited remarkably similar temporal profiles across experimental conditions, suggesting a coordinated regulation over time. This parallel trend may reflect the establishment of a dynamic balance between pro-inflammatory and anti-inflammatory cues within the ovarian microenvironment, whereby MCP-1–mediated immune cell recruitment is accompanied by IL-10 driven regulatory mechanisms aimed at limiting excessive inflammation. Such a coordinated behavior is consistent with evidence indicating that IL-10 can modulate

MCP-1 expression and function in inflammatory settings, contributing to immune homeostasis rather than purely antagonistic regulation (109,110).

While MCP-1 has been functionally linked to IL-6 and IL-8 within pro-inflammatory networks (102), its association with IL-10 observed here supports a broader role in fine-tuning inflammatory responses. In this context, the coexistence of MCP-1 and IL-10 signaling may represent a compensatory mechanism that balances immune activation and resolution processes. Although the relationship between MCP-1 and angiogenic mediators such as VEGF is generally considered indirect and context-dependent (109,111), the temporal concordance between MCP-1 and IL-10 highlights the importance of regulatory cytokine interplay in shaping the ovarian inflammatory milieu under both physiological and treatment-related conditions.

Finally, IP-10 showed a distinct temporal behavior and limited association with the other cytokines analyzed. This observation is consistent with previous findings indicating that IP-10 primarily exerts selective effects on stromal and immune compartments, with relatively weak interactions with IL-6-, IL-8-, and VEGF-associated signaling networks (112).

Overall, the cytokine patterns observed in this study suggest the presence of a complex network of synergistic and modulatory interactions within cultured ovarian tissue. The apparent reduction in cytokine production following chemotherapy and combined treatments may be associated with chemotherapy-induced cellular damage affecting both ovarian and immune compartments, whereas elevated cytokine levels under CTRL and OLA conditions may reflect stress-related responses to tissue manipulation and non-physiological culture conditions.

In interpreting these findings, the cytokine results should also be considered together with histological and immunohistochemical observations. CD45 immunohistochemistry revealed no, or only very rare, positive cells in the analyzed ovarian tissue sections, arguing against a substantial contribution of infiltrating leukocytes to the cytokine levels measured in this experimental setting. At the same time, Masson’s trichrome staining showed a relatively abundant collagen component within the ovarian tissue, suggesting the presence of a stromal microenvironment characterized by marked extracellular matrix deposition. Although no definitive

conclusion can be drawn on the cellular source of cytokine release, these findings may support the hypothesis that resident stromal cells, including fibroblasts, contributed, at least in part, to the cytokine production detected in the culture medium. This interpretation remains speculative, but it is biologically plausible in light of the recognized association between ovarian fibrosis, fibroblast activity, extracellular matrix deposition, and inflammatory remodeling (63,113,114). Given the preliminary nature of the data and the absence of statistical analyses, these interpretations should be considered exploratory and warrant further investigation.

5.5 Brussels internship experiments

5.5.1 Morphological assessment of follicular stages and atresia

The classification of follicles according to their developmental stage confirmed that primordial and transitional follicles were the predominant populations across all treatment groups, consistent with the expected composition of ovarian cortical tissue. Notably, Olaparib alone did not induce substantial alterations in follicular distribution, as the relative proportions of primordial, transitional, primary, and secondary follicles remained comparable to control. This suggests that PARP inhibition does not appear to trigger premature follicular activation nor to induce stromal remodeling that could accelerate follicle recruitment and depletion.

In contrast, cyclophosphamide (4HC) exposure resulted in a slightly broader variability, particularly within transitional and primary follicles, indicating a higher degree of tissue disruption. However, the combination of 4HC and Olaparib did not consistently exacerbate this variability, suggesting that Olaparib does not synergize with chemotherapy to aggravate follicular dysregulation under the tested conditions.

Follicular atresia analysis further supported these observations. While 4HC led to increased degenerative structures, Olaparib-treated tissues displayed atresia levels similar to control, and the 4HC + Olaparib group did not show a marked increase beyond chemotherapy alone. Taken together, these preliminary findings suggest that Olaparib may be less detrimental to follicle survival compared with standard alkylating agents, although definitive conclusions await statistical validation.

A key aspect emerging from this study concerns the qualitative and quantitative differences between ovarian tissues from Brussels compared with those from Genoa. Brussels-derived samples displayed markedly higher follicle counts and better-preserved morphology, despite comparable or even more advanced chronological age in some donors. This observation highlights how chronological age does not always accurately reflect biological ovarian age and reinforces the concept that ovarian reserve declines at an individual pace, strongly influencing tissue responsiveness to genotoxic stress.

The superior follicle abundance observed in the Brussels cohort allowed more robust analysis and further underscores the critical role of initial ovarian reserve in determining tissue resilience.

Importantly, all interpretations must be considered preliminary, as no statistical analysis has yet been performed and experimental collection is still ongoing. Nevertheless, the emerging trends suggest that Olaparib does not substantially impair follicular morphology or survival when administered alone and does not appear to potentiate chemotherapy-induced atresia. Further investigation on larger cohorts will be required to determine whether PARP inhibitors could represent a more fertility-compatible therapeutic option, particularly in BRCA mutation carriers.

5.5.2 Immunostaining results

The analysis of DNA damage markers revealed heterogeneous responses across treatment groups and between BRCA-mutated and non-mutated samples. When focusing on the effect of Olaparib, either alone or in combination with cyclophosphamide, an overall trend of moderate increase in DNA damage markers was observed compared with control conditions, although not to the extent induced by 4HC monotherapy, which consistently showed the highest TUNEL and γH2AX positivity. These preliminary observations suggest that Olaparib alone does not elicit substantial DNA toxicity in ovarian follicles within the tested exposure window, and that its damaging potential is markedly lower than that of chemotherapy.

Interestingly, when combined with 4HC, Olaparib did not further exacerbate the DNA damage induced by chemotherapy, particularly in granulosa cells, where the response appeared comparable or slightly reduced relative to 4HC alone. Although this could indicate a potential modulatory interaction, caution is warranted as no statistical validation is currently available, and experiments are still ongoing.

Comparison between BRCA-mutated and non-mutated samples did not reveal a clear sensitization to Olaparib, as both groups displayed similar levels of positivity across markers and cell types. This may suggest that the synthetic lethality observed in BRCA-deficient tumor cells is not necessarily recapitulated in quiescent ovarian follicles, possibly due to lower proliferative activity or alternative repair mechanisms active in non-dividing cells.

A consistent pattern across datasets was the lower frequency of DNA damage in oocytes compared with granulosa cells, indicating either higher intrinsic resilience of oocytes or rapid elimination of severely damaged oocytes, preventing their accumulation. The low incidence of simultaneous positivity in both cell types (GC + oocyte) further suggests that complete follicular collapse is relatively uncommon, even under 4HC exposure.

The lack of detectable toxicity after short-term exposure to olaparib should be interpreted considering the mechanism of action of PARP inhibitors. These agents impair PARP-mediated DNA repair and their cytotoxic effect typically emerges after progressive accumulation of unrepaired DNA damage rather than immediately after exposure (115). In particular, in BRCA-deficient contexts, cell death results from synthetic lethality occurring when DNA lesions cannot be adequately resolved (116,117). Therefore, limited damage observed after a 3-day exposure may reflect insufficient time for endogenous DNA damage to accumulate to a measurable threshold rather than true biological safety.(115,117)

This interpretation is supported by preliminary dose-response assays in BRCA-mutated MDA-MB-436 cells, where olaparib induced a progressive time-dependent reduction in viability, especially at higher concentrations, while human cumulus cells did not exhibit appreciable viability reduction at any concentration or time point. These findings suggest that the detection of toxicity may depend on cellular context,

including proliferative activity and baseline DNA damage burden. Moreover, PARP inhibition may plausibly enhance toxicity when combined with DNA-damaging treatments by preventing repair of chemotherapy-induced lesions, providing a mechanistic explanation for the increased toxicity observed in the combination setting.

Importantly, all interpretations remain exploratory, as no statistical analysis has yet been performed and the dataset is still in expansion. The current findings must therefore be considered descriptive rather than conclusive. Nevertheless, these early trends raise the possibility that PARP inhibition may be less harmful to the ovarian reserve than conventional chemotherapy, and that its combination with alkylating agents may not necessarily exert additive toxicity. Further investigation with increased sample size and quantitative validation will be essential to determine whether Olaparib could be compatible with fertility preservation strategies, particularly in BRCA mutation carriers undergoing cancer treatment.

6. Study limitations

This study presents several and considerable limitations that should be acknowledged when interpreting the results.

The ovarian tissue samples were obtained from patients aged between 35 and 45 years, a relatively advanced reproductive window in which the follicular reserve is already physiologically reduced as previously reported (45). Therefore, the number of follicles available for analysis was limited, preventing a patient-based evaluation. To ensure a meaningful assessment, data therefore had to be interpreted in relation to follicle count rather than on an individual level.

Moreover, the manipulation of the tissue, specifically, the freezing and thawing procedures, may have affected not only the stromal component but also the intrinsic quality of the follicles. This hypothesis is supported by previous evidence showing that cryopreservation can impact ovarian tissue integrity and follicular viability (105–107). Consistently with these findings, a relatively high proportion of atretic follicles was observed in the CTRL condition in the present study, which could indicate that cryopreservation introduced some degree of bias in the evaluation of follicular health, although this cannot be stated with certainty.

In addition, another limitation of the study concerns the lack of standardization in tissue fragment size. The ovarian cortical pieces used were not cut to a uniform thickness or area, unlike the approach adopted by other research groups working with in vitro culture of cryopreserved ovarian cortical tissue, such as the Brussels group (58), which may have contributed to variability in follicular survival and growth outcomes.

Finally, one of the initial aims of the study was to explore whether the presence of a *BRCA* mutation might influence ovarian reserve both at baseline and after exposure to the targeted therapy Olaparib. Due to the limited availability of non-*BRCA*-mutated ovarian tissue comparable to the BRCA-mutated samples, this question could not be conclusively addressed within the present study, but it remains an important line of investigation for future research.

7. Conclusions

This study employed four complementary molecular markers: TUNEL, pH2AX, cleaved caspase-3 and YAP1, alongside morphological assessment of follicular atresia to investigate the effects of Olaparib (OLA), chemotherapy (CB+PTX), their combined exposure (OLA+CB+PTX), and untreated controls (CTRL). Each marker captured a distinct dimension of follicular integrity: TUNEL detected DNA fragmentation, pH2AX indicated the presence of DNA double-strand breaks, cleaved caspase-3 reflected activation of the apoptotic cascade, while YAP1 provided insight into pro-survival or proliferative signaling through modulation of the Hippo pathway (67,85,88).

Starting from the total follicle count, the control condition displayed the highest number of follicles, whereas all treatment groups showed a comparable reduction, with fewer than 20 follicles overall approximately half of those observed in the control. Regarding follicular atresia, both the control and Olaparib groups exhibited a higher proportion of healthy follicles compared to chemotherapy condition and combined treatment condition. In fact, this chemotherapy (CB+PTX) and the combined treatment (OLA+CB+PTX) displayed the opposite pattern, with more than 60% of follicles showing signs of atresia. These differences were statistically significant ($p = 0.0054$), indicating a treatment-dependent effect on follicular integrity.

A similar trend emerged across two out of three apoptotic molecular markers, where control and Olaparib behaved comparably, in contrast to CB+PTX and OLA+CB+PTX, which displayed a similar response pattern. Cleaved caspase-3 exemplified this trend particularly well, with a markedly elevated proportion of positively stained follicles (close to complete staining in the CB+PTX and OLA+CB+PTX groups). The data regarding chemotherapy is in line with existing evidence on chemotherapy-induced apoptotic damage (79,91,118). Data regarding the combined treatment highly positive staining of apoptotic follicles is emerging from this significant analysis (Fisher's exact test $p < 0.05$). A comparable pattern was observed for pH2AX: while control and Olaparib remained below 50% positivity,

CB+PTX and OLA+CB+PTX displayed a higher fraction of follicles with DNA double-strand breaks, particularly in chemotherapy with Olaparib condition the percentage of positive stained follicles is higher than 70%. These differences were statistically significant (Fisher's exact test, $p < 0.05$), indicating a clear treatment-dependent increase in DNA damage. The only marker diverging from this trend was TUNEL. In this case, Olaparib showed a proportion of DNA-fragmented follicles more closely aligned with CB+PTX and OLA+CB+PTX (around 88%), rather than with the control (approximately 65%). Notably, TUNEL was the only apoptotic marker for which no statistically significant (Fisher's exact test, $p > 0.05$), differences were detected among conditions, suggesting that further investigation with additional assays may be necessary to clarify this outcome.

Lastly, concerning YAP1, a well-established effector of the Hippo pathway involved in cellular survival and proliferation, it is important to note that its nuclear localization reflects its activated state. In fact, YAP1 is normally retained in the cytoplasm in a phosphorylated form; when dephosphorylated, it escapes kinase-mediated sequestration and translocates to the nucleus, where it functions as a transcriptional co-activator. Since Hippo signaling negatively regulates YAP1 activity, its nuclear translocation indicates Hippo pathway inactivation and consequent loss of growth control(66,67). In this context, the high proportion of nuclear staining in granulosa cells observed in the CB+PTX group, the most pronounced among all conditions — may suggest an increased proliferative or pro-survival response to chemotherapy-induced stress. Although further validation is required, this finding is reminiscent of the "burnout" phenomenon described in the literature, where chemotherapy triggers premature follicular activation followed by accelerated depletion of the follicular pool (94,119,120).

In contrast**,** the combined treatment (OLA+CB+PTX) displayed the highest proportion of follicles lacking positive YAP1 staining. This difference was statistically significant (Fisher's exact test $p < 0.05$) and it could tentatively be interpreted as a shift towards apoptosis due to insufficient proliferative or survival signaling, in line with evidence suggesting that suppression of YAP1 activity may sensitize cells to programmed cell death under stress conditions(121). However, this

hypothesis requires additional investigation before definitive conclusions can be drawn.

Overall, the cytokine analyses performed in this study did not allow the identification of a clear, condition-specific inflammatory signature. Nonetheless, a consistent trend emerged across experimental groups, with CTRL and OLA displaying broadly comparable cytokine profiles, while CB+PTX and OLA+CB+PTX exhibited a similar pattern characterized by lower cytokine concentrations. This paired behavior suggests the presence of shared biological responses within each treatment group and appears to correlate with the observations made in IHC and IF analyses, thereby providing additional contextual information that complements the morphological, immunohistochemical, and functional data presented throughout this study.

In this context, the reduced cytokine levels detected under chemotherapy and combined treatment conditions may reflect an overall decrease in cytokine production by ovarian tissue exposed to cytotoxic stress. Conversely, the relatively higher cytokine concentrations observed under CTRL and OLA conditions may be associated with stress-related responses induced by tissue manipulation, cryopreservation, and in vitro culture, rather than representing a physiological inflammatory state. However, the release of anti-inflammatory cytokines is also evident, which could help balance this condition. Nevertheless, given the exploratory nature of these analyses and the technical limitations related to cytokine detectability, these observations should be interpreted cautiously and cannot be considered conclusive.

Accordingly, the cytokine data should be viewed as complementary to the other experimental findings rather than as standalone evidence. Their integration with histological, immunohistochemical, and functional analyses contributes to a broader and more nuanced interpretation of ovarian tissue responses under the different treatment conditions, thereby providing a framework for addressing the main research questions of the present study.

Taken together, and in relation to the first research question, namely whether Olaparib exerts gonadotoxic effects, the present data do not provide a definitive answer.

However, the overall profile of Olaparib was consistently more aligned with the control condition than with chemotherapy or the combined treatment, suggesting that Olaparib is unlikely to be overtly gonadotoxic, although this assumption warrants further investigation.

As for the second research question, concerning whether the presence of a *BRCA* mutation may affect ovarian reserve at baseline or after treatment exposure, this could not be conclusively addressed due to the lack of a non-*BRCA*-mutated cohort. Moreover, comparison with the non-*BRCA* group treated in Brussels was not appropriate, as the age distribution differed substantially from that of the *BRCA*-mutated patients analyzed in this study. If anything, the marked discrepancy in follicle counts between the two populations further reinforces the dominant role of age as a determinant of both follicle quantity and quality.

The results obtained in this work represent an important starting point for understanding how molecular target therapy such as Olaparib can influence follicular integrity and ovarian tissue physiology in *BRCA*-mutated patients. Despite the limitations related to sample availability and follicle number, the study provides meaningful insights and outlines several promising directions for future research.

A primary objective will be to continue the collection of both *BRCA*-mutated and non-mutated ovarian tissues, compatibly with the opportunities offered by ovarian tissue donations. Lowering the age threshold for inclusion may be particularly beneficial, as it would allow the collection of tissue with a higher follicular density, thereby increasing the number of analyzable structures and improving the statistical robustness of future findings.

Another relevant step will be the completion of immunological analyses on the culture medium, aimed at identifying possible release of inflammatory mediators in response to the different treatments. These data could provide further insight into the mechanisms of tissue stress and repair in the in vitro environment.

Furthermore, the immunostaining results obtained so far could be strengthened by performing molecular biology analyses on the remaining BRCA ovarian tissue samples. Specifically, evaluating the expression of selected molecular targets involved in DNA damage response, apoptosis, and survival pathways would make it

possible to correlate protein localization with transcriptional activity, thus offering a deeper mechanistic understanding of the observed phenomena.

Lastly, it will be important to investigate to what extent the stromal compartment is affected by the treatments applied. Given the key role of the stroma in supporting follicular development and maintaining tissue homeostasis, understanding its response will be essential to clarify how the microenvironment contributes to follicular health and resilience.

Overall, the integration of these approaches ranging from histological and immunological to molecular analyses will enable a more comprehensive characterization of ovarian tissue behavior under stress conditions. Such knowledge could contribute to the optimization of fertility preservation strategies and to the development of more effective in vitro culture systems, ultimately improving the reproductive outcomes and quality of life of oncological and high-risk patients.

Bibliography

1. Siegel RL, Miller KD, Wagle NS, Jemal A. Cancer statistics, 2023. CA Cancer J Clin. 2023 Jan;73(1):17–48. doi:10.3322/caac.21763 PubMed PMID: 36633525.

2. Lambertini M, Goldrat O, Clatot F, Demeestere I, Awada A. Controversies about fertility and pregnancy issues in young breast cancer patients: current state of the art. Curr Opin Oncol. 2017 Jul;29(4):243–52. doi:10.1097/CCO.0000000000000380 PubMed PMID: 28463857.

3. Lambertini M, Anserini P, Levaggi A, Poggio F, Del Mastro L. Fertility counseling of young breast cancer patients. J Thorac Dis. 2013 Jun;5 Suppl 1(Suppl 1):S68-80. doi:10.3978/j.issn.2072-1439.2013.05.22 PubMed PMID: 23819030; PubMed Central PMCID: PMC3695540.

4. Kerr JB, Hutt KJ, Michalak EM, Cook M, Vandenberg CJ, Liew SH, et al. DNA damage-induced primordial follicle oocyte apoptosis and loss of fertility require TAp63-mediated induction of Puma and Noxa. Mol Cell. 2012 Nov 9;48(3):343–52. doi:10.1016/j.molcel.2012.08.017 PubMed PMID: 23000175; PubMed Central PMCID: PMC3496022.

5. Nguyen QN, Zerafa N, Liew SH, Findlay JK, Hickey M, Hutt KJ. Cisplatin- and cyclophosphamide-induced primordial follicle depletion is caused by direct damage to oocytes. Mol Hum Reprod. 2019 Aug 1;25(8):433–44. doi:10.1093/molehr/gaz020 PubMed PMID: 30953068.

6. Luan Y, Yu SY, Abazarikia A, Dong R, Kim SY. TAp63 determines the fate of oocytes against DNA damage. Sci Adv. 8(51):eade1846. doi:10.1126/sciadv.ade1846 PubMed PMID: 36542718; PubMed Central PMCID: PMC9770984.

7. Ben-Aharon I, Bar-Joseph H, Tzarfaty G, Kuchinsky L, Rizel S, Stemmer SM, et al. Doxorubicin-induced ovarian toxicity. Reprod Biol Endocrinol RBE. 2010 Mar 4;8:20. doi:10.1186/1477-7827-8-20 PubMed PMID: 20202194; PubMed Central PMCID: PMC2838903.

8. Wang Y, Liu M, Johnson SB, Yuan G, Arriba AK, Zubizarreta ME, et al. Doxorubicin obliterates mouse ovarian reserve through both primordial follicle atresia and overactivation. Toxicol Appl Pharmacol. 2019 Oct 15;381:114714. doi:10.1016/j.taap.2019.114714 PubMed PMID: 31437492; PubMed Central PMCID: PMC6745286.

9. Lande Y, Fisch B, Tsur A, Farhi J, Prag-Rosenberg R, Ben-Haroush A, et al. Short-term exposure of human ovarian follicles to cyclophosphamide metabolites seems to promote follicular activation in vitro. Reprod Biomed Online. 2017 Jan;34(1):104–14. doi:10.1016/j.rbmo.2016.10.005 PubMed PMID: 27815062.

10. Rosario R, Stewart HL, Spears N, Telfer EE, Anderson RA. Anti-Mullerian hormone attenuates both cyclophosphamide-induced damage and PI3K signalling activation, while rapamycin attenuates only PI3K signalling activation, in human ovarian cortex in vitro. Hum Reprod Oxf Engl. 2023 Dec 9;39(2):382–92. doi:10.1093/humrep/dead255 PubMed PMID: 38070496; PubMed Central PMCID: PMC10833070.

11. Shai D, Aviel-Ronen S, Spector I, Raanani H, Shapira M, Gat I, et al. Ovaries of patients recently treated with alkylating agent chemotherapy indicate the presence of acute follicle

activation, elucidating its role among other proposed mechanisms of follicle loss. Fertil Steril. 2021 May;115(5):1239–49. doi:10.1016/j.fertnstert.2020.11.040 PubMed PMID: 33485607.

12. Bedoschi G, Navarro PA, Oktay K. Chemotherapy-induced damage to ovary: mechanisms and clinical impact. Future Oncol. 2016 Oct;12(20):2333–44. doi:10.2217/fon-2016-0176 PubMed PMID: 27402553; PubMed Central PMCID: PMC5066134.

13. Lambertini M, Del Mastro L, Pescio MC, Andersen CY, Azim HA, Peccatori FA, et al. Cancer and fertility preservation: international recommendations from an expert meeting. BMC Med. 2016 Jan 4;14:1. doi:10.1186/s12916-015-0545-7 PubMed PMID: 26728489; PubMed Central PMCID: PMC4700580.

14. Shapiro CL. Cancer Survivorship. N Engl J Med. 2018 Dec 20;379(25):2438–50. doi:10.1056/NEJMra1712502 PubMed PMID: 30575480.

15. Vaz-Luis I, Masiero M, Cavaletti G, Cervantes A, Chlebowski RT, Curigliano G, et al. ESMO Expert Consensus Statements on Cancer Survivorship: promoting high-quality survivorship care and research in Europe. Ann Oncol Off J Eur Soc Med Oncol. 2022 Nov;33(11):1119–33. doi:10.1016/j.annonc.2022.07.1941 PubMed PMID: 35963481.

16. Dias Nunes J, Ntemou E, Van den Steen G, Findikli N, Fastrez M, Delbaere A, et al. Carboplatin and paclitaxel induced-gonadotoxicity on the ovarian reserve of young breast cancer patients with BRCA1 mutation. Hum Reprod Oxf Engl. 2025 Sep 1;40(9):1709–19. doi:10.1093/humrep/deaf133 PubMed PMID: 40646715.

17. Lambertini M, Goldrat O, Toss A, Azim HA, Peccatori FA, Ignatiadis M, et al. Fertility and pregnancy issues in BRCA-mutated breast cancer patients. Cancer Treat Rev. 2017 Sep;59:61–70. doi:10.1016/j.ctrv.2017.07.001 PubMed PMID: 28750297.

18. Lambertini M, Olympios N, Lequesne J, Calbrix C, Fontanilles M, Loeb A, et al. Impact of Taxanes, Endocrine Therapy, and Deleterious Germline BRCA Mutations on Anti-müllerian Hormone Levels in Early Breast Cancer Patients Treated With Anthracycline- and Cyclophosphamide-Based Chemotherapy. Front Oncol. 2019 Jul 12;9:575. doi:10.3389/fonc.2019.00575 PubMed PMID: 31355134; PubMed Central PMCID: PMC6640206.

19. Turan V, Lambertini M, Lee DY, Wang E, Clatot F, Karlan BY, et al. Association of Germline BRCA Pathogenic Variants With Diminished Ovarian Reserve: A Meta-Analysis of Individual Patient-Level Data. J Clin Oncol. 2021 Jun 20;39(18):2016–24. doi:10.1200/JCO.20.02880 PubMed PMID: 33891474; PubMed Central PMCID: PMC8260903.

20. Sighinolfi G, Grandi G, Barbieri E, Venturelli M, Piombino C, Melotti C, et al. Reduced reproductive potential in young healthy women with hereditary breast and/or ovarian cancer syndrome. Commun Med. 2025 Mar 8;5(1):70. doi:10.1038/s43856-025-00788-9 PubMed PMID: 40057639; PubMed Central PMCID: PMC11890596.

21. Gasparri ML, Di Micco R, Zuber V, Taghavi K, Bianchini G, Bellaminutti S, et al. Ovarian reserve of women with and without BRCA pathogenic variants: A systematic review and meta-analysis. Breast Edinb Scotl. 2021 Dec;60:155–62. doi:10.1016/j.breast.2021.09.006 PubMed PMID: 34627117; PubMed Central PMCID: PMC8501498.

22. C E DK, C van TT, J C EM, G W M LE, Irene H, Mariette G, et al. The Impact of BRCA1- and BRCA2 Mutations on Ovarian Reserve Status. Reprod Sci Thousand Oaks Calif. 2023

Jan;30(1):270–82. doi:10.1007/s43032-022-00997-w PubMed PMID: 35705781; PubMed Central PMCID: PMC9810575.

23. Winship AL, Alesi LR, Stringer JM, Cao Y, Lewis YM, Tu L, et al. Conditional loss of Brca1 in oocytes causes reduced litter size, ovarian reserve depletion, and impaired oocyte in vitro maturation with advanced reproductive age in mice. eBioMedicine. 2024 Jul 30;106:105262. doi:10.1016/j.ebiom.2024.105262 PubMed PMID: 39084071; PubMed Central PMCID: PMC11342213.

24. Meirow D, Nugent D. The effects of radiotherapy and chemotherapy on female reproduction. Hum Reprod Update. 2001;7(6):535–43. doi:10.1093/humupd/7.6.535 PubMed PMID: 11727861.

25. Oktem O, Oktay K. Quantitative assessment of the impact of chemotherapy on ovarian follicle reserve and stromal function. Cancer. 2007 Nov 15;110(10):2222–9. doi:10.1002/cncr.23071 PubMed PMID: 17932880.

26. Meirow D, Biederman H, Anderson RA, Wallace WHB. Toxicity of chemotherapy and radiation on female reproduction. Clin Obstet Gynecol. 2010 Dec;53(4):727–39. doi:10.1097/GRF.0b013e3181f96b54 PubMed PMID: 21048440.

27. Oktay K, Harvey BE, Partridge AH, Quinn GP, Reinecke J, Taylor HS, et al. Fertility Preservation in Patients With Cancer: ASCO Clinical Practice Guideline Update. J Clin Oncol Off J Am Soc Clin Oncol. 2018 Jul 1;36(19):1994–2001. doi:10.1200/JCO.2018.78.1914 PubMed PMID: 29620997.

28. Scavone G, Ottonello S, Blondeaux E, Arecco L, Scaruffi P, Stigliani S, et al. The Role of Cyclin-Dependent Kinases (CDK) 4/6 in the Ovarian Tissue and the Possible Effects of Their Exogenous Inhibition. Cancers. 2023 Oct 10;15(20):4923. doi:10.3390/cancers15204923 PubMed PMID: 37894292; PubMed Central PMCID: PMC10605229.

29. Frontiers | Confirming the efficacy and safety of CDK4/6 inhibitors in the first-line treatment of HR+ advanced breast cancer: a systematic review and meta-analysis [Internet]. [cited 2025 Sep 16]. Available from: https://www.frontiersin.org/journals/pharmacology/articles/10.3389/fphar.2024.1369420/full

30. Himpe J, Lammerant S, Van den Bergh L, Lapeire L, De Roo C. The Impact of Systemic Oncological Treatments on the Fertility of Adolescents and Young Adults-A Systematic Review. Life Basel Switz. 2023 May 18;13(5):1209. doi:10.3390/life13051209 PubMed PMID: 37240854; PubMed Central PMCID: PMC10223569.

31. Cui W, Rocconi RP, Thota R, Anderson RA, Bruinooge SS, Comstock IA, et al. Measuring ovarian toxicity in clinical trials: an American Society of Clinical Oncology research statement. Lancet Oncol. 2023 Oct;24(10):e415–23. doi:10.1016/S1470-2045(23)00390-X PubMed PMID: 37797647.

32. Eden CO, Haslam A, Prasad V. Cancer Therapy, Gonadal Function, and Fertility Preservation: Narrative Review. JCO Oncol Pract. 2024 Dec;20(12):1580–7. doi:10.1200/OP.23.00468 PubMed PMID: 38954787.

33. Arecco L, de Moura Leite L, Gentile G, Jankovic K, Stana M, Ottonello S, et al. Gonadotoxicity of immunotherapy and targeted agents in patients with cancer and impact on subsequent

pregnancies. Hum Reprod Oxf Engl. 2025 Aug 1;40(8):1452–66. doi:10.1093/humrep/deaf096 PubMed PMID: 40482082; PubMed Central PMCID: PMC12314150.

34. Wang X, Zhao S, Xin Q, Zhang Y, Wang K, Li M. Recent progress of CDK4/6 inhibitors' current practice in breast cancer. Cancer Gene Ther. 2024 Sep;31(9):1283–91. doi:10.1038/s41417-024-00747-x PubMed PMID: 38409585; PubMed Central PMCID: PMC11405274.

35. Ragupathi A, Singh M, Perez AM, Zhang D. Targeting the BRCA1/2 deficient cancer with PARP inhibitors: Clinical outcomes and mechanistic insights. Front Cell Dev Biol. 2023;11:1133472. doi:10.3389/fcell.2023.1133472 PubMed PMID: 37035242; PubMed Central PMCID: PMC10073599.

36. Maiorano BA, Maiorano MFP, Lorusso D, Di Maio M, Maiello E. Efficacy, and safety of PARP inhibitors in elderly patients with advanced ovarian cancer: a systematic review and meta-analysis. Int J Gynecol Cancer Off J Int Gynecol Cancer Soc. 2022 Nov 7;32(11):1410–8. doi:10.1136/ijgc-2022-003614 PubMed PMID: 36229080; PubMed Central PMCID: PMC9664098.

37. Winship AL, Griffiths M, Lliberos Requesens C, Sarma U, Phillips KA, Hutt KJ. The PARP inhibitor, olaparib, depletes the ovarian reserve in mice: implications for fertility preservation. Hum Reprod Oxf Engl. 2020 Aug 1;35(8):1864–74. doi:10.1093/humrep/deaa128 PubMed PMID: 32604417.

38. Nakamura K, Takae S, Shiraishi E, Shinya K, Igualada AJ, Suzuki N. Poly (ADP-ribose) polymerase inhibitor exposure reduces ovarian reserve followed by dysfunction in granulosa cells. Sci Rep. 2020 Oct 13;10:17058. doi:10.1038/s41598-020-74087-9 PubMed PMID: 33051529; PubMed Central PMCID: PMC7553950.

39. Williams CJ, Erickson GF. Morphology and Physiology of the Ovary. In: Feingold KR, Ahmed SF, Anawalt B, Blackman MR, Boyce A, Chrousos G, et al., editors. Endotext [Internet]. South Dartmouth (MA): MDText.com, Inc.; 2000 [cited 2025 Sep 16]. Available from: http://www.ncbi.nlm.nih.gov/books/NBK278951/ PubMed PMID: 25905186.

40. McLaughlin EA, McIver SC. Awakening the oocyte: controlling primordial follicle development. Reprod Camb Engl. 2009 Jan;137(1):1–11. doi:10.1530/REP-08-0118 PubMed PMID: 18827065.

41. Mossa F, Carter F, Walsh SW, Kenny DA, Smith GW, Ireland JLH, et al. Maternal undernutrition in cows impairs ovarian and cardiovascular systems in their offspring. Biol Reprod. 2013 Apr;88(4):92. doi:10.1095/biolreprod.112.107235 PubMed PMID: 23426432.

42. Erickson GF, Shimasaki S. The physiology of folliculogenesis: the role of novel growth factors. Fertil Steril. 2001 Nov;76(5):943–9. doi:10.1016/s0015-0282(01)02859-x PubMed PMID: 11704115.

43. McGee EA, Hsueh AJ. Initial and cyclic recruitment of ovarian follicles. Endocr Rev. 2000 Apr;21(2):200–14. doi:10.1210/edrv.21.2.0394 PubMed PMID: 10782364.

44. Edson MA, Nagaraja AK, Matzuk MM. The mammalian ovary from genesis to revelation. Endocr Rev. 2009 Oct;30(6):624–712. doi:10.1210/er.2009-0012 PubMed PMID: 19776209; PubMed Central PMCID: PMC2761115.

45. Wallace WHB, Kelsey TW. Human ovarian reserve from conception to the menopause. PloS One. 2010 Jan 27;5(1):e8772. doi:10.1371/journal.pone.0008772 PubMed PMID: 20111701; PubMed Central PMCID: PMC2811725.

46. Broekmans FJ, Kwee J, Hendriks DJ, Mol BW, Lambalk CB. A systematic review of tests predicting ovarian reserve and IVF outcome. Hum Reprod Update. 2006;12(6):685–718. doi:10.1093/humupd/dml034 PubMed PMID: 16891297.

47. Collins JK, Jones KT. DNA damage responses in mammalian oocytes. Reprod Camb Engl. 2016 Jul;152(1):R15-22. doi:10.1530/REP-16-0069 PubMed PMID: 27069010.

48. Vollenhoven B, Hunt S. Ovarian ageing and the impact on female fertility. F1000Research. 2018;7:F1000 Faculty Rev-1835. doi:10.12688/f1000research.16509.1 PubMed PMID: 30542611; PubMed Central PMCID: PMC6259486.

49. Park SU, Walsh L, Berkowitz KM. Mechanisms of ovarian aging. Reprod Camb Engl. 2021 Jul 14;162(2):R19–33. doi:10.1530/REP-21-0022 PubMed PMID: 33999842; PubMed Central PMCID: PMC9354567.

50. Cavalcante MB, Sampaio OGM, Câmara FEA, Schneider A, de Ávila BM, Prosczek J, et al. Ovarian aging in humans: potential strategies for extending reproductive lifespan. GeroScience. 2023 Aug;45(4):2121–33. doi:10.1007/s11357-023-00768-8 PubMed PMID: 36913129; PubMed Central PMCID: PMC10651588.

51. Malhotra N, Gupta P, Kamboj S, Chaturvedi P, Kutum R. 'Age specific variations in ovarian reserves in healthy fertile and infertile women: A cross sectional study. PloS One. 2024;19(10):e0308865. doi:10.1371/journal.pone.0308865 PubMed PMID: 39446778; PubMed Central PMCID: PMC11500972.

52. Turan V, Bedoschi G, Moy F, Oktay K. Safety, and feasibility of performing two consecutive ovarian stimulation cycles with the use of letrozole-gonadotropin protocol for fertility preservation in breast cancer patients. Fertil Steril. 2013 Dec;100(6):1681-1685.e1. doi:10.1016/j.fertnstert.2013.08.030 PubMed PMID: 24055050; PubMed Central PMCID: PMC3888552.

53. Lambertini M, Moore HCF, Leonard RCF, Loibl S, Munster P, Bruzzone M, et al. Gonadotropin-Releasing Hormone Agonists During Chemotherapy for Preservation of Ovarian Function and Fertility in Premenopausal Patients With Early Breast Cancer: A Systematic Review and Meta-Analysis of Individual Patient-Level Data. J Clin Oncol Off J Am Soc Clin Oncol. 2018 Jul 1;36(19):1981–90. doi:10.1200/JCO.2018.78.0858 PubMed PMID: 29718793; PubMed Central PMCID: PMC6804855.

54. von Mengden L, Klamt F, Smitz J. Redox Biology of Human Cumulus Cells: Basic Concepts, Impact on Oocyte Quality, and Potential Clinical Use. Antioxid Redox Signal. 2020 Mar 10;32(8):522–35. doi:10.1089/ars.2019.7984 PubMed PMID: 31861967; PubMed Central PMCID: PMC7038817.

55. O'Brien N, Conklin D, Beckmann R, Luo T, Chau K, Thomas J, et al. Preclinical Activity of Abemaciclib Alone or in Combination with Antimitotic and Targeted Therapies in Breast Cancer. Mol Cancer Ther. 2018 May;17(5):897–907. doi:10.1158/1535-7163.MCT-17-0290 PubMed PMID: 29483214.

56. Torres-Guzmán R, Calsina B, Hermoso A, Baquero C, Alvarez B, Amat J, et al. Preclinical characterization of abemaciclib in hormone receptor positive breast cancer. Oncotarget. 2017 Sep 19;8(41):69493–507. doi:10.18632/oncotarget.17778 PubMed PMID: 29050219; PubMed Central PMCID: PMC5642494.

57. Bosnjak M, Jesenko T, Markelc B, Janzic L, Cemazar M, Sersa G. PARP inhibitor olaparib has a potential to increase the effectiveness of electrochemotherapy in BRCA1 mutated breast cancer in mice. Bioelectrochemistry Amst Neth. 2021 Aug;140:107832. doi:10.1016/j.bioelechem.2021.107832 PubMed PMID: 33984694.

58. Dias Nunes J, Ntemou E, Van den Steen G, Findikli N, Fastrez M, Delbaere A, et al. Carboplatin and paclitaxel induced-gonadotoxicity on the ovarian reserve of young breast cancer patients with BRCA1 mutation. Hum Reprod Oxf Engl. 2025 Sep 1;40(9):1709–19. doi:10.1093/humrep/deaf133 PubMed PMID: 40646715.

59. Gene Expression Analyses in Human Follicles. United States; 2023. doi:10.3791/64807

60. Gougeon A. Dynamics of follicular growth in the human: a model from preliminary results. Hum Reprod Oxf Engl. 1986 Feb;1(2):81–7. doi:10.1093/oxfordjournals.humrep.a136365 PubMed PMID: 3558758.

61. Lopes F, Liu J, Morgan S, Matthews R, Nevin L, Anderson RA, et al. Single and combined effects of cisplatin and doxorubicin on the human and mouse ovary in vitro. Reprod Camb Engl. 2020 Feb;159(2):193–204. doi:10.1530/REP-19-0279 PubMed PMID: 31821159; PubMed Central PMCID: PMC6993208.

62. Zhou Y, Lan H, Dong Z, Li W, Qian B, Zeng Z, et al. Rhamnocitrin Attenuates Ovarian Fibrosis in Rats with Letrozole-Induced Experimental Polycystic Ovary Syndrome. Oxid Med Cell Longev. 2022 May 26;2022:5558599. doi:10.1155/2022/5558599 PubMed PMID: 35663203; PubMed Central PMCID: PMC9162838.

63. Zhu Y, Sun H, Gao T, Hou S, Li Y, Xu Y, et al. Ovarian remodeling and aging-related chronic inflammation and fibrosis in the mammalian ovary. J Ovarian Res. 2025 Jun 18;18:133. doi:10.1186/s13048-025-01715-1 PubMed PMID: 40533804; PubMed Central PMCID: PMC12175466.

64. Valdiglesias V, Giunta S, Fenech M, Neri M, Bonassi S. γH2AX as a marker of DNA double strand breaks and genomic instability in human population studies. Mutat Res. 2013;753(1):24–40. doi:10.1016/j.mrrev.2013.02.001 PubMed PMID: 23416207.

65. Hurst PR, Mora JM, Fenwick MA. Caspase-3, TUNEL and ultrastructural studies of small follicles in adult human ovarian biopsies. Hum Reprod Oxf Engl. 2006 Aug;21(8):1974–80. doi:10.1093/humrep/del109 PubMed PMID: 16670195.

66. Clark KL, George JW, Przygrodzka E, Plewes MR, Hua G, Wang C, et al. Hippo Signaling in the Ovary: Emerging Roles in Development, Fertility, and Disease. Endocr Rev. 2022 Nov 25;43(6):1074–96. doi:10.1210/endrev/bnac013 PubMed PMID: 35596657; PubMed Central PMCID: PMC9695108.

67. Hsueh AJW, Kawamura K. Hippo signaling disruption and ovarian follicle activation in infertile patients. Fertil Steril. 2020 Sep;114(3):458–64. doi:10.1016/j.fertnstert.2020.07.031 PubMed PMID: 32782158.

68. Tosatti JAG, Sóter MO, Ferreira CN, Silva I de FO, Cândido AL, Sousa MO, et al. The hallmark of pro- and anti-inflammatory cytokine ratios in women with polycystic ovary syndrome. Cytokine. 2020 Oct;134:155187. doi:10.1016/j.cyto.2020.155187 PubMed PMID: 32645538.

69. Du Y, Carranza Z, Luan Y, Busman-Sahay K, Wolf S, Campbell SP, et al. Evidence of cancer therapy-induced chronic inflammation in the ovary across multiple species: A potential cause of persistent tissue damage and follicle depletion. J Reprod Immunol. 2022 Mar;150:103491. doi:10.1016/j.jri.2022.103491 PubMed PMID: 35176661; PubMed Central PMCID: PMC9224575.

70. Kunicki M, Rzewuska N, Gross-Kępińska K. Immunophenotypic profiles and inflammatory markers in Premature Ovarian Insufficiency. J Reprod Immunol. 2024 Aug;164:104253. doi:10.1016/j.jri.2024.104253 PubMed PMID: 38776714.

71. Adamczak R, Ukleja-Sokołowska N, Lis K, Dubiel M. Function of Follicular Cytokines: Roles Played during Maturation, Development, and Implantation of Embryo. Medicina (Mex). 2021 Nov 16;57(11):1251. doi:10.3390/medicina57111251 PubMed PMID: 34833469; PubMed Central PMCID: PMC8625323.

72. Sirotkin AV. Cytokines: signalling molecules controlling ovarian functions. Int J Biochem Cell Biol. 2011 Jun;43(6):857–61. doi:10.1016/j.biocel.2011.03.001 PubMed PMID: 21382504.

73. Field SL, Dasgupta T, Cummings M, Orsi NM. Cytokines in ovarian folliculogenesis, oocyte maturation and luteinisation. Mol Reprod Dev. 2014 Apr;81(4):284–314. doi:10.1002/mrd.22285 PubMed PMID: 24273059.

74. Demeestere I, Simon P, Englert Y, Delbaere A. Preliminary experience of ovarian tissue cryopreservation procedure: alternatives, perspectives, and feasibility. Reprod Biomed Online. 2003 Nov;7(5):572–9. doi:10.1016/s1472-6483(10)62074-3 PubMed PMID: 14680552.

75. Demeestere I, Simon P, Buxant F, Robin V, Fernandez SA, Centner J, et al. Ovarian function, and spontaneous pregnancy after combined heterotopic and orthotopic cryopreserved ovarian tissue transplantation in a patient previously treated with bone marrow transplantation: case report. Hum Reprod Oxf Engl. 2006 Aug;21(8):2010–4. doi:10.1093/humrep/del092 PubMed PMID: 16585122.

76. Tuppi M, Kehrloesser S, Coutandin DW, Rossi V, Luh LM, Strubel A, et al. Oocyte DNA damage quality control requires consecutive interplay of CHK2 and CK1 to activate p63. Nat Struct Mol Biol. 2018 Mar;25(3):261–9. doi:10.1038/s41594-018-0035-7 PubMed PMID: 29483652.

77. Morgan S, Lopes F, Gourley C, Anderson RA, Spears N. Cisplatin, and doxorubicin induce distinct mechanisms of ovarian follicle loss; imatinib provides selective protection only against cisplatin. PloS One. 2013;8(7):e70117. doi:10.1371/journal.pone.0070117 PubMed PMID: 23922929; PubMed Central PMCID: PMC3726485.

78. Wei Q, Ding W, Shi F. Roles of poly (ADP-ribose) polymerase (PARP1) cleavage in the ovaries of fetal, neonatal, and adult pigs. Reprod Camb Engl. 2013 Dec;146(6):593–602. doi:10.1530/REP-13-0174 PubMed PMID: 24062568.

79. Titus S, Szymanska KJ, Musul B, Turan V, Taylan E, Garcia-Milian R, et al. Individual-oocyte transcriptomic analysis shows that genotoxic chemotherapy depletes human primordial follicle reserve in vivo by triggering proapoptotic pathways without growth activation. Sci

Rep. 2021 Jan 11;11(1):407. doi:10.1038/s41598-020-79643-x PubMed PMID: 33431979; PubMed Central PMCID: PMC7801500.

80. Dias Nunes J, Demeestere I, Devos M. BRCA Mutations and Fertility Preservation. Int J Mol Sci. 2023 Dec 22;25(1):204. doi:10.3390/ijms25010204 PubMed PMID: 38203374; PubMed Central PMCID: PMC10778779.

81. Fan Y, Flanagan CL, Brunette MA, Jones AS, Baker BM, Silber SJ, et al. Fresh and cryopreserved ovarian tissue from deceased young donors yields viable follicles. FS Sci. 2021 Aug;2(3):248–58. doi:10.1016/j.xfss.2021.06.003 PubMed PMID: 35146457; PubMed Central PMCID: PMC8823279.

82. Albamonte MS, Willis MA, Albamonte MI, Jensen F, Espinosa MB, Vitullo AD. The developing human ovary: immunohistochemical analysis of germ-cell-specific VASA protein, BCL-2/BAX expression balance, and apoptosis. Hum Reprod Oxf Engl. 2008 Aug;23(8):1895–901. doi:10.1093/humrep/den197 PubMed PMID: 18534994.

83. Chao T, Shih HT, Hsu SC, Chen PJ, Fan YS, Jeng YM, et al. Autophagy restricts mitochondrial DNA damage-induced release of ENDOG (endonuclease G) to regulate genome stability. Autophagy. 2021 Nov;17(11):3444–60. doi:10.1080/15548627.2021.1874209 PubMed PMID: 33465003; PubMed Central PMCID: PMC8632313.

84. Liu J, Wu Y, Meng S, Xu P, Li S, Li Y, et al. Selective autophagy in cancer: mechanisms, therapeutic implications, and future perspectives. Mol Cancer. 2024 Jan 24;23(1):22. doi:10.1186/s12943-024-01934-y PubMed PMID: 38262996; PubMed Central PMCID: PMC10807193.

85. Onishi M, Yamano K, Sato M, Matsuda N, Okamoto K. Molecular mechanisms and physiological functions of mitophagy. EMBO J. 2021 Feb 1;40(3):e104705. doi:10.15252/embj.2020104705 PubMed PMID: 33438778; PubMed Central PMCID: PMC7849173.

86. Lin W, Titus S, Moy F, Ginsburg ES, Oktay K. Ovarian Aging in Women With BRCA Germline Mutations. J Clin Endocrinol Metab. 2017 Oct 1;102(10):3839–47. doi:10.1210/jc.2017-00765 PubMed PMID: 28938488; PubMed Central PMCID: PMC5630253.

87. Oktay K, Turan V, Titus S, Stobezki R, Liu L. BRCA Mutations, DNA Repair Deficiency, and Ovarian Aging. Biol Reprod. 2015 Sep;93(3):67. doi:10.1095/biolreprod.115.132290 PubMed PMID: 26224004; PubMed Central PMCID: PMC4710189.

88. Talibova G, Bilmez Y, Tire B, Ozturk S. The DNA double-strand break repair proteins γH2AX, RAD51, BRCA1, RPA70, KU80, and XRCC4 exhibit follicle-specific expression differences in the postnatal mouse ovaries from early to older ages. J Assist Reprod Genet. 2024 Sep;41(9):2419–39. doi:10.1007/s10815-024-03189-4 PubMed PMID: 39023827; PubMed Central PMCID: PMC11405603.

89. Yeung CK, Wang G, Yao Y, Liang J, Tenny Chung CY, Chuai M, et al. BRE modulates granulosa cell death to affect ovarian follicle development and atresia in the mouse. Cell Death Dis. 2017 Mar 23;8(3):e2697. doi:10.1038/cddis.2017.91 PubMed PMID: 28333135; PubMed Central PMCID: PMC5386581.

90. Matikainen T, Perez GI, Zheng TS, Kluzak TR, Rueda BR, Flavell RA, et al. Caspase-3 gene knockout defines cell lineage specificity for programmed cell death signaling in the ovary.

Endocrinology. 2001 Jun;142(6):2468–80. doi:10.1210/endo.142.6.8078 PubMed PMID: 11356696.

91. Hurst PR, Mora JM, Fenwick MA. Caspase-3, TUNEL and ultrastructural studies of small follicles in adult human ovarian biopsies. Hum Reprod Oxf Engl. 2006 Aug;21(8):1974–80. doi:10.1093/humrep/del109 PubMed PMID: 16670195.

92. Glamoclija V, Vilović K, Saraga-Babić M, Baranović A, Sapunar D. Apoptosis, and active caspase-3 expression in human granulosa cells. Fertil Steril. 2005 Feb;83(2):426–31. doi:10.1016/j.fertnstert.2004.06.075 PubMed PMID: 15705385.

93. Stringer JM, Alesi LR, Winship AL, Hutt KJ. Beyond apoptosis: evidence of other regulated cell death pathways in the ovary throughout development and life. Hum Reprod Update. 2023 Jul 5;29(4):434–56. doi:10.1093/humupd/dmad005 PubMed PMID: 36857094; PubMed Central PMCID: PMC10320496.

94. Lv X, He C, Huang C, Wang H, Hua G, Wang Z, et al. Timely expression, and activation of YAP1 in granulosa cells is essential for ovarian follicle development. FASEB J Off Publ Fed Am Soc Exp Biol. 2019 Sep;33(9):10049–64. doi:10.1096/fj.201900179RR PubMed PMID: 31199671; PubMed Central PMCID: PMC6704445.

95. M D, J G, I D. Interaction between PI3K/AKT and Hippo pathways during in vitro follicular activation and response to fragmentation and chemotherapy exposure using a mouse immature ovary model. Biol Reprod. 2020 Mar 13;102(3). doi:10.1093/biolre/ioz215 PubMed PMID: 31786608.

96. Devos M, Dias Nunes J, Donfack Jiatsa N, Demeestere I. Regulation of follicular activation signaling pathways by in vitro inhibition of YAP/TAZ activity in mouse ovaries. Sci Rep. 2023 Sep 15;13(1):15346. doi:10.1038/s41598-023-41954-0 PubMed PMID: 37714905; PubMed Central PMCID: PMC10504383.

97. Zhao H, Wu L, Yan G, Chen Y, Zhou M, Wu Y, et al. Inflammation and tumor progression: signaling pathways and targeted intervention. Signal Transduct Target Ther. 2021 Jul 12;6:263. doi:10.1038/s41392-021-00658-5 PubMed PMID: 34248142; PubMed Central PMCID: PMC8273155.

98. Tan B, Wang J, Tan B, Wang J. Role of IL-6 in Physiology and Pathology of the Ovary. Clin Exp Obstet Gynecol. 2024 Sep 19;51(9):208. doi:10.31083/j.ceog5109208

99. Pan Y, Pan C, Zhang C. Unraveling the complexity of follicular fluid: insights into its composition, function, and clinical implications. J Ovarian Res. 2024 Nov 26;17(1):237. doi:10.1186/s13048-024-01551-9 PubMed PMID: 39593094; PubMed Central PMCID: PMC11590415.

100. Guzmán A, Hernández-Coronado CG, Gutiérrez CG, Rosales-Torres AM. The vascular endothelial growth factor (VEGF) system as a key regulator of ovarian follicle angiogenesis and growth. Mol Reprod Dev. 2023 Apr;90(4):201–17. doi:10.1002/mrd.23683 PubMed PMID: 36966489.

101. Guo Y, Xue L, Tang W, Xiong J, Chen D, Dai Y, et al. Ovarian microenvironment: challenges and opportunities in protecting against chemotherapy-associated ovarian damage. Hum Reprod Update. 2024 Oct 1;30(5):614–47. doi:10.1093/humupd/dmae020 PubMed PMID: 38942605; PubMed Central PMCID: PMC11369228.

102. Zhang R, Roque DM, Reader J, Lin J. Combined inhibition of IL-6 and IL-8 pathways suppresses ovarian cancer cell viability and migration and tumor growth. Int J Oncol. 2022 May;60(5):50. doi:10.3892/ijo.2022.5340 PubMed PMID: 35315502; PubMed Central PMCID: PMC8973967.

103. Spears N, Lopes F, Stefansdottir A, Rossi V, De Felici M, Anderson RA, et al. Ovarian damage from chemotherapy and current approaches to its protection. Hum Reprod Update. 2019 Nov 5;25(6):673–93. doi:10.1093/humupd/dmz027

104. Kawano M, McKey J, Batchvarov IS, Capel B. Granulosa cell death is a significant contributor to DNA-damaging chemotherapy-induced ovarian insufficiency†. Biol Reprod. 2025 May 13;112(5):906–15. doi:10.1093/biolre/ioae181 PubMed PMID: 40178377; PubMed Central PMCID: PMC12078076.

105. Lee S, Ryu KJ, Kim B, Kang D, Kim YY, Kim T. Comparison between Slow Freezing and Vitrification for Human Ovarian Tissue Cryopreservation and Xenotransplantation. Int J Mol Sci. 2019 Jul 8;20(13):3346. doi:10.3390/ijms20133346 PubMed PMID: 31288388; PubMed Central PMCID: PMC6651588.

106. Wang T ren, Yan J, Lu C ling, Xia X, Yin T lang, Zhi X, et al. Human single follicle growth in vitro from cryopreserved ovarian tissue after slow freezing or vitrification. Hum Reprod Oxf Engl. 2016 Apr;31(4):763–73. doi:10.1093/humrep/dew005 PubMed PMID: 26851603.

107. Ramos L, Galbinski S, Nacul A, Jiménez MF, Frantz N, Bos-Mikich A. Detailed Morphological Analysis of Cryoinjury in Human Ovarian Tissue Following Vitrification or Slow Freezing. Reprod Sci Thousand Oaks Calif. 2022 Aug;29(8):2374–81. doi:10.1007/s43032-021-00716-x PubMed PMID: 34398410.

108. Wen J, Zhao Z, Huang L, Wang L, Miao Y, Wu J. IL-8 promotes cell migration through regulating EMT by activating the Wnt/β-catenin pathway in ovarian cancer. J Cell Mol Med. 2020 Jan;24(2):1588–98. doi:10.1111/jcmm.14848 PubMed PMID: 31793192; PubMed Central PMCID: PMC6991660.

109. Arici A, Oral E, Bukulmez O, Buradagunta S, Bahtiyar O, Jones EE. Monocyte chemotactic protein-1 expression in human preovulatory follicles and ovarian cells. J Reprod Immunol. 1997 Feb;32(3):201–19. doi:10.1016/s0165-0378(97)82476-x PubMed PMID: 9080384.

110. Al-Shahat A, Hulail MAE, Soliman NMM, Khamis T, Fericean LM, Arisha AH, et al. Melatonin Mitigates Cisplatin-Induced Ovarian Dysfunction via Altering Steroidogenesis, Inflammation, Apoptosis, Oxidative Stress, and PTEN/PI3K/Akt/mTOR/AMPK Signaling Pathway in Female Rats. Pharmaceutics. 2022 Dec 10;14(12):2769. doi:10.3390/pharmaceutics14122769 PubMed PMID: 36559263; PubMed Central PMCID: PMC9786155.

111. Bouet PE, Chao de la Barca JM, Boucret L, Descamps P, Legendre G, Hachem HE, et al. Elevated Levels of Monocyte Chemotactic Protein-1 in the Follicular Fluid Reveals Different Populations among Women with Severe Endometriosis. J Clin Med. 2020 May 1;9(5):1306. doi:10.3390/jcm9051306 PubMed PMID: 32370059; PubMed Central PMCID: PMC7291127.

112. Yates-Binder CC, Rodgers M, Jaynes J, Wells A, Bodnar RJ, Turner T. An IP-10 (CXCL10)-derived peptide inhibits angiogenesis. PloS One. 2012;7(7):e40812. doi:10.1371/journal.pone.0040812 PubMed PMID: 22815829; PubMed Central PMCID: PMC3397949.

113. Orisaka M, Mizutani T, Miyazaki Y, Shirafuji A, Tamamura C, Fujita M, et al. Chronic low-grade inflammation, and ovarian dysfunction in women with polycystic ovarian syndrome, endometriosis, and aging. Front Endocrinol. 2023;14:1324429. doi:10.3389/fendo.2023.1324429 PubMed PMID: 38192421; PubMed Central PMCID: PMC10773729.

114. Machlin JH, Barishansky SJ, Kelsh J, Larmore MJ, Johnson BW, Pritchard MT, et al. Fibroinflammatory Signatures Increase with Age in the Human Ovary and Follicular Fluid. Int J Mol Sci. 2021 May 5;22(9):4902. doi:10.3390/ijms22094902 PubMed PMID: 34063149; PubMed Central PMCID: PMC8125514.

115. Helleday T. The underlying mechanism for the PARP and BRCA synthetic lethality: clearing up the misunderstandings. Mol Oncol. 2011 Aug;5(4):387–93. doi:10.1016/j.molonc.2011.07.001 PubMed PMID: 21821475; PubMed Central PMCID: PMC5528309.

116. Bryant HE, Schultz N, Thomas HD, Parker KM, Flower D, Lopez E, et al. Specific killing of BRCA2-deficient tumours with inhibitors of poly(ADP-ribose) polymerase. Nature. 2005 Apr 14;434(7035):913–7. doi:10.1038/nature03443 PubMed PMID: 15829966.

117. Farmer H, McCabe N, Lord CJ, Tutt ANJ, Johnson DA, Richardson TB, et al. Targeting the DNA repair defect in BRCA mutant cells as a therapeutic strategy. Nature. 2005 Apr 14;434(7035):917–21. doi:10.1038/nature03445 PubMed PMID: 15829967.

118. Kim YY, Kim WO, Liu HC, Rosenwaks Z, Kim JW, Ku SY. Effects of paclitaxel and cisplatin on in vitro ovarian follicle development. Arch Med Sci AMS. 2019 Oct;15(6):1510–9. doi:10.5114/aoms.2019.81730 PubMed PMID: 31749880; PubMed Central PMCID: PMC6855155.

119. Masciangelo R, Hossay C, Chiti MC, Manavella DD, Amorim CA, Donnez J, et al. Role of the PI3K and Hippo pathways in follicle activation after grafting of human ovarian tissue. J Assist Reprod Genet. 2020 Jan;37(1):101–8. doi:10.1007/s10815-019-01628-1 PubMed PMID: 31732846; PubMed Central PMCID: PMC7000614.

120. Hu LL, Su T, Luo RC, Zheng YH, Huang J, Zhong ZS, et al. Hippo pathway functions as a downstream effector of AKT signaling to regulate the activation of primordial follicles in mice. J Cell Physiol. 2019 Feb;234(2):1578–87. doi:10.1002/jcp.27024 PubMed PMID: 30078193.

121. Lv X, He C, Huang C, Hua G, Chen X, Timm BK, et al. Reprogramming of Ovarian Granulosa Cells by YAP1 Leads to Development of High-Grade Cancer with Mesenchymal Lineage and Serous Features. Sci Bull. 2020 Aug 15;65(15):1281–96. doi:10.1016/j.scib.2020.03.040 PubMed PMID: 34888112; PubMed Central PMCID: PMC8654108.